



FACULDADE DE TECNOLOGIA SENAI CIMATEC
PROGRAMA DE POS-GRADUAÇÃO STRICTO SENSU
GESTÃO E TECNOLOGIA INDUSTRIAL

PEDRO DE ANDRADE MATO GROSSO E PEDREIRA BAMBERG

**STUDY OF THE MECHANICAL CHARACTERIZATION OF
DISSIMILAR AND SIMILAR SINGLE LAP JOINTS BONDED BY
EPOXY STRUCTURAL ADHESIVE: An experimental approach**

**ESTUDO DA CARACTERIZAÇÃO MECÂNICA DE JUNTAS
SOBREPOSTAS SIMPLES DISSIMILARES E SIMILARES UNIDAS
POR ADESIVO ESTRUTURAL DE EPÓXI: Uma abordagem
experimental**

Salvador

2016

PEDRO DE ANDRADE MATO GROSSO E PEDREIRA BAMBERG

STUDY OF THE MECHANICAL CHARACTERIZATION OF DISSIMILAR AND
SIMILAR SINGLE LAP JOINTS BONDED BY EPOXY STRUCTURAL ADHESIVE:

An experimental approach

ESTUDO DA CARACTERIZAÇÃO MECÂNICA DE JUNTAS SOBREPOSTAS
SIMPLES DISSIMILARES E SIMILARES UNIDAS POR ADESIVO ESTRUTURAL

DE EPÓXI: Uma abordagem experimental

Dissertação de mestrado apresentada ao Programa de Pós-
Graduação Stricto Sensu da Faculdade Tecnologia SENAI
CIMATEC como requisito final para a obtenção do título de
Mestre em Gestão e Tecnologia Industrial

Orientador: Prof^a.Dr^a. Josiane Dantas Viana Barbosa

Co-orientador: Prof.Dr.-Ing Rodrigo Santiago Coelho

Salvador

2016

Ficha catalográfica elaborada pela Biblioteca da Faculdade de Tecnologia SENAI CIMATEC

B199e Bamberg, Pedro de Andrade Mato Grosso e Pedreira

Estudo da caracterização mecânica de juntas sobrepostas simples dissimilares e similares unidas por adesivo estrutural de epóxi: uma abordagem experimental / Pedro de Andrade Mato Grosso e Pedreira Bamberg. – Salvador, 2016.

105 f. : il. color.

Orientador: Prof. Dr.^a Josiane Dantas Viana Barbosa.

Coorientador: Prof. Dr. Rodrigo Santiago Coelho.

Dissertação (Mestrado em Gestão e Tecnologia Industrial - GETEC) – Programa de Pós-Graduação, Faculdade de Tecnologia SENAI CIMATEC, Salvador, 2016.

Inclui referências.

1. Adesivos estruturais. 2. Juntas sobrepostas dissimilares. 3. Distribuição de tensão. 4. Correlação digital de imagens. I. Faculdade de Tecnologia SENAI CIMATEC. II. Barbosa, Josiane Dantas Viana. III. Coelho, Rodrigo Santiago. IV. Título.

CDD: 621.825

Faculdade de Tecnologia SENAI CIMATEC

Mestrado Profissional em Gestão e Tecnologia Industrial

A Banca Examinadora, constituída pelos professores abaixo listados, aprova a Defesa de Mestrado, intitulada "Estudo da caracterização mecânica de juntas sobrepostas simples dissimilares e similares unidas por adesivo estrutural de epóxi: Uma abordagem experimental", apresentada no dia 14 de dezembro de 2016, como parte dos requisitos necessários para a obtenção do Título de Mestre em Gestão e Tecnologia Industrial.

Orientadora:



Prof. Dr. Josiane Dantas Viana Barbosa
SENAI CIMATEC

Coorientador:



Prof. Dr. Rodrigo Santiago Coelho
SENAI CIMATEC

Membro Interno:



Prof. Dr. Valter Estevão Beal
SENAI CIMATEC

Membro Externo:



Prof. Dr. Leona Pêter Correia da Silva Andrade
FIEB

Dedico este trabalho à minha
mãe, Lílian, pelo exemplo e incentivo concedidos no dia a dia.

*I dedicate this work to my mother,
Lílian, for being my role model and for the daily given support.*

ACKNOWLEDGEMENT

First, I would like to say thanks to God for the guidance, motivation and faith. With Him the path is lighter. To my family and friends, I say thanks for all the support given and affection. From the bottom of my heart, I thank and acknowledge my mother, LÍlian, and my brother, Bernhard, for being always present in the most important moments and decisions through my whole life, especially during the development of this work while abroad. Special thanks to SENAI CIMATEC and GETEC program, with distinction to Dr. Josiane Dantas and Dr. Rodrigo Coelho, for the provided orientation on the current work, to my colleagues from ISI – SENAI Institute for Innovation – due to the productive discussions and teamwork, and also to the creators of the “Young Talents” trainee program for believing in the potential and results of our group. Finally, I have no words to describe how thankful I am for all the coaching, good will, interest, technical support and friendship from ISF – Institute für Schweißtechnik und Füge-technik – where the experimental part of this work was performed. To Prof. Dr. Uwe Reisgen, Mr. Alex Schiebahn and Mr. Bernd Marx, I would like to say thanks for this unique opportunity. To Mr. Matthias Angerhausen, Mr. Alexandros Pipinikas, Mr. Martin Christ and all the other Institute friends and colleagues, thank you very much for the kindness, patience and friendship, which I will carry with me for the rest of my life.

“Andá com fé eu vou, que a fé não costuma faiá”.
(Gilberto Gil)

RESUMO

Este trabalho abrange o estudo de juntas sobrepostas simples, formadas por materiais similares e dissimilares, unidas por adesivos estruturais. O objetivo foi avaliar o efeito do comprimento de sobreposição, espessura da camada adesiva e tensão de escoamento do substrato, na resistência à tração da junta. Para isso, ensaios mecânicos de tração foram realizados em amostras contendo três diferentes comprimentos de sobreposição, três diferentes espessuras de camada adesiva e dois substratos com tensão de escoamento diferentes. Além disto, foram feitas análises de correlação digital de imagens para a análise do estado de tensão das juntas, a presença de concentradores de tensão e a incidência de deformações plásticas nos substratos. Como resultado, foi possível aferir que o comprimento de sobreposição possui a maior influência sobre a resistência a tração das juntas. O efeito é reduzido à medida que este comprimento aumenta. A tensão de escoamento do substrato também apresentou grande influência, de modo que deformações plásticas no substrato favoreceram a incidência de *peeling stresses*, que reduzem significativamente a resistência das juntas. A espessura da camada adesiva possui menor efeito sobre a resistência mecânica. Quanto mais espessa, menor é a resistência mecânica da junta, quando não há grande incidência de deformação plástica nos substratos. No entanto, quando ocorrem deformações plásticas nos substratos, o estado de tensão é mais complexo e esta relação pode variar. O estudo das juntas unidas por adesivos estruturais e entendimento sobre o efeito das variáveis sobre o seu estado de tensão se mostrou fundamental no projeto de estruturas coladas. Além das propriedades mecânicas do adesivo e dos aderentes, as interações entre as variáveis podem configurar juntas com propriedades adequadas ou inadequadas para determinada aplicação, dependendo do seu estado de tensão. Além disto, há fatores dessas variáveis a serem considerados como o seu impacto em custo, peso e propriedades de corrosão das juntas.

Palavras-chave: Adesivos estruturais; Juntas sobrepostas; Correlação digital de imagens; Comprimento de sobreposição; Distribuição de tensão; Juntas dissimilares; Similares; HSS; DP600; Ligas de alumínio; AA5083.

ABSTRACT

This work encompasses the study of the mechanical behavior of overlap joints with similar and dissimilar materials, joined by structural adhesives. The objective was to evaluate the effect the variables overlap length, adhesive layer thickness and adherend yield strength over the SLJ FL. Mechanical experiments of tensile tests were performed with samples containing three different overlap lengths, three different adhesive thicknesses and two different materials used as adherends with high and low yield strength. In addition, digital image correlation (DIC) analyses were done in order to study the stress state of the single lap joints, the presence of stress concentrators and the incidence of plastic strain at the adherends. At the end of this work, it was possible to confirm that the overlap length has the highest direct influence over the single lap joints (SLJ) FL. This effect is reduced as the length is increased. Plastic strains at the adherends allow the incidence of peeling stresses, which reduce considerably the joints FL. The adhesive layer thickness has lower effect over the joints FL. For the cases free of plastic strain, the relationship is inverse. However, when the adherends face plastic strain, the stress state of the SLJ is more complex and this relationship is not true. The study of the bonded joints and proper understanding about the effects of the studied variables over the stress state proved to be fundamental in the design of bonded structures. Further than the mechanical properties of the adhesive and adherends, the interactions between the studied variables can configure joints suitable proper or inappropriate for a certain application, depending on its stress state. In addition, there are factors attached to these variables to be considered, as its impact over cost, weight and corrosion properties of such joints.

Keywords: Structural adhesives; Single lap joints, Digital image correlation; overlap length; Stress state; Dissimilar joints; Similar; HSS (DP600), Al alloys; AA5083

FIGURES LIST

Figure 1 - Case of study: The rail segment design change. Source: Jamestown (2016).	7
Figure 2 - Rail segment design (before). Source: Jamestown (2016).	8
Figure 3 - Rail segment design (after). Source: Jamestown (2016).	8
Figure 4 - PMMA molecule overview. Source: Da Silva et al. (2011).	14
Figure 5 - Electrostatic bonding example. Source: Pocius (2012).	15
Figure 6 - Diffusion bonding. Source: Adhesive and glue (2016).	16
Figure 7 – Mechanical interlocking. Source: Pocius (2012).	17
Figure 8 – Wetting and dewetting examples. Source: Author.	18
Figure 9 – Contact angle of a liquid over a surface. Source: Kinloch (1987).	18
Figure 10 - Contact angle vs. wettability. Source: Adhesives.org (2015).	19
Figure 11 - Adhesive bonding main forces. Source: Adhesives.org (2015).	20
Figure 12 - Main adhesive bonded joint types. Source: The Aluminum Joining Manual (2015).	21
Figure 13 - Tensile/Shear load condition. Source: Nashett (2015).	22
Figure 14 - Tensile load condition. Source: Nashett (2015).	23
Figure 15 - Peeling stress on a bonded joint. Source: Plastech (2011).	24
Figure 16 – Cleavage load condition. Source: Plastech (2011).	24
Figure 17 – Torsion stress condition. Source: Hussey and Wilson (1996).	25
Figure 18 – Bending moment on SLJ. Source: Tsai and Morton (1994).	25
Figure 19 - OL effect vs. plastic strain. Source: Pocius (2012).	27
Figure 20 – Untreated surface and its contaminants. Source: Pocius (2012).	29
Figure 21 - The SLJ specimen. Source: Bamberg et al. (2016).	33
Figure 22 – The experimental setup. Source: Author.	34
Figure 23 – The alignment tabs. Source: Modified from Guo, Dillard and Plautc, (2006).	36
Figure 24 - Sample preparing process overview. Source: Author.	36
Figure 25 - Surface treatment sequence. Source: Author.	37
Figure 26 - The ultrasound cleaner. Source: Author.	38
Figure 27 – Sandblasting example. Source: Author.	39
Figure 28 – The sandblasting machine (left) and chamber (right). Source: Author.	39

Figure 29 - Treated samples. Source: Author.....	40
Figure 30 - Marking the bonding area. Source: Author.....	40
Figure 31 – Samples in the alignment mold. Source: Author.....	41
Figure 32 - Cured sample. Source: Author.....	43
Figure 33 - The DIC example. Source: www.limess.com.....	44
Figure 34 - Preparing samples for DIC. Source: Author.....	44
Figure 35 - Air brushing the DIC sample. Source: Author.....	45
Figure 36 - Sample ready for the DIC. Source: Author.....	45
Figure 37 – The DIC analysis model. Source: Modified from Guo, Dillard and Plautc, (2006).	46
Figure 38 - The LaGrange strain model. Source: DILL, (2006).....	47
Figure 39 - Mixed failure mode pattern on SLJ. Source: ISO 10365.	48
Figure 40 - Normal probability. Source: Author.	51
Figure 41 - Residuals vs. fitted values. Source: Author.	52
Figure 42 - Histogram. Source: Author.	52
Figure 43 - Variables main effects over the SLJ FL. Source: Author.....	53
Figure 44 - Overlap length vs. failure load. Source: Author.....	54
Figure 45 - Adhesive thickness vs. failure load. Source: Author.....	55
Figure 46 - Interaction between OL and YS vs. SLJ FL. Source: Author.....	56
Figure 47 - Interaction between OL and AT vs. SLJ FL. Source: Author.....	57
Figure 48 - Interaction between YS and AT vs. SLJ FL. Source: Author.....	58
Figure 49 - Output optimization. Source: Author.	59
Figure 50 - Stress strain curve from AA SLJ. Source: Author.....	60
Figure 51 - Stress strain curve from the dissimilar SLJ. Source: Author.....	61
Figure 52 - Stress strain curve from HSS SLJ. Source: Author.....	63
Figure 53 - DIC analysis of the SLJ with 7mm of OL. Source: Author.....	65
Figure 54 - DIC analysis of the SLJ with 12.5mm of OL. Source: Author.....	67
Figure 55 - DIC analysis of the SLJ with 25mm of OL. Source: Author.....	70
Figure 56 - DIC analysis of AT effect. Source: Author.....	72
Figure 57 – Failure modes of the SLJ: geometric aspects.....	74
Figure 58 – Failure modes of the SLJ: YS aspects.....	75

TABLES LIST

Table 1 – Comparison between joining methods. Source: adapted from Dunn (2003).	6
Table 2 - Bonding vs. welding costs comparison. Source: adapted from Jamestown (2016).	9
Table 3 - Experimental inputs and outputs. Source: Author.	32
Table 4 - Materials mechanical properties. Source: Author.....	33
Table 5 – Bonded joints failure mode classification. Source: ISO 10365.....	48
Table 6 – The experiments results. Source: Author.....	49
Table 7 - ANOVA results. Source: Author.	50
Table 8 - DIC results summary. Source: Author.....	64

ACRONYM LIST

SLJ	Single lap joints
DIC	Digital image correlation
HSS	High strength steel
AA	Aluminum alloy
BMI	Bismaleimide
PI	Polyimide
DOE	Design of experiments
ANOVA	Analysis of variance
OL	Overlap length
AT	Adhesive thickness
YS	Yield strength
RSW	Resistance spot welding
NVH	Noise vibration and harshness
PMMA	Polymethylmethacrylate
AF	Adhesion failure
SCF	Special cohesion failure
ACFP	Adhesion and cohesion failure with peeling
FL	Failure load
DF	Degrees of freedom

SUMMARY

1	INTRODUCTION	1
1.1	Motivation.....	1
1.2	Goals	2
1.2.1	General goals	2
1.2.2	Specific goals.....	2
1.3	Research matters	2
1.4	Limits and restraints	3
1.5	Work organization	3
2	BACKGROUND	4
2.1	Structural adhesives	4
2.1.1	Structural adhesives in the industry.....	4
2.1.2	Structural adhesives advantages and disadvantages	5
2.1.3	Adhesive types.....	9
2.2	Basic definitions	13
2.2.1	Adhesion.....	13
2.2.2	Wetting	17
2.2.3	Cohesion	19
2.3	Joint types	20
2.4	Main loads	21
2.4.1	Tensile shear	22
2.4.2	Tensile.....	23
2.4.3	Peeling	23
2.4.4	Cleavage	24
2.4.5	Torsion.....	24
2.4.6	Bending moment.....	25
2.5	Main geometric variables and mechanical properties.....	27
2.5.1	Overlap length	27
2.5.2	Adhesive layer thickness	28
2.5.3	Adherend yield strength.....	28
2.6	Adhesive curing methods	28
2.7	Surface treatment	29
3	RESEARCH METHODOLOGY.....	31

3.1	Methodology.....	31
3.2	Mechanical characterization	34
3.2.1	Tensile tests apparatus	35
3.2.2	DIC technique	43
3.2.3	LaGrange Principal strains	46
3.2.4	Failure mode analysis	47
4	RESULTS AND DISCUSSIONS	49
4.1	SLJ tensile tests results	49
4.1.1	ANOVA	50
4.1.2	Stress x strain curves analysis of plastic deformation	59
4.1.3	DIC analyses	63
4.1.4	Failure mode analysis	73
5	CONCLUSIONS	77
6	FUTURE WORKS.....	78
	REFERENCES.....	79
	APPENDICES	84
	ATTACHMENTS	89

1 INTRODUCTION

Industries like automotive, aerospace and shipbuilding has materials joining as one of the main fabrication process and it has great influence over important matters, as weight and cost. According to Carle and Blount (1999), the car structure contributes to 25% of the car weight. Nowadays, the pursuit for performance and reduce fuel consumption leads the companies to open up the materials portfolio for others than steel, which is steel the most used material in such industries, according to The Aluminum Joining Manual (2015). The usage of aluminum and other light weight metal alloys, as well as composites and polymers, led efforts to find alternative material joining processes other than resistance spot welding (RSW), which is the main process of metal sheet joining, according to Grant et al. (2009). RSW is well known for its speed and reliability (BAMBERG et al., 2016; BRISKHAM, 2006). However, this process faces many difficulties when it comes to the joining of dissimilar materials and some light weight metal alloys, such as aluminum, mainly due to the high conductivity of aluminum, existence of an oxide film with high fusion temperature (around 2000 °C), as discussed by Pocius (2012). Also, the formation of brittle precipitations while welding it is an obstacle, as stated by Coelho et al. (2012). In order to overcome these problems, the automotive industry started using adhesives in structural and non-structural applications as an alternative of conventional welding processes to join light weight structures and dissimilar materials. As output some benefits other than weight downsizing were granted, for example: better crash test performance, noise, vibration and harshness (NVH) characteristics, improved fatigue and corrosion resistance, unconventional mechanical properties combinations and joints sealing (POCIUS, 2012; BARTCZAK, MUCHA and TRZEPIECINSKI, 2013).

1.1 Motivation

Facing the current industrial context of Brazil, in which opportunities for innovation and development are constantly pursuit, the adhesive bonding process as an alternative for certain conventional welding takes place. It is already being used largely at the European automotive and aircraft industries and can deliver several advantages. Particularly, the use of light weight material in automotive and aircraft

structures opens a very interesting range of innovation opportunities, since it faces challenges for dissimilar joining. The durability, mechanical behavior and properties of such kind of joint motivated an investigation about the stress state and main variables of the single lap bonded joints. In addition, the technological gap between the Brazilian and the European industries can be shortened as result from collaborative researches. The current one is one example of collaborative work between SENAI CIMATEC, in Brazil, and ISF RWTH, in Germany, with the purpose of approximate both research institutes.

1.2 Goals

1.2.1 General goals

Study the adhesive bonding method as an alternative for sheet metal joining and understand the effect of the main variables over determined mechanical properties of single lap joints (SLJ).

1.2.2 Specific goals

- To study the effect of the overlap length, adhesive thickness and material yield strength over the SLJ FL;
- To analyze the stress state of SLJ under tensile stress load;
- To understand the influence of plastic strain at the adherends over SLJ FL;
- To perform a business case of the costs associated to the AB technique in comparison with a conventional joining method in a similar application of this work.

1.3 Research matters

Despite the fact that there are several works developed about adhesive bonding subject, SLJ and mechanical characterization of it, there are still several opportunities of development inside the fields of dissimilar material joining, variables effects over FL and stress state of such joints. Most of the researches include high strength adherends, which provides a stress state free of plastic deformation. Further, several works study the bonded joints mechanical characterization under shear stress

condition. Yet, to study the joining of dissimilar materials through adhesive bonding is still not very common. Finally, the use of digital image correlation in this research characterizes an innovative method that not only provides better precision over mechanical tests data, but also analysis of the behavior of the samples when submitted to it.

1.4 Limits and restraints

The results found in this research as well as the discussions are limited to the use of compatible metallic sheets of aluminum and steel joined by structural adhesive of epoxy. Also the variables, samples preparations method and general conditions must be observed for comparable studies purposes.

1.5 Work organization

This work is composed by three main sections named “Background”, “Research Methodology and Techniques” and “Results and Discussions”. The first section starts with the introduction of bibliography research supporting the subject, describing the important definitions, components, aspects, variables, inputs and outputs of the current study. The second section scrutinizes the experimental program adopted in order to fulfill the determined goals. It covers the definition of the variables, test array, main aspects of the used standards, samples preparation and methodology. The final section presents the results, discussing the effects of the proposed variables over the SLJ FL and bringing other authors works results for matters of comparison.

2 BACKGROUND

2.1 Structural adhesives

Adhesive is a general term that includes materials such as cement, glue and pastes. Polymeric adhesives consist of polymers that are able to develop forces of adhesion in solid surfaces allowing stiffness to the formed joint. According to Pocius (2012), the use of adhesives is described in the ancient Egypt, found in recipes that explain how to prepare it from clay, linseed and iron dust. By that period the adhesives were used as joining method for roof tiles, bricks and other construction applications, which had no safety or design requirements. However, in the beginning of the 20th century, the development of polymeric adhesives had a great improvement due to the synthetic and chemical preparing methods. Da Silva et al. (2011) and Grant et al. (2009) describe structural adhesive as an adhesive that can resist substantial loads and is responsible for the strength and stiffness of the structure. In another study, Hussey and Wilson (1996) state that the structural adhesives must perform a significant load bearing function within their designed application lifetime.

The structural adhesives started to be used as structural joining method in the aircraft industry, about the year of 1950, as an alternative or reinforcement of riveted metallic plates, according to Kinloch (1987). Currently, the automotive makes large use of adhesives both for structural and nonstructural reasons, as described in the introduction of this work. That demand, initially, took place due to the fact that adhesive bonding does not make use of any heat input and thus reveal great capacity to join dissimilar materials (THE ALUMINUM JOINING MANUAL, 2015). According to Kinloch (1987), adhesive bonding is a material joining process in which a structural adhesive material is placed between solid surfaces, called adherends, joining it.

2.1.1 Structural adhesives in the industry

The application of aluminum alloys in automotive structures, despite the presented difficulties, keeps growing. According to CARLE and BLOUNT (1999), the percentage in weight of the total aluminum used in a vehicle exceeds 10%. “The key

enabler for the use of aluminum in automotive applications proved to be the series application of non-heat involving joining techniques like mechanical joining and adhesive bonding” (THE ALUMINUM JOINING MANUAL, 2015). In 2001, the usage of structural adhesives in cars was of about 10 meters. Currently, over 150 meters of bonded joints is used in the construction of the car body, according to Adhesives.org (2015).

Despite this is a not new joining method, the aircraft industry started using adhesive bonding in the middle of the last century and in the last 30 years the automotive industry started to use it with great emphasis as an alternative to more traditional joining methods, as resistance spot welding, screws and rivets (POCIUS, 2012, p.7).

That action enabled several kinds of materials to be used in car bodies and structures, configuring multi material joints, such as dissimilar metals panels, as well as combinations between metals and polymers or composites. As result, it was possible the combination of different mechanical properties, weight reduction associated with high structural stiffness, better fatigue resistance, improvement of noise, vibration and harshness attributes, and others. Adhesives are stronger under shear, compression and tension loads, but perform less efficiency under peel and cleavage loading (XU et al., 2013).

2.1.2 Structural adhesives advantages and disadvantages

Adhesive bonding, such as any joining method, have its advantages and disadvantages. Some of the main known advantages are the high shear strength, possibility of dissimilar material combination, linear stress distribution and lack of heat input, (HER, 1999). The main disadvantages are high temperature limitations, adhesive cure time and surface preparation (POCIUS, 2012). The Table 1 presents some comparisons about the vantages and disadvantages of adhesive bonding when compared to conventional welding methods, such as resistance spot welding.

Table 1 – Comparison between joining methods. Source: adapted from Dunn (2003).

Comparison of assembly methods for metals					
	Adhesive bonding	Mechanical fastening	Arc welding	RSW	Riveting
Joint stresses	Excellent	Bad	Fair	Bad	Bad
Fatigue resistance	Excellent	Fair	Fair	Bad	Good
Dissimilar materials	Excellent	Good	Bad	Bad	Good
Joint preparation	Fair	Fair	Good	Excellent	Fair
Temperature resistance	Fair	Excellent	Excellent	Excellent	Excellent
Joint appearance	Good	Bad	Fair	Bad	Bad
Production speed	Fair to Good	Bad to fair	Excellent	Excellent	Excellent
Materials costs	Good	Bad	Good	Good	Bad
Operating costs	Good	Fair	Bad	Fair	Fair
Capital costs	Good	Good	Bad	Bad	Good

Da Silva et al. (2011) state that currently it is difficult to imagine a product that does not use adhesives or sealants in some manner, including home, industry, transportation or any other application field. When it comes to lightweight alloys, multi-material and multi-metal joining, some factors should be considered. The use of AA in industries like the automotive has been growing during the last years. It grew from 83kg in 1991 to 113kg in 1999 per vehicle, according to Dunn (2003). Recently, the use of AA in lightweight vehicles is of about 151kg, with a projection of 200kg in 2025, according to European Aluminum (2016). AA are 60% lighter than an equivalent iron and steel alloys structure in terms of mechanical properties. Another alternative for mild steel in automotive industry was the high strength steel (HSS) that has surged in the early 2000's as an alternative for body in white vehicles structures. Currently, nearly 50% of a car body mass is made up of HSS, (BENEVENTO, 2015). Using both materials, however, present challenges with conventional joining methods, such as RSW, arc welding and rivets. When it comes to multi material joining, such methods present problems like galvanic corrosion and microstructure incompatibility. In case of aluminum joining, the problems can vary from a high energy input, bad microstructure and unfeasibility, (COELHO et al, (2012); BRISHKHAM et al., (2006)).

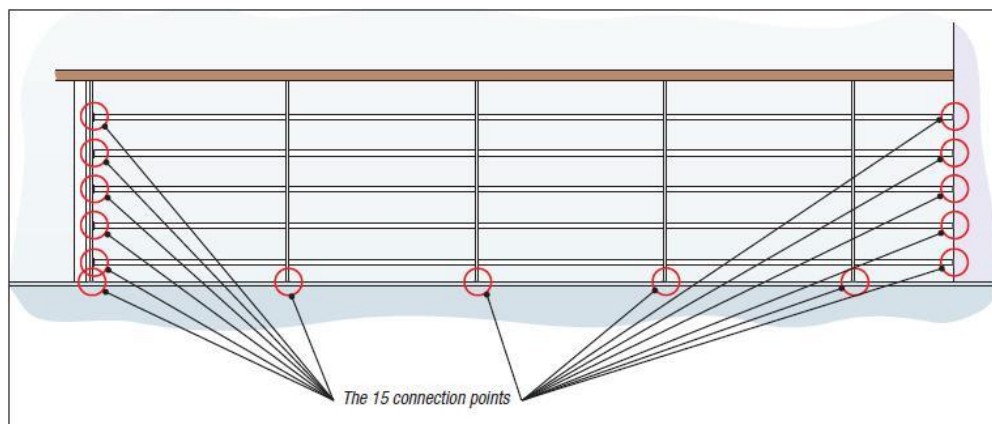
The structural adhesives surged as an enabling technology for the joining of such materials, according to Benevento, (2015) and The Aluminum Advantage (2015). A deeper look in the advantages presented in Table 1 brings attention to joining of

dissimilar materials and possibilities of cost reduction. This last advantage is one of the most desired improvements of industries like the automotive, shipbuilding and others. So, a case of study about design change and its effect over cost is presented below.

2.1.2.1 Adhesive bonding case of study – cost management

The cost of an adhesive bonding as well as other joining processes (such as RSW) is theme of discussions. Briskhan (2006) includes spends with energy, maintenance, consumables, equipment and labor to calculate the overall RSW cost for an automotive application. For an adhesive process it is not straight forward to compare such costs because of different basis of comparison, lack of financial comparisons and information from industrial cases of study. However, the company Sikaflex performed a practical cost comparison between using adhesive bonding and arc welding to join a marine structure, (JAMESTOWN, 2016). It was design change about the joining of a rail segment to the deck of a boat. The structure is shown in Figure 1.

Figure 1 - Case of study: The rail segment design change. Source: Jamestown (2016).



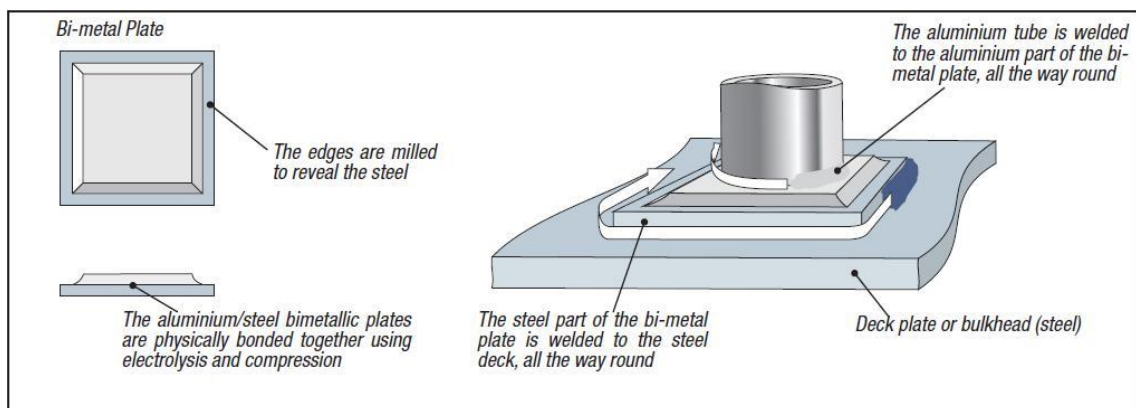
The rail segment is composed by multi materials, such as hardened plastic, wood, steel and aluminum. The traditional design of joining this structure was described by Jamestown (2016) as follows:

Using traditional methods, welding aluminum to steel requires the use of specially made bimetal plates that are costly and difficult to manufacture. First of all, the two metals must be bonded together

using compression rolling and electrolysis. Then the edges of the aluminum need to be milled away to expose the steel, enabling the plates to be welded to the steel deck. The aluminum tubes are then welded onto the aluminum side of the plates. The complete process must be carried out with care to ensure a quality finish, (JAMESTOWN, 2016).

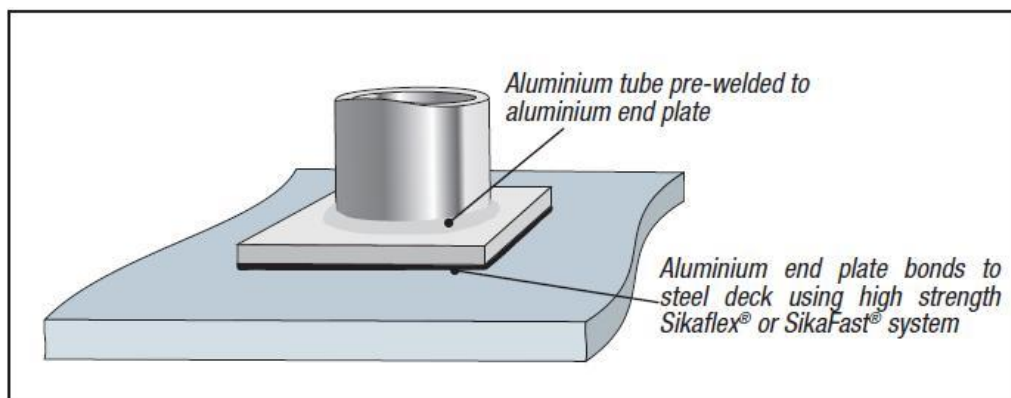
An overview of this joining process is shown in Figure 2.

Figure 2 - Rail segment design (before). Source: Jamestown (2016).



Joining this structure using adhesive bonding method in this case helped to simplify considerably the joining process due to the ability of the structural adhesive to join dissimilar materials, as well as bond and seal in a single process. The result of this design change is shown in Figure 3.

Figure 3 - Rail segment design (after). Source: Jamestown (2016).



This design change encompassed a cost saving of approximately 66%, as it is shown in Table 2. Other aspects as mechanical properties, weight, corrosion resistance and other positive attributes of the structural adhesives were not considered in the study but also have positive impacts.

Table 2 - Bonding vs. welding costs comparison. Source: adapted from Jamestown (2016).

Bonding *costs			Arc welding *costs		
		Cost			Cost
Material (Structural adhesive)		57	Welding material		
Working time	Time	Cost	14 bimetal milled plates		139
Cleaning and ventilating	20	11	Weld material for 5.24m		49
Grinding bonding surface	30	17	Working time	Time	Cost
Cleaning and ventilating	20	11	Positioning, adaptation and fixing	300	165
Primer application	30	17	Welding the crossways	150	83
Adhesive application	30	17	Welding the pillars	90	50
Positioning and bonding	60	33			
Overall time taken	190	106	Overall time taken	540	298
Total cost		163	Total cost		486

*Values in dollar.

The adhesive bonding method helped to reduce the number of individual components of the structure and encouraged a modular approach. The discussed results of this design change were about saving in process time and cost. However, it can be extended to weight reduction, as more AA parts were included in place of steel, better corrosion resistance, as structural adhesives have the ability of reducing galvanic corrosion by isolating dissimilar materials from salt bridges, and provide excellent fatigue properties, according to Dunn (2003).

2.1.3 Adhesive types

Currently, there are several types of adhesives available in the market, which can be classified in different ways, as the intended application and chemical base, for example. One section of these applications is the structural adhesives, explained in the introduction of this work. The structural adhesives also differ from many aspects, as chemical composition, curing method, mechanical properties and recommended application that can cover from packing to automotive or aircraft industry. This work is focused in the structural adhesives applied on metal sheet adherends with medium

and high strength. Inside that field, some of the main adhesives are presented within its characteristics in the next topics, according to Hussey and Wilson (1996) classification.

2.1.3.1 Epoxy

The epoxy adhesive, which was used in this work, is often used when the application requires high shear strength and endurance, as in the automotive, aircrafts and shipbuilding industries. Among its characteristics, the epoxy adhesives have good adhesion to several types of surface and substrates, a wide range of high mechanical properties and several ways of curing methods. For many years, they have dominated the high-performance adhesives market, but the desire for increased service temperatures has led to the development of new adhesives based on imide polymers (e.g.: PI and BMI). Usually the epoxy resins start to lose properties within 30°C above the curing temperature limit (around 150 °C), which is common for some automotive engine application and aircraft fuselages, (POCIUS, 2012). The cure of epoxy adhesives, according to Hussey and Wilson (1996), may have a range of curing temperatures, from room temperature up to round about 175 °C. The epoxy adhesives are available as pastes (one or two-part) or films.

2.1.3.2 Imide

Hussey and Wilson (1996) describe that the term “Imide” is used to group together BMI and PI adhesive composites. Both are classified as high temperature limit adhesives, which are higher than those based on epoxy resins. BMI has a temperature capability of about 230 °C, excellent electrical properties, not high peeling resistance and polymerization method involving addition reaction. PI has a temperature limit up to 300°C and it also excellent electrical properties. Its polymerization method can be done by addition or condensation method. The addition consists in a polymerization reaction that hardens the adhesive by bonding together monomers via rearrangement of links. No water or atom is lost during the curing process. The condensation, however, is a polymerization reaction in which the adhesive hardens when molecules join together by losing water during the curing. Both reactions involve application of temperature and pressure, (POCIUS, 2012).

2.1.3.3 Acrylic

Acrylic adhesives have been used to join several materials as plastic, ceramic and metal as deliver a secure bond between oily or contaminated surfaces. This kind of adhesive also gives improved aesthetics. However, acrylic adhesives are known for some questionable aspects as they high levels of odor, that could cause health concerns, longer set times that slow assembly processes, lower impact resistance, that result in brittle bonds, and limited shelf life. Currently, studies are being performed in order to improve the quality and performance of this type of adhesive, providing characteristics as high overlap shear strength and high impact resistance increasing the industrial applicability requesting less surface preparation. The curing of acrylic adhesives includes chemical agents, which can be mixed with the adhesive or applied at the adherend prior to bonding, ultraviolet light application or electron-beam radiation. Structural applications of acrylic adhesives can be found at computer, cars manufacturing, aircrafts and wood work industries.

2.1.3.4 Anaerobic

The anaerobic type of adhesive is commonly used on metallic components filling gaps and voids, increasing the sealing and clamp load of bolted and riveted joints. It also prevents losses caused from vibration besides protect the joint from corrosion and rust that can result from moisture. According to Hussey and Wilson (1996), one of its main features is that they cure rapidly in the absence of oxygen to produce strong bond. The anaerobic adhesives also have a good chemical resistance to a variety of substances, for example oils and solvents.

2.1.3.5 Cyanoacrylate

Cyanoacrylate adhesives started to be used in the middle of last century. It was known, by the time, for their brittleness, leading to poor tolerance to impact, peel, heat and thermal cycling. Furthermore, it had lot of problems of curing and pungent odor. According to Hussey and Wilson (1996), many of these issues are now solved due to modifications in the formulations. For example, the addition of surface activating agents has reduced the cure sensitivity. Additions of rubber polymers also toughened cyanoacrylates, improving significantly its mechanical properties. This

adhesive is not recommended when an application with creep resistance is required, (POCIUS, 2012).

Currently, cyanoacrylates adhesives are used to joining small parts, particularly in commercial and domestic applications where an 'instant' bond is needed, avoiding the need for clamping or heating.

2.1.3.6 Polyurethane

Polyurethane structural adhesives are formulated by the addition of polyols and isocyanates. This type of adhesive is known not for high strength of shear modulus, but for its high capability to absorb mechanical energy, such as noise and vibration (damping characteristics). Also, this type of adhesive offers certain flexibility associated with a modest level of mechanical strength, of about 7 to 14 MPa, according to Pocius (2012). Other features which polyurethane adhesives are known for are the good adhesion to a variety of adherends, good chemical resistance to oils and solvents and availability in many ways, such as pastes, films and powders, according to Hussey and Wilson (1996). On the other hand, its application relies on previous mixing and bringing it to molten state with the use of heat input if needed. Its curing methods depends on the type of polyol and cyanate, which can involve the application of a catalyst or temperature-based curing, which range from room temperature.

2.1.3.7 Phenolic

Phenolic structural adhesives are polymers formed by the reaction of phenol and formaldehyde. This structural adhesive is used in wood products, for bonding abrasive materials in tools (such as grinding discs and sand papers), as binders for molding sands and for friction components (such as brake linings, clutches and automatic transmissions composites). It can also be used in fiber-reinforced composites been used with all major types of reinforcing materials, according to Hussey and Wilson (1996). The main features of this type of adhesive are high mechanical strength, good solvent and water resistance, high thermal stability and flame retardant. Pocius (2012) describes some limitations like relevant atmospheric

pollution and low shelf life, being necessary to keep it under low temperature to retard premature cure during storage.

2.1.3.8 Hot melt

Hot melt adhesives are classified as thermoplastic which requires heating in order to melt the polymer prior to bonding. Since 1950, several different types of thermoplastic polymers were developed with different properties and providing a wide range of potential hot-melts, including adding tackifiers to promote adhesion and waxes to reduce viscosity and costs. Hussey and Wilson (1996) report some characteristics of the hot melt adhesives like rapid setting times, easy adaptation for specific applications, ease of use (easy application and/or automation), long term stability, which requires no special storage conditions, and availability in many shapes and forms, as pellets, film, powder or cylinders.

The hot melt adhesives are split in low performance and high performance. The first is mostly applied packaging, textiles and furniture. The second is often applied for metal and glasses bonding, like windshield joining.

2.2 Basic definitions

The adhesive bonding is based in the main forces of adhesion and cohesion, as well as the property of wettability. These three principles, which have high influence over bonded joints main mechanical properties, will be discussed in the following topics.

2.2.1 Adhesion

Adhesion is defined as the state in which two surfaces are held together by interphase forces, according to the standard ASTM D907. Pocius (2012) describe it as the capacity that the adhesive has to distribute an applied load over the solid bonded surface of the adherend. The adhesion phenomenon relies in some main theories, such as adsorption, electrostatic, diffusion and mechanical interlocking. Despite no one of them can describe the whole adhesion phenomenon or predict perfectly the mechanical properties of an adhesive bond, these classic theories emphasize different aspects of a more comprehensive adhesion model, regarding

from molecular disposition in the region of interest, to macroscopic properties of an adhesive joint, according to Da Silva *et al.* (2011).

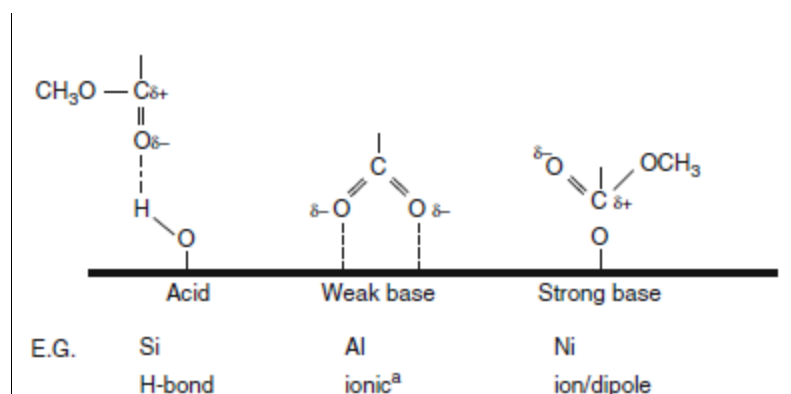
2.2.1.1 Adsorption theory

The adsorption theory can be first recognized in the initial moment of the bonding, when the adhesive and the adherend get in contact. At this moment, forces of attraction are created between them and the adhesive will spread over the adherend. Both are dependent on the chemical nature of the material surfaces, on the intensity of these forces and the level of wettability, which is explained further in this work. This is an important moment at adhesive bonding process since it is when the primary bonding forces surge, which can be identified as primary covalent forces and secondary Van der Waals and dipole-dipole forces. These forces must be sufficient to resist high bond strength and durability within hostile environments, according to Da Silva *et al.* (2011).

The adsorption theory is mostly related to molecular interactions. “The essential idea of the adsorption theory of adhesion is that whenever there is contact between two materials at a molecular level, there will be adhesion”, (DA SILVA *et al.* (2011)).

Leadley and Watts (1997) did an experiment to analyze the molecular bonding of PMMA and oxidized surfaces of metal or silicon, by using adhesion promoters to bond epoxy to metal and glass adherends, using X-ray photoelectron spectroscopy. Evidences of hydrogen links, ionic links and ionic-dipole interactions were found, as it is illustrated in Figure 4, which indicates the adsorption theory primary links and plays significant role by enhancing the bond strength, according to Da Silva *et al.* (2011).

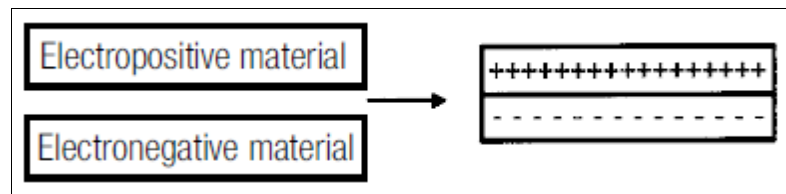
Figure 4 - PMMA molecule overview. Source: Da Silva *et al.* (2011).



2.2.1.2 Electrostatic theory

The electrostatic theory, explained by Da Silva et al. (2011), is based in the fact that free charges exist in any condensed material, even in the best dielectrics, and there will always be an electromechanical potential difference across the interface between two materials in contact, such as the adhesive and the adherend. That electronegativity difference of the materials will lead the adhesive bond due to the transfer of charge from an electropositive material to and electronegative material, as illustrated in Figure 5.

Figure 5 - Electrostatic bonding example. Source: Pocius (2012).

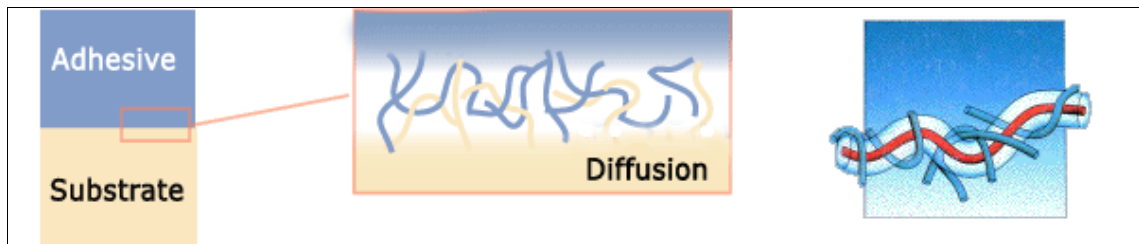


A solid surface can, however, be characterized as electropositive or electronegative if the static energy at the surface is considered. According to Pocius (2012), in terms of adhesion science, it can be said that surfaces electropositive in character are bases and surfaces in electronegative character are acids.

2.2.1.3 Diffusion theory

The diffusion theory is mostly related with the adhesion of polymers as adherends. Da Silva et al. (2011) describes the theory as an interdiffusion between the molecules of two compatible materials (i.e. the adhesive and adherend) in such way that the interface becomes diffuse and disappear, configuring a bond between the polymeric chains of both materials at the contact area. Pocius (2012) describes it as the situation in which two soluble materials are put in close contact. The result is a diffusive bonding, creating an interphase with no longer true interface, with a gradual change of mechanical properties from one material in the other. Both descriptions converge, as they state the creation of an interphase between both materials and elimination of a real boundary. Figure 6 illustrates it.

Figure 6 - Diffusion bonding. Source: Adhesive and glue (2016).



As stated before, for a diffusion bonding to successfully happen, both materials must be soluble (or compatible). Da Silva et al. (2011) state the criterion for the spontaneous formation of a solution based in the sign and magnitude of the Gibbs free energy theory. This is represented by Eq.1, which should be positive or zero for a solution to be formed. The Gibbs free energy of mixing ΔG_m is related to the enthalpy (heat) of mixing ΔH_m and entropy of mixing ΔS_m by the usual second Law equation”:

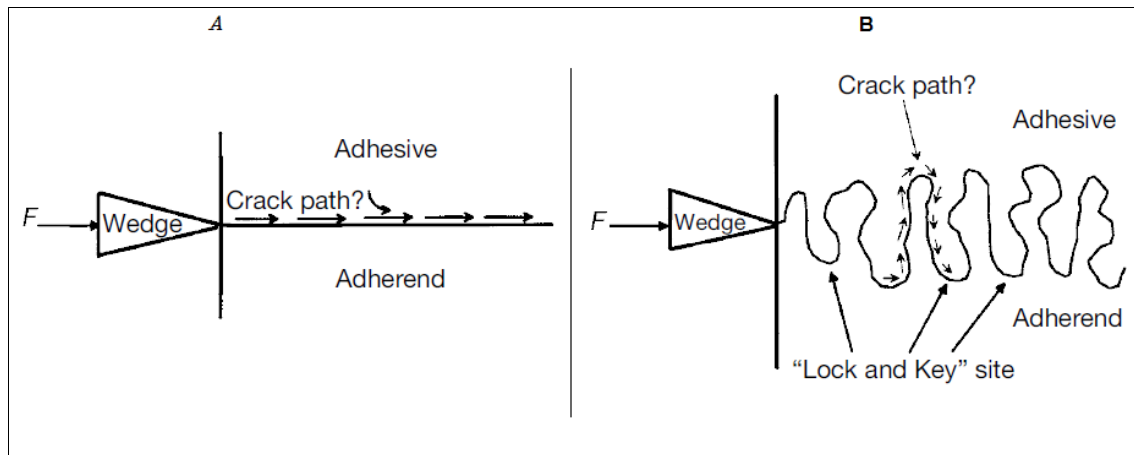
$$\Delta G_m = \Delta H_m - T * \Delta S_m \quad (1)$$

Where T is the absolute temperature. As mixing always increases disorder, ΔS_m is positive, it follows that the $- T\Delta S_m$ term is always negative, and therefore favors mixing. However, where polymers are involved, the long chain molecules mean that the entropy gain is much smaller than when compounds with small molecules are mixed. The term “T x ΔS_m ”, although negative, tends to be small in magnitude.

2.2.1.4 Mechanical interlocking theory

The mechanical interlocking along with adhesive cohesion are the main reasons that provide strength to adhesive bonding at materials that are impermeable to the adhesive, such as metals, according to Pocius (2012). The Figure 7 represents how this adhesion phenomenon works. Supposing that a wedge is pressed against the edge in which adhesive and the adherend are joined together it starts to propagate a crack between these two materials. In the left size of Figure 7, a crack propagates over a flat adherends surface that does not offer physical barrier to the crack path.

Figure 7 – Mechanical interlocking. Source: Pocius (2012).



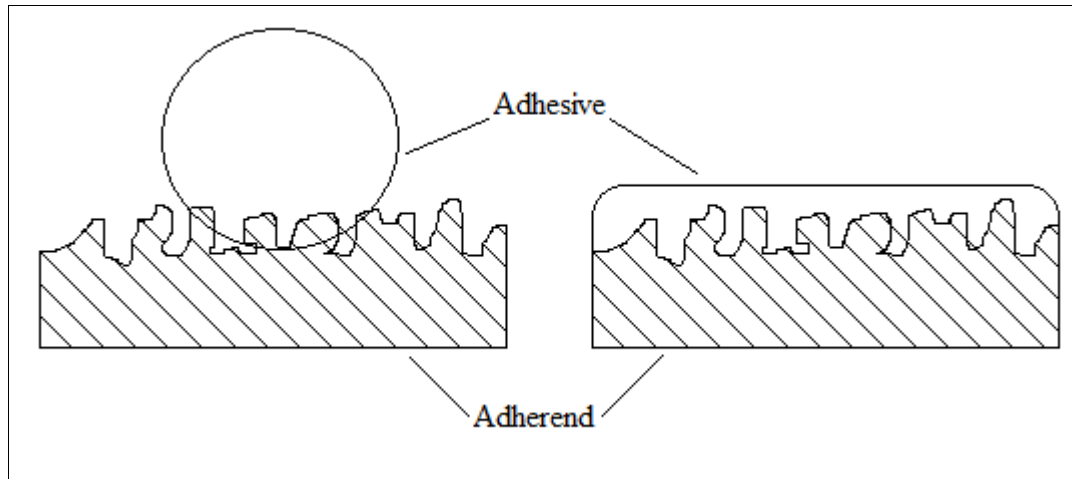
In the right side, the adherends surface is rough and the hardened adhesive fills up the crevices of it. In that second case, for a crack to propagate, it must go through the way indicated by the small arrows in Figure 7, which is a considered a tortuous way by Pocius (2012). The crack needs constantly to change its direction, which reduces the energy state of the strain. This pair composed by the hardened adhesive and the threads of the prepared adherend also configures a barrier for the movement of the strain, known as “locking and key” effect. For the applied load to continue both adhesive and adherend should deform plastically, which also consumes energy, according to Pocius (2012). Da Silva et al. (2011) complements the mechanical interlocking theory by adding that rough surfaces provide higher adhesion, however it relies in good wetting of the adhesive over the adherend. The good contact between the adhesive and the adherend will avoid the presence of voids and, in consequence, stress concentrators, what would decrease the strength of the bonded joint. Wetting is further explained in the next topic.

2.2.2 Wetting

For a good adhesion to take place, the adhesive and the adherend must come to an intimate contact, according to Pocius (2012). A prerequisite for a good adhesion is that the adhesive is able to reach most of the adherends surface, which is not uniform and composed by several crevices and peaks. To make it happen, a good wetting property is required, so the adhesive can spontaneously spread over the adherend surface, reaching as maximum bonding area as possible and minimizing or

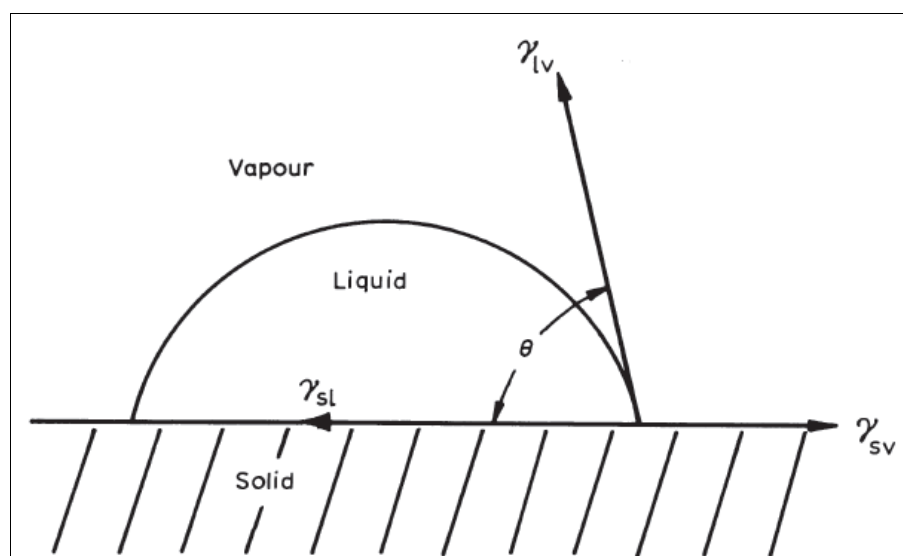
eliminating voids and empty points. This phenomenon is illustrated in Figure 8, where the case in the left side shows a bad wettability situation and in the right side a good wettability case.

Figure 8 – Wetting and dewetting examples. Source: Author.



According to Da Silva *et al.* (2011) and Adhesive and Sealants Council (2015), wetting is the ability of liquids to form interfaces (contact) with solid surfaces. This can be determined measuring the angle of contact (θ in Figure 9) between the liquid and the solid surface, as it is shown in Figure 9.

Figure 9 – Contact angle of a liquid over a surface. Source: Kinloch (1987).

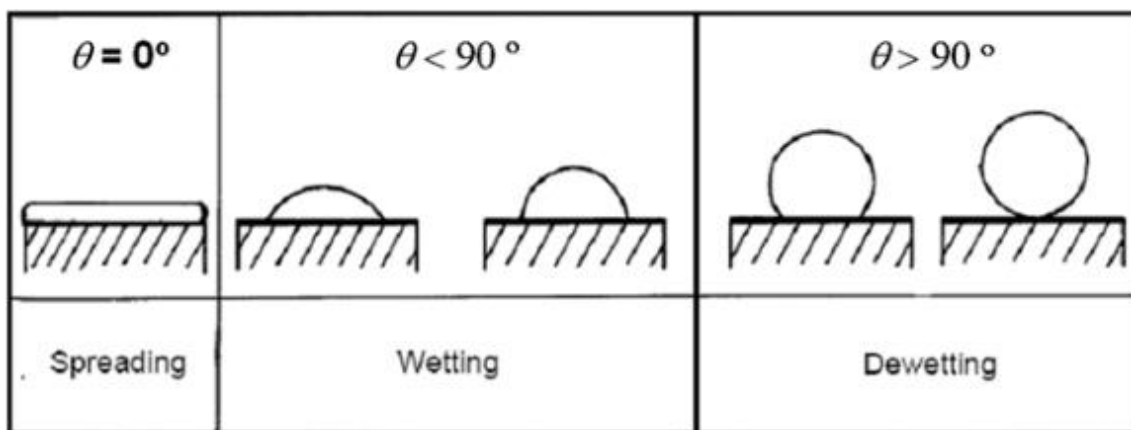


The lower the angle, the more the liquid will spread over a solid surface, which allows a better adhesion from the adhesive to the adherend. The other way around tends to concentrate the adhesive without great contact of the adhesive on the surface of the adherend, increasing the contact angle, which is worse for the adhesion. For the wetting to occur, the surface free energy of the adherend must be higher than of the adhesive, according to Kinloch (1987). To calculate it, is it possible to use the Eq.2, known as Young's equation.

$$\gamma_{sv} = \gamma_{sl} + \gamma_{lv} * \cos(\theta) \quad (2)$$

In the Eq.2, which encompasses the tensions at the three-phase contact point, γ_{sv} represents the surface free energy of the solid adherend in vapor, γ_{sl} is the tension of the solid/liquid point and γ_{lv} the tension on the liquid/vapor point. The contact angle (θ in Eq.2) can be measured in the equipment called goniometer, which records the moment in which a liquid drop reaches a solid surface. According to Da Silva et al. (2011), the range of possible angles vary from $0^\circ \leq \theta \leq 180^\circ$, which relates to wetting and contact angle as shown in Figure 10.

Figure 10 - Contact angle vs. wettability. Source: Adhesives.org (2015).

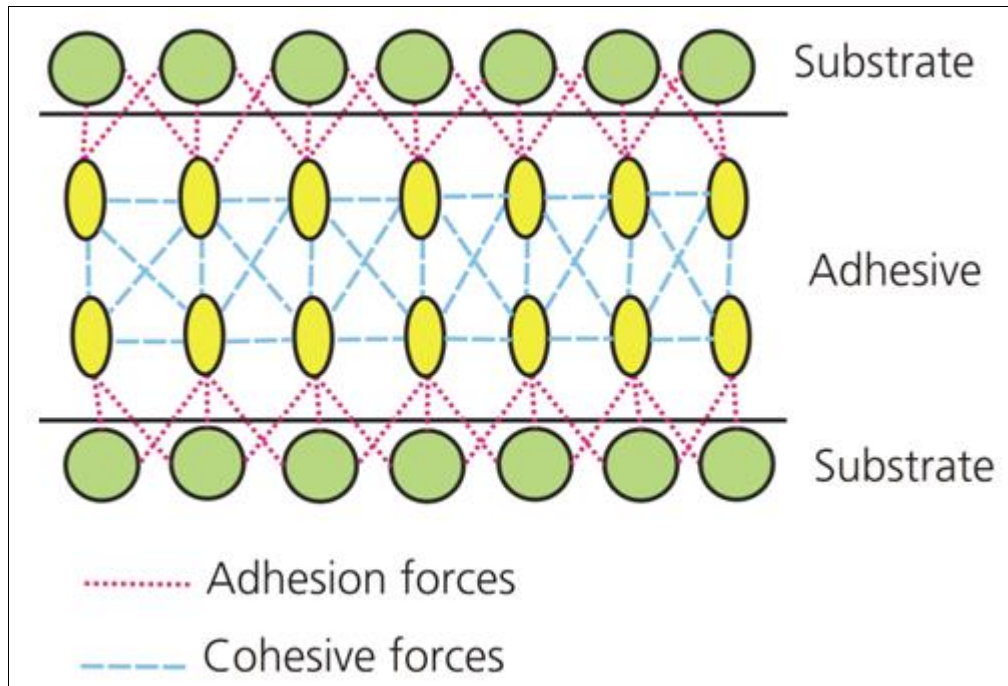


2.2.3 Cohesion

While adhesion is related to the surface interactions between the adhesive and the adherend, cohesion is related to the internal strength of the adhesive. It is based on its chemical bonds and links of the adhesive polymeric base, according to Adhesive

and Sealants Council (2015). Figure 11 illustrates the scheme of a bonded joint and the actuation of both adhesion and cohesion forces.

Figure 11 - Adhesive bonding main forces. Source: Adhesives.org (2015).



The properties of cohesion of an adhesive are based in four cohesive forces: a) the chemical bonds within the adhesive polymers; b) the chemical bonds resulting from crosslinking of the polymer; c) the intermolecular interactions between the molecules in the adhesive, and d) the mechanical adhesion between various molecules in the adhesive.

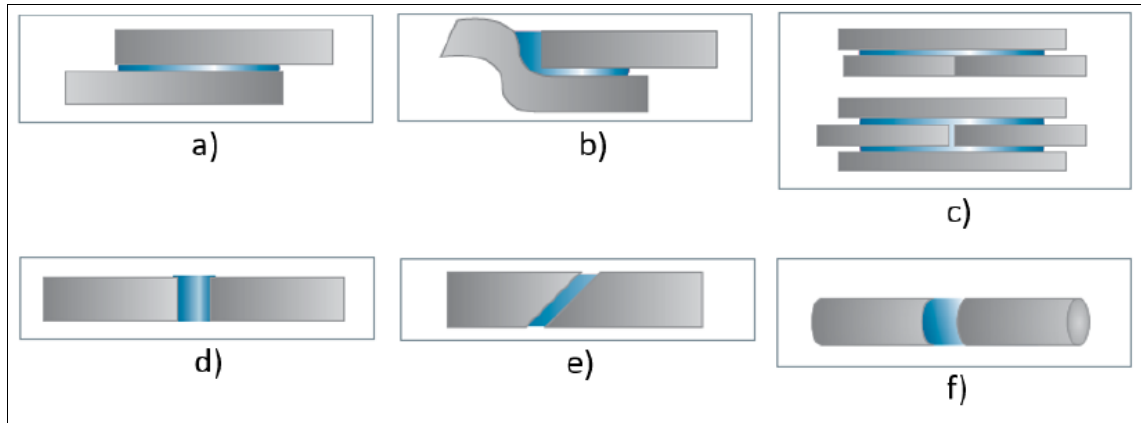
Together, adhesion and cohesion play important role in the strength of a bonded joint and the weakest link will probably determine the amount of load that such joint can tolerate.

2.3 Joint types

The adhesive bonded joints can be set in several ways, depending on the type of loading, desired mechanical properties, resistance to a specific phenomenon and others. Known as joint design, the main difference is the disposition of the adherends and adhesive, however great effect can be acquired from that and the cost and assembly time and efficiency can vary a lot. The adhesive joint must be selected and

prepared to use the structural adhesive best characteristics, such as high resistance to shear, tension and compressive loads, avoiding high incidence of peeling and cleavage stresses. Figure 12 presents the some of the most common types of bonded joints.

Figure 12 - Main adhesive bonded joint types. Source: The Aluminum Joining Manual (2015).



According to The Aluminum Joining Manual (2015), the bonded joints illustrated in Figure 12 are known as: a) single lap (overlap) joint; b) offset lap joint; c) strap joint (single or double), which is a combination of overlap and butt joint; d) butt joint; e) scarf joint (angular butt joint) and; f) cylindrical butt joint. In this work, it was selected the single lap joint (SLJ), due to the fact that it makes usage of the better mechanical properties of the structural adhesives (shear strength – further explained in the next sections), to its simplicity and large usage in the industry. According to Da Silva *et al.* (2009), the SLJ is the most common and used adhesive joint. In addition, this kind of joint has simple design rules, well established standards and high resistance to shear load. More information about the joints geometry, specifications and variables are presented in the following sections and in the methodology section of this work.

2.4 Main loads

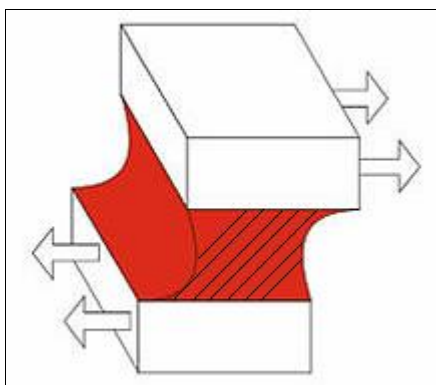
As discussed in the previous topic, the adhesive joints must be designed accordingly with the type of load and other aspects. The SLJ is supposed to receive tensile load at its ends, which submit the adhesive layer to a shear load stress state and also generates secondary stresses known as peeling forces. The pure shear load state is the theoretical condition in which the SLJ can develop its full strength, according to

Da Silva et al. (2009). However, due to the misalignment between the joint center line and the stress transfer line, bending moment is generated through the joint, which is a problem because it generates secondary normal forces of peeling over the bonded area. The edge of the bonded area is the critical part of it and is the point where the peeling forces have higher intensity, being this the principal aspect that leads SLJ to fail, Silva and Nunes (2014). Below it is presented the main resulting stress states of the SLJ when submitted to tensile load:

2.4.1 Tensile shear

As discussed before, the tensile shear stress state is the one in which the SLJ have its best strength, due to the fact that the adhesive can develop its full shear strength, according to Pocius (2012). Figure 13 illustrates this condition of loading.

Figure 13 - Tensile/Shear load condition. Source: Nashett (2015).



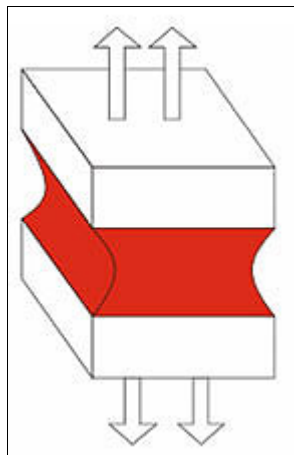
When both ends of the single lap joints are under tensile load (arrows in at the edges of the adherends), the adhesive layer tends to resist to such load being submitted to a shear load condition in consequence to the first. In that case, basically, the whole bonded area is under stress, resisting to the displacement resulted by the load, providing the best strength to the joints. The adhesion forces hold both adherends and the cohesion forces resist the applied load based in the huge amount of polymeric links and bonds (discussed in previous topics) of its composition. Most bonded joints are set to resist this type of load, since it is the most efficient way to design such joints, according to Hussey and Wilson (1996). The pure shear state is the condition in which overlap joints present the highest strength, but it is a very difficult stress state to reach in SLJ, due to the load transfer characteristics. However,

there are ways to help the joint to keep a close to pure shear state, enhancing its strength. i.e.: set SLJ with short overlaps, thin adhesive thickness layers and high yield strength adherends.

2.4.2 Tensile

The tensile type of loading occurs when the bonded area is stressed in the perpendicular direction of the overlap length, as it is shown in Figure 14. According to Hussey and Wilson (1996), the strength of the joint to this kind of loading relies mainly in the adhesion forces from the adhesive to the adherend, which relies heavily on the surface treatment of the latter. This arrangement can be negatively influenced by peeling stresses when the adherends present distortion or strain. In this case, thicker or stiffer adherends are recommended to enhance the strength of the bonded joint.

Figure 14 - Tensile load condition. Source: Nashett (2015).

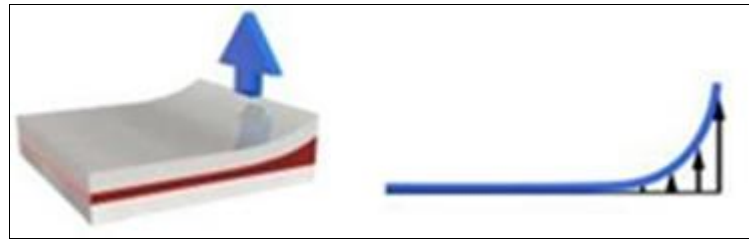


2.4.3 Peeling

Resistance to peeling stresses is one of the lowest strength of a structural adhesive (HUSSEY AND WILSON, 1996; Da SILVA et al., 2009; SILVA and NUNES, 2014; POCIUS, 2012). Peeling stresses is a consequence of the bending moment and is also related with plastic strain at the adherends. It results from the application of a tensile load at the adherends of an overlapped joint and provokes a displacement in the vertical direction of the SLJ, as presented in Figure 15. The applied load is resisted by a very narrow part of the bonded joint, leading it to a fast propagation of

cracks or wedges. Great part of incidence of failures of SLJ loaded in tension are result of peeling stresses generated at the edges of the overlap, which quickly propagates cracks through the bonded area, in such way that most of the adhesive layer is not under load, (NASHETT, 2015).

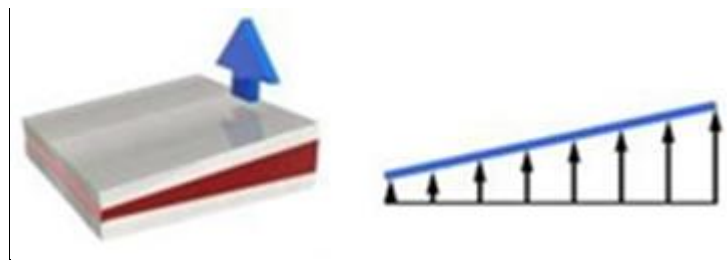
Figure 15 - Peeling stress on a bonded joint. Source: Plastech (2011).



2.4.4 Cleavage

Like the peeling stress, the cleavage loads bring the bonded joints to a very inefficient or fragile condition. However, the cleavage load results from perpendicular forces applied to the edges of rigid adherends without encompass relevant plastic strain. The edges of the bonded region resist more load than the rest of it, creating stress concentrators, (HUSSEY AND WILSON, 1996).

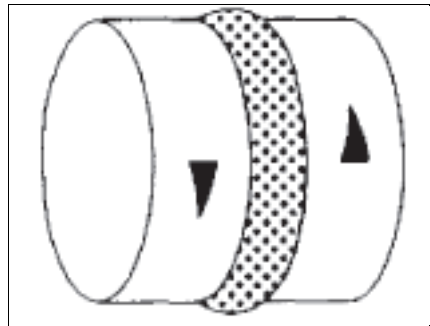
Figure 16 – Cleavage load condition. Source: Plastech (2011).



2.4.5 Torsion

Adhesively bonded joints designed to deal with torsional stresses can be accepted, since it is not an uncommon type of load (direct load or geometric effect). However, some kinds of joints may be avoided and some reinforcement should be foreseen, once that the adhesive strength to this kind of load is not as high as shear stress.

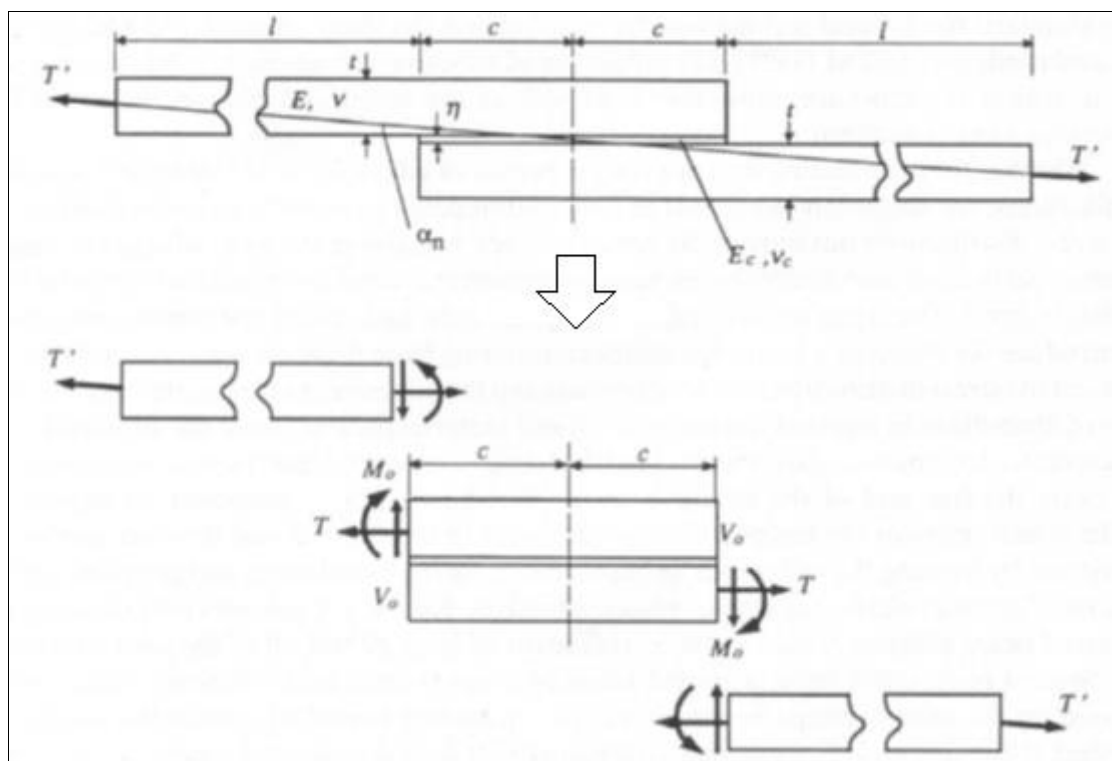
Figure 17 – Torsion stress condition. Source: Hussey and Wilson (1996).



2.4.6 Bending moment

Despite the fact that bending moment is not a kind of load, it is an important condition to be understood in order to properly estimate the strength of a bonded joint, according to Zhao, Adams and Da Silva (2010). Bending moment is a mechanical behavior of the SLJ when under load, due to its geometrical disposition. It can be described as a momentum that is the result of the longitudinal load applied at overlap joints. It has its highest incidence at the edges of the bonded area, according to Silva and Nunes (2014).

Figure 18 – Bending moment on SLJ. Source: Tsai and Morton (1994).



The Figure 18 shows an overview of Tsai and Morton's free body diagram of a SLJ. When a load (T) is applied at the ends of a SLJ, its eccentricity (α angle) induces a bending moment (M_0) in both adherends, which modifies the direction of the path resultant load (T'). From this combination of vectors, a secondary force (V_0) is generated and changes the stress state of the SLJ from pure shear to in a combination of shear and peeling load condition, according to Tsai and Morton (1994). That secondary forces of peeling are the main responsible for most failures of bonded SLJ, (SILVA and NUNES, 2014; ZHAO, ADAMS and Da SILVA, 2010; Da SILVA et al., 2009). The amount of bending moment generated at SLJ relies on several factors, such as geometric variables and material properties.

Tsai and Morton (1994) explain the calculus of the bending moment at the edge of the bonded area based in the geometric parameters of free length of the adherend, overlap length, thickness of the adherend and adhesive, (l , $2c$, t and n in Figure 18, respectively). The adherend and adhesive Young's modulus and Poisson's ratio also should be considered and is denoted by E , E_c , ν and ν_c in Figure 18. Silva and Nunes (2014) scribed the equation below in order to calculate the bending moment at the edge of the bonded area (M_0):

$$M_0 = T[\alpha_n * l - w_1] \quad (3)$$

Where T is the applied load, α_n is the force-eccentricity angle, l is the free length of the adherend and w_1 is vertical displacement. The force-eccentricity angle can be calculated using the equation below:

$$\alpha_n = (t + ta)/(2l + c) \quad (4)$$

Where t and ta are the thickness of the adherend and adhesive, respectively, l is the free length of the adherend (distance from the OL area edge and the grip) and c is half of the overlap length. The force-eccentricity path of a SLJ is where the bonding moment is generated and modifies the load path. This behavior gives rise to a non-linear geometric problem, which results in second order peeling stresses (DA SILVA et al., 2009; SILVA and NUNES, 2014). In the following topics is discussed how the overlap length, adhesive thickness and adherends yield strength affect the SLJ strength.

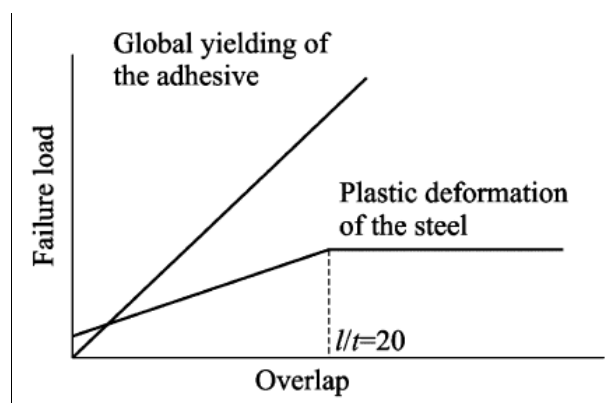
2.5 Main geometric variables and mechanical properties

Several studies analyze how variables affect the strength of SLJ. These variables are mainly classified as geometric dimensions and material properties. Geometric variables can be defined as overlap length, adhesive layer thickness, adherend thickness and width. Da Silva et al. (2009) simply attribute that the SLJ strength is improved increasing the overlap length, adherend thickness and width, and also reducing the adhesive layer thickness. The material property that affects the most the SLJ strength is the adherend yield strength. The higher the yield strength is, the more resistant the SLJ is. In this work it was selected as variable of analysis the OL, AT and adherend YS. Below it is presented listed some of the known relations of these variables with the SLJ strength and stress state.

2.5.1 Overlap length

The overlap length is the variable responsible for increasing the bonded area, which increases directly the strength of the joint. Increasing the overlap and the bonded area, in consequence, increase also the amount of adhesion and cohesion forces that strengthen a SLJ. However, increasing the overlap length of a SLJ also increases the misalignment of it in reference of the applied load, which can be seen in Figure 18. The higher the misalignment, the higher is the bending moment over the adherends of the SLJ and the incidence of peeling stresses (which is the main responsible for SLJ failures, as described previously) at the edges of the bonded area (SILVA and NUNES, 2014; Da SILVA et al., 2009).

Figure 19 - OL effect vs. plastic strain. Source: Pocius (2012).



Pocius (2012) also demonstrated that increasing the OL increases the bonding area, which produces a higher SLJ strength. However, it may encompass plastic deformation both at the adherends and adhesive. As shown in Figure 19, the presence plastic deformation at the adherends tends to reduce the effect of increasing the SLJ strength as effect of increasing the OL – a plateau is expected.

2.5.2 Adhesive layer thickness

The adhesive layer thickness is also related to the SLJ strength in an inverse proportion, according to Silva and Nunes (2014) and Da Silva et al. (2009). Increasing the adhesive thickness also increases the misalignment of the joint, as it is shown in Figure 18, which causes the same impacts of bending moment and peeling stresses as increasing the overlap length. Another negative aspect of increasing the adhesive layer thickness is that, when under application of load, thicker layers tend to propagate failures, cracks and air bubbles (when is there any) faster and with less load, according to Grant et al. (2009).

2.5.3 Adherend yield strength

The mechanical property of yield strength of the adherend has direct impact at the SLJ strength. Increasing the yield strength minimizes the bending moment as well as the peeling stresses at the adherends, as it requires higher loads to allow plastic strain and, in consequence, the adherends to bend. High adherends yield strength makes it easier to keep a stress distribution closer to pure shear condition, which is optimum for the SLJ strength.

2.6 Adhesive curing methods

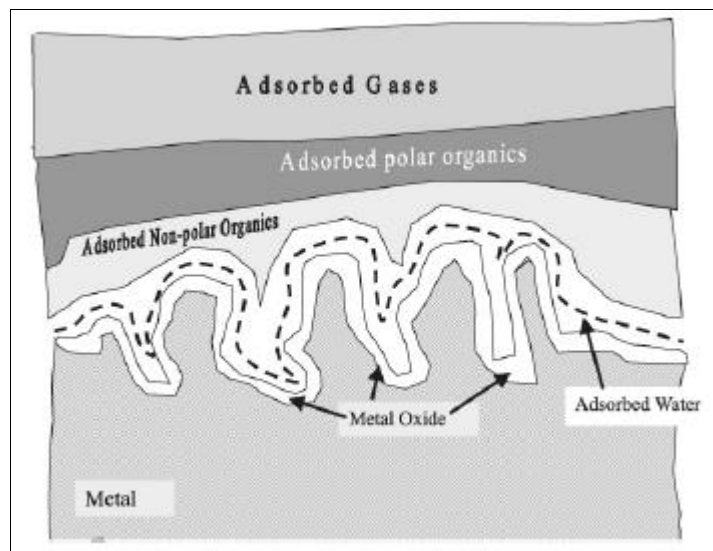
The curing method represents the way in which the structural adhesives pass from the liquid form, as when applied in the overlap area, to rigid state, which grants stiffness and strength to the SLJ. Some structural adhesives curing methods are addition of catalyst agent, heat input, contact with oxygen and ultraviolet light exposure. In this work the used epoxy adhesives is composed by two components known as the epoxy resin and the hardening agent, the hardener catalyst. This

reaction can be accelerated by high temperature, putting the SLJ inside an oven, however the room temperature curing was selected instead.

2.7 Surface treatment

The treatment of the adherends surface prior to the bonding process is indispensable to perform an adhesive bond able to resist high loads. The objective is to prepare the surface of the adherends in order to remove contaminants, dust, oil, grease and other adhesion inhibitors, as well as increase the free surface energy, allowing the adhesive to develop its adhesion phenomena properly. The Figure 20 represents how an untreated metal surface is received for bonding prior to treatment. The oxides, gases, water particles and others restrain or reduce the lock and key effect, explained in 2.4.1.4 topic, which may reduce significantly the adhesion phenomena.

Figure 20 – Untreated surface and its contaminants. Source: Pocius (2012).



In addition to improve adhesion, the adherend treatment is particularly important to provide a reproducible surface so that the bonding operation is consistent, according to Pocius (2012). The most common surface treatments are split in two main types: a) chemical treatment; and b) mechanical treatment. The first consist in deposition of chemical agents with the objective of increasing the adhesion through the adsorption, diffusion and electrostatic theories (free electrons, surface free energy and solubility), which is used mostly for polymers adherends bonding. The second has the objective

of increasing the adhesion through the adsorption and mechanical interlocking theories. It consists a sequence of actions (shown in the next topic) to turn the metal adherend surface condition presented in Figure 7a into the condition presented in the Figure 7b, increasing the surface roughness and releasing components present on the untreated surface (shown in Figure 20) that decrease the adhesion, as discussed previously in the last topic.

Depending on the conditions of the adherend, requirements of the bonding process (level of adhesion) and economic aspects, some surface treatments are available. Simple methods like the use of a detergent are efficient to remove surface dust, dirt and oil present in the surface without complexity. However, the presence of certain greases, oxides and other chemical contaminants may demand more severe treatment methods, like deoxidizing, ultrasound or even mechanical cleaning, which involves brushing, grinding or polishing. Economic aspects can as well impact the demand for a fast and/or cost efficient method, as in the automotive industry, for example. In that case it is common to immerse the whole body structure in a chemical treatment bath, which is fast and very efficient for bonding automotive metal alloys, according to The Aluminum Joining Manual (2015).

3 RESEARCH METHODOLOGY

3.1 Methodology

The methodology of the present work is divided in two parts: a) quantitative analysis of the tensile/shear strength of SLJ by analyzing its failure load (FL) when submitted to tensile tests and; b) DIC of the tested samples with the aid of a cameras system in order to analyze the SLJ behavior when under load.

For the first part of this work, the significance of the variables (input factors) overlap length (OL), adhesive thickness (t_a) and adherend material yield strength (y_s) over the failure load (FL) of SLJ is analyzed. The overlap length (7, 12.5 and 25mm) and adhesive thickness (0.1, 0.5 and 1mm) were set as quantitative factors (levels 0, 1 and 2) and the yield strength configurations (similar AA, similar HSS and dissimilar SLJ – levels AA5083, DP600 and AA5083/DP600) qualitative factor.

The OLs were defined based on a proposal of automotive reduction of body structure flanges (7mm), previous studies (SILVA and NUNES (2014); and Da SILVA et al., (2009)) and DIN EN 1465 (both 12.5 and 25mm levels). The selected adhesive thicknesses for the current work were 0.1, 0.5 and 1mm. It was defined based on the used adhesive datasheet, Da SILVA et al. (2009) and GRANT et al. (2009) works. The first work used adhesive thicknesses of 0.5, 1 and 2mm, while the second used 0.1, 0.5, 1, 2 and 3mm. In both studies, the FL decreased as the adhesive thickness was increased and presented a large drop after 1mm (larger than 40%). So it was planned to narrow the investigation to a shorter interval in order to observe the effect over the output (FL). A draft of the sample and its geometric variables is presented in Figure 21. The adherends of the SLJ were configured in three combinations: a) both adherends of AA (similar AA); b) one adherend of AA and the other of HSS (dissimilar) and; c) both adherends of HSS (similar HSS). These configurations are very common in industries such as aircraft (similar AA and dissimilar) and automotive (similar AA, dissimilar and similar HSS) and also are used in some reference works like Da Silva et al. (2009), Karachalios et al. (2013) and Karachalios et al. (2013). The dissimilar application is one of the main points of this work: analyze the effects of the adherends YS over the SLJ FL.

In order to accomplish the analysis successfully, a DOE full factorial program (3 factors with 3 levels each) was set and the combination of factors and levels resulted in a total of 27 treatments with 6 replicates for each. It was used the software Minitab® to design the experiment and analyze the results. In Table 3 it is shown the DOE of this work.

Table 3 - Experimental inputs and outputs. Source: Author.

Design of experiment - DOE			
	Inputs (Factors)		
Factors levels	Overlap length (mm)	Adhesive thickness (mm)	Yield strength (MPa)
0	7	0.1	AA
1	12.5	0.5	Dissimilar
2	25	1	HSS
Output (N)			
Failure load			

The confidence level set for the full factorial analysis was of 5% (α). The significance of each factor and its interaction was verified based on an ANOVA analysis. A statistical hypothesis testing was performed, measuring the respective P-value. A hypothesis reflects some conjecture about the problem situation, (MONTGOMERY, 2012). In this work, as discussed previously, it is established an assumption (hypothesis) that the variables OL, AT and YS have significance over the output SLJ failure load (Da SILVA, 2009). Then, null hypothesis (H_0) denying the assumption was defined in order to apply a statistical hypothesis test. I.e.:

- H_0 – The response (output) to the factors levels are equal: $FL_0=FL_1=FL_2$.

The rejection of H_0 for each factor using an α of 5% will be discussed in the results chapter. Another ANOVA tool used in this work was the statistical analysis of the F-value, named the variability of the datum, (MONTGOMERY, 2012). It indicates the significance and level of influence of the factors and its interactions based on the mean square of the treatments divided by the mean square of the errors. This calculated F-value should be compared to a standard F-value from the table shown in Attachment A.

The structural adhesive selected for this work was the epoxy bi-component DP 460, from 3M, and the adherends were the AA 5083 and HSS DP600. The mechanical properties of the adherends and adhesives are shown in Table 4.

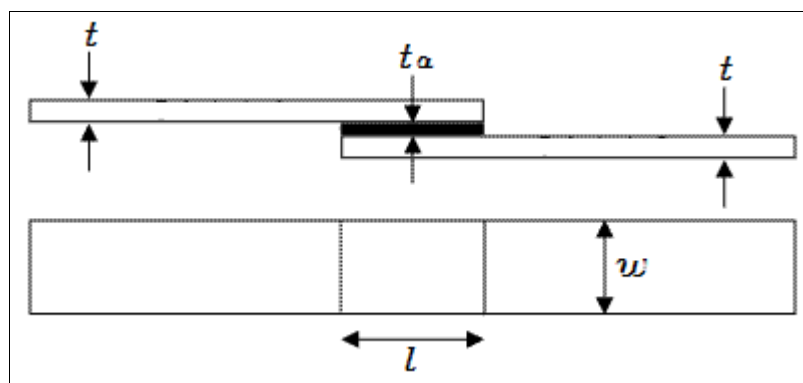
Table 4 - Materials mechanical properties. Source: Author.

Adhesive	3M DP460	Adherend	HSS DP600	AA 5083
Shear strength (MPa)	31	Tensile strength (MPa)	580	275-350
Hardness (D)	75-80	Yield strength (MPa)	400	125
Basis density (g/cm ³)*	1.2	Density (g/cm ³)	8	2.65
Hardener density (g/cm ³)*	1	Modulus of elasticity (GPa)	207	72

*Liquid state

Figure 21 shows the SLJ specimen geometry, recommended by the standard DIN EN 1465 and used in this work, in which it is possible to visualize the geometric variables overlap length (l) and adhesive thickness (t_a) analyzed in this work. The adherend width (w) was of 25mm for all the treatments and the other geometries were described in the beginning of this section (factor levels).

Figure 21 - The SLJ specimen. Source: Bamberg et al. (2016).



The procedure followed the standard DIN EN 1465, which states the conditions of a quasi-static tensile test of SLJ composed by two rigid metal (adherends) joined by the application of a structural adhesive. It will be described in the following topics in this chapter. According to Singh (2007), “deformation of solid bodies plays a crucial

role in materials and structures analysis and design. Deformation is either needed to control them or the equations of equilibrium are not sufficient to solution of stresses.” The second part of the experimental design is based in using a DIC system, in order to correlate the tensile shear test results to the mechanical behavior of the used joints. This method quantifies the amount of strain of a SLJ during the mechanical test. By doing this, it is possible to understand how the factors influence the stress distribution, the presence of stress concentrators, peeling stresses and bending moment on SLJ. Figure 22 shows an overview of the experimental setup used in this work. In the picture, the tensile test machine grips are indicated by letter A, the SLJ sample by letter B, the DIC spotlights by letter C and the DIC cameras system with the fixing support by letter D.

Figure 22 – The experimental setup. Source: Author.



3.2 Mechanical characterization

To perform the tensile tests two standards were used. The first one was the DIN EN 1465, in order to determine the samples manufacturing, test conditions and procedure, technical apparatus and results reporting. The second standard was the ISO 10365 that designates main failure patterns for the tested samples, which

consists in analyze the bonded area of the SLJ after the tensile tests. The results feed statistical analyses of ANOVA, in order to estimate the relevance of each factor over the output SLJ FL and factors interaction, and also normal distribution curve, P-value, results dispersion and optimization.

3.2.1 Tensile tests apparatus

As stated before, the DIN EN 1465 is responsible for specifying the methods to determine the tensile lap-shear strength of bonded SLJ, such as samples preparation, testing conditions and other recommendations. According to the standard, adhesive lap-shear bond strength is determined by stressing in shear a SLJ, composed by two rigid adherends, by applying to the adherends a tensile force which is parallel to the bonded area and to the major axis of the specimen. It is reported the observed force or stress at the rupture.

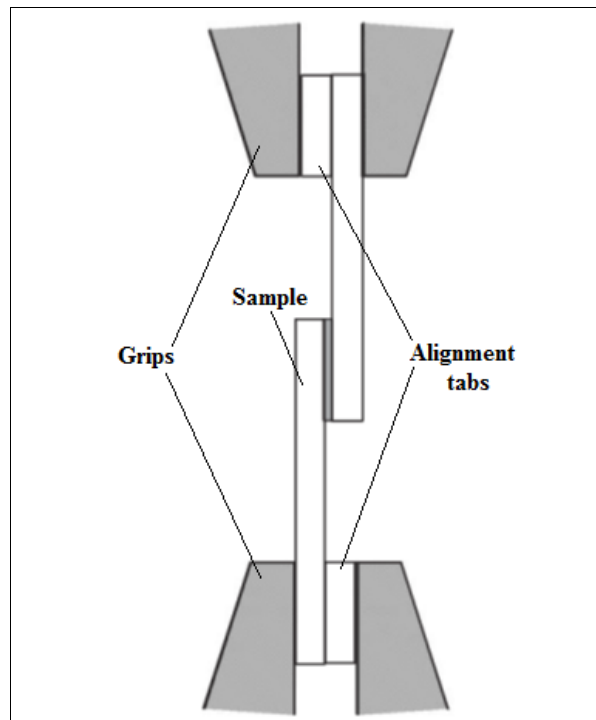
3.2.1.1 Tests settings and equipment

The standard DIN EN 1465 specifies that the used tensile machine should have a response time short enough to not affect the accuracy with which the force applied at the time of rupture can be measured. Also, it shall be capable of applying a tensile force that increases at a steady rate. The tensile load test machine used in this work was an Instron 4210, which has a load cell of 100kN, from INSTRON GmbH, Darmstadt, Germany. This equipment was used to apply load at samples in a longitudinal way, resulting in shear load for the SLJ samples.

The standard recommends that the duration of each sample test lasts between 65 ± 20 seconds. In order to obey that, preliminary tests were done with different test speed and it was verified that the speed of 4mm/min attended this condition for all the different overlap configurations.

The standard recommends the use of self-aligned grips and jaws or alignment shims and tabs, reducing misalignment and bending moment, described in the section 2.6.6. As the used tensile load machine was not equipped with self-aligning grips, machined alignment tabs were used to attach the samples, as it is shown in Figure 23, providing a better condition for the tensile tests.

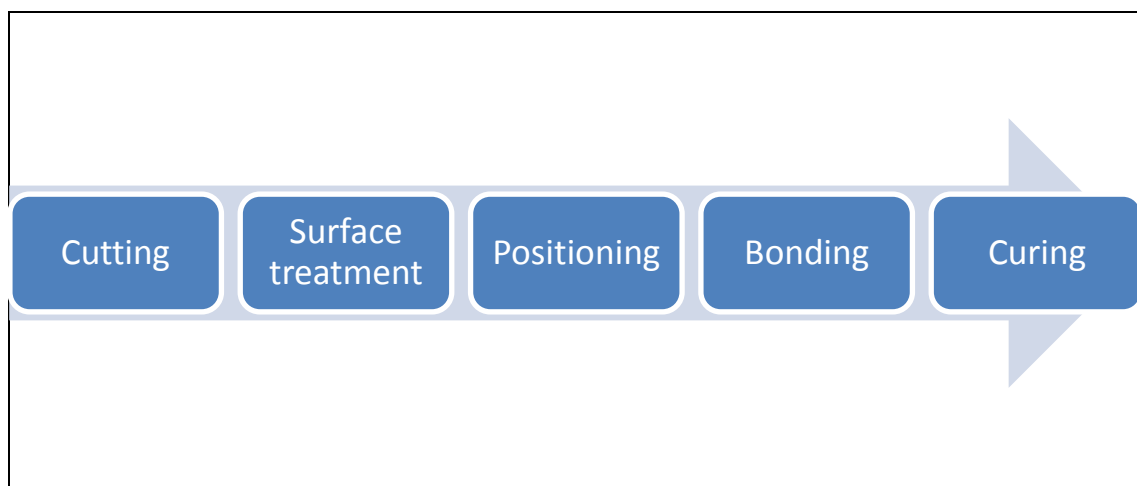
Figure 23 – The alignment tabs. Source: Modified from Guo, Dillard and Plautc, (2006).



3.2.1.2 Preparing samples for tensile tests

The adherend surface shall be prepared, in order to obtain an optimum bond, and reported. It is advised that the surface treatment follows the adhesive manufacturer recommendations for the type of used adherend. If no recommendation is available, it is suggested to follow the standard DIN 13887, however the current work followed specialists' recommendations which are described in the following topics.

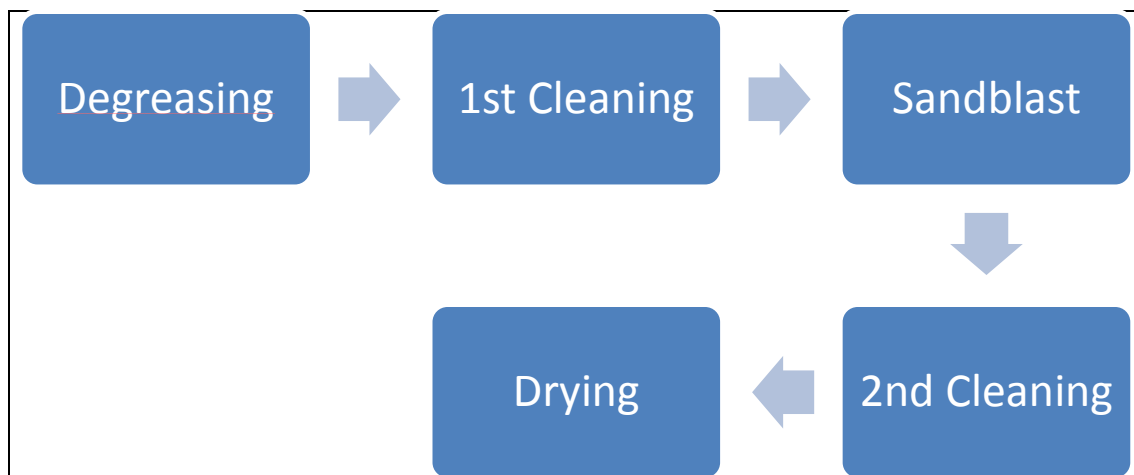
Figure 24 - Sample preparing process overview. Source: Author.



The manufacturing of the SLJ samples used in this work - overviewed in Figure 24 - followed the recommendations from the DIN EN 1465 and the instructions of previous works (Da SILVA et al., 2012; Da SILVA et al., 2009; KARACHALIOS, ADAMS and Da SILVA, 2013; SILVA and NUNES, 2014; POCIUS, 2012).

The samples preparation starts with the cutting of the adherends with dimensions specified on the topic 3.2.1.2. In order to minimize the effects of the cutting, Da Silva et al. (2012) recommend the machining of the adherends in order to improve the results precision. However, in this work, an industrial guillotine (metal cutter) was used based on good statistical data (low variance and standard deviation) of the preliminary results, shown in Appendix E, done with similar adherends of AA and the 3M DP460 adhesive. The adherends were cut from a 2000 x 1000mm (width x length) sheet to the dimensions of 1.5 x 25 x 100mm (thickness x width x length). After cutting, the adherends were submitted to a surface treatment, shown in Figure 25, with the objective of increasing the adhesion by enhancing the surface free energy and improving the lock and key effect, as explained in the topic 2.2.1.4.

Figure 25 - Surface treatment sequence. Source: Author.



The untreated surface of metal plates when received for bonding usually contain several contaminants such as presented in Figure 20. So, first, a degreasing is necessary in order to remove some impurities, such as oils, fat, grease, dust, dirt, water and other contaminants present on the adherends surface. Using the industrial neutral degreasing soap, the samples were cleaned manually at the sink. The adherends were then submitted then to the first cleaning, in order to remove the

degreasing agent as well as contaminants left over previously to the sandblast. This must avoid that the sandblast process drag contaminants deeper into the crevices what would be harder to remove and would impact negatively the surface treatment process. The samples bonding area were positioned inside an ultrasound cleaner, shown in Figure 26, which was filled with isopropanol and is able to remove dirties, particles and others by creating micro bubbles in the surface of the adherends.

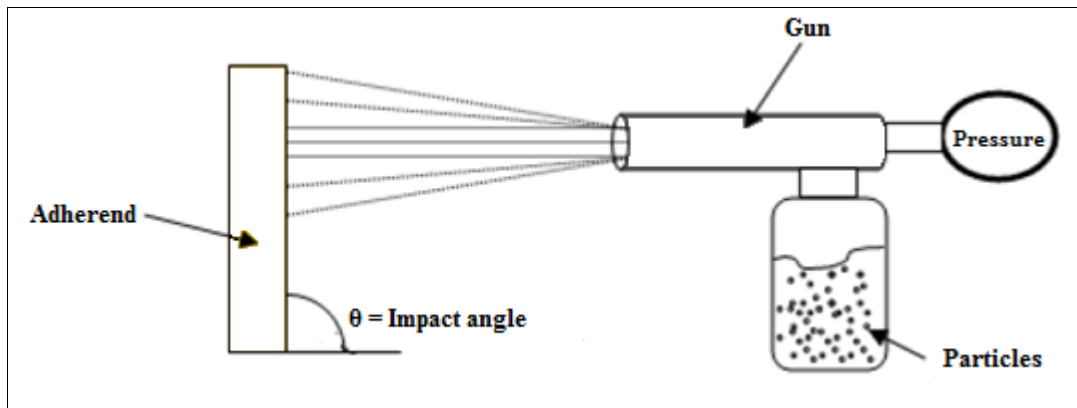
Figure 26 - The ultrasound cleaner. Source: Author.



The first cleaning lasted for five minutes at room temperature of 23 °C using the ultrasound cleaner 460/H, from the company Elma Transsonic, shown in Figure 26, using a frequency of 35 kHz. The ultrasound cleaner removes dirties, particles, oil and greases, by creating micro bubbles that apply a very high pressure over the surface of the adherends, known as micro cavitation.

After the first cleaning, the adherends were sandblasted, increasing the roughness of the bonding area (demonstrated in Figure 7b), improving the “lock and key” effect and the adhesion, in consequence. The procedure consists in displacing the adherends inside the sandblasting chamber and spraying abrading particles in high speed over the area intended to bond (as illustrated in Figure 27). Despite its irregular shape, the blasted particles, which are usually composites, have mean size a variable of control. The compressed air pressure and impact angle are also controlled. After the sandblasting the adherends surface is plastically deformed like the one presented in Figure 7b.

Figure 27 – Sandblasting example. Source: Author.



The machine used in the current work was a sandblasting cabin from the company Heinrich Schlick KG GmbH, shown in Figure 28. The air pressure was of 3 psi, spray angle round about 45°, the abrading particles were made of iron and silicon material with a grain size between 150 and 212 μm (F80 Corundum Fe-Si, Radler & Ruf Sandstrahl- und Druckluftbedarf GmbH). The blasting time was of around 10 seconds over 6 adherends positioned side by side.

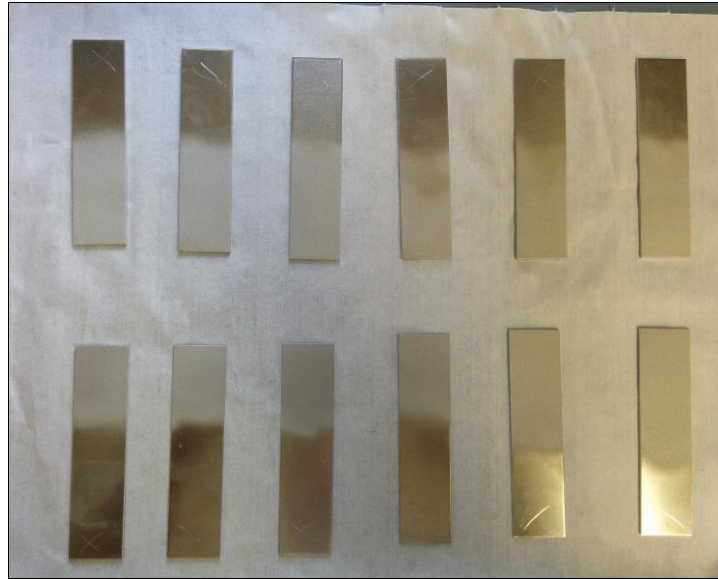
Figure 28 – The sandblasting machine (left) and chamber (right). Source: Author.



After the sandblasting it was used compressed air at 3 psi to remove the residual particles from the surface and also a tissue with isopropanol. After that a second cleaning was performed in the ultrasound cleaner for five more minutes with the same parameter of the first one, when the already abraded adherends are left there for five more minutes. After the second cleaning, a special care was taken with the prepared area in order to preserve a high surface energy from the treatment. So it

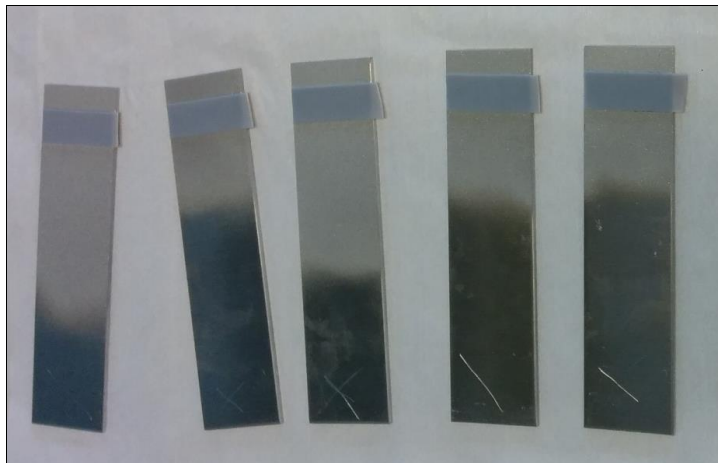
was avoided any contact with anything that could left residuals particles, by letting the samples to dry inside a clean room at laboratory temperature of 23 °C and 45% of humidity for 10 minutes and packing it with a cleaning wipe that leave no residuals (reference 3M 34567), as shown in Figure 29.

Figure 29 - Treated samples. Source: Author.



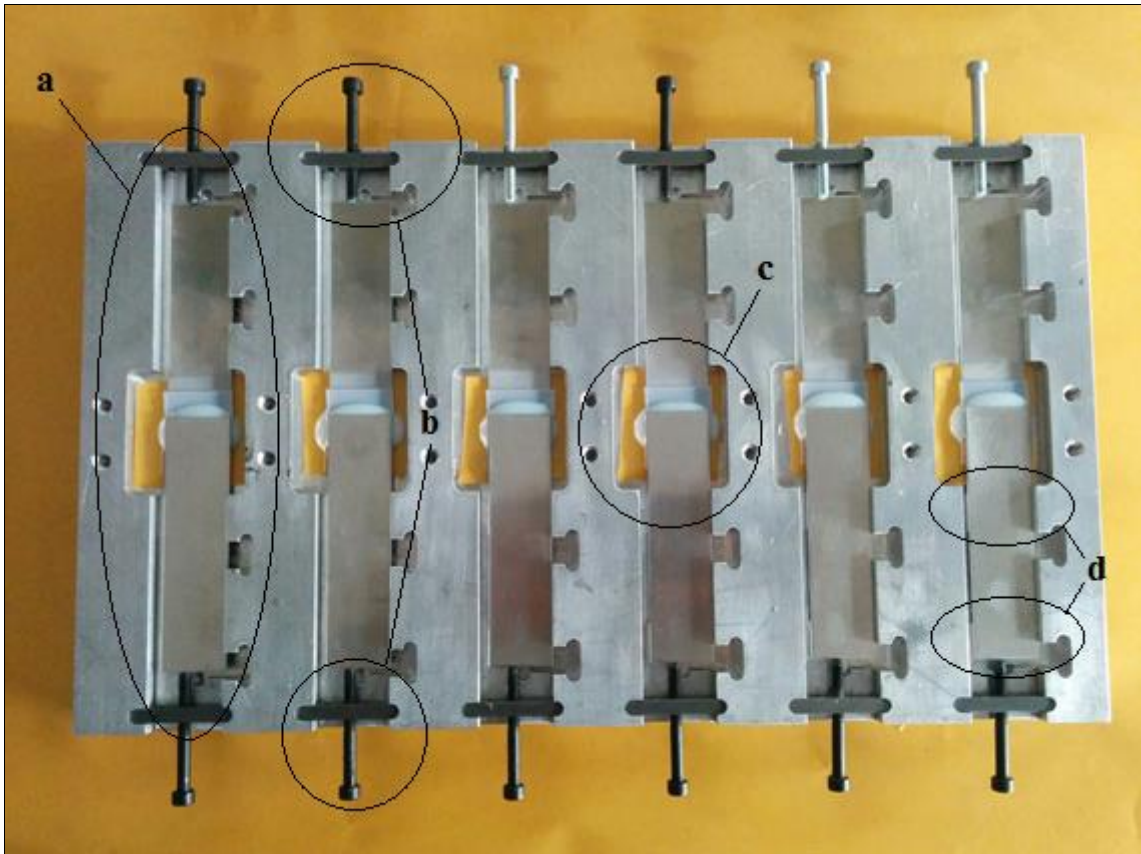
The next step consists in measuring and marking the bonding area so it can be ready to be bonded. It was used a caliper ruler to measure the desired overlap length and then a rigid tape was inserted to mark and control the bonding area, as shown in Figure 30. After that step, the adherends are ready to be positioned inside the mold for the structural adhesive application.

Figure 30 - Marking the bonding area. Source: Author.



Special care is recommended for the positioning of each adherend and specimen, to ensure proper alignment of the adherends and adhesive layer thicknesses uniform and constant as possible. In order to get these variables under control, an alignment mold was used. It is shown in Figure 31 with 6 samples already positioned in it.

Figure 31 – Samples in the alignment mold. Source: Author.



The mold used in this work was built based on the recommendation of Da Silva et al. (2012). It is very important to prepare SLJ for ASTM D1002 and DIN EN 1456 standards for several reasons:

- Controls the samples geometric variables of overlap length, adhesive thickness;
- Helps to align the adherends prior and after displacing the structural adhesive;
- Keeps samples static during the curing period (both in room temperature or inside the oven);

- Prepare 6 samples together each time under the same conditions of temperature, time and pressure during the curing period, which increases the reliability and accuracy of the results.

The alignment mold was made by machining an aluminum block and can develop the functions listed above because of the following characteristics indicated in Figure 31: a) machined flat paths (cavities) that are responsible for keeping both adherends (top and bottom) aligned and fixed during the bonding and curing of the samples; b) adjustable screws that are responsible for controlling the overlap length; c) centered square hole in order to position a Teflon paper, avoiding the structural adhesive to bond to the mold; d) machined calibrated shims are positioned inside the flat paths (shown in Figure 31a) in order to control the adhesive thickness. The length between the screws of each sample cavity was measured with a caliper rule in order to control the overlap length. Then the bottom adherend was positioned in mold with its right edge fully in contact with the flat wall of the cavity, controlling the alignment of it. To control the adhesive thickness, the standards DIN EN 1465 and ASTM D1002 recommend the use of glass beads or calibrated wire to control the adhesive layer thickness. Da Silva et al. (2012), however, suggest the use of shims to control the thickness and the angle of the adhesive layer. In this work, calibrated shims were positioned in the mold, under the upper adherend, to control the thickness of the adhesive layer. It was used calibrated shims of 1.6, 2 and 2.5mm of thickness under the top adherends, in order to grant adhesive thicknesses of 0.1, 0.5 and 1mm, respectively, as it is shown in Figure 31d. The adhesive is then displaced over the bonded area using the 3M applicator pistol EPX Plus II. Some adhesive was first squeezed out of the pistol in order to get an uniform mix between the adhesive and the hardener and avoiding air bubbles within the adhesive layer, as recommended by Da Silva et al. (2012). After that, the upper adherend was placed over the lower one also with its edge fully touching the cavity's wall. The alignment of each sample was checked and corrected, when necessary. Then it was applied calibrated weights of 800 grams over each sample by the centered square hole area (Figure 31c).

The 3M DP 460 datasheet provides mechanical properties for different curing methods with or without temperature. The samples of this work were all cured in laboratory temperature of about 23 °C and humidity around 45% during 7 days (first 48 hours inside the mold under the 800grams mass), as suggested in the adhesive's

datasheet. After this curing time, the samples were taken carefully from the molds, is it can be seen in Figure 32.

Figure 32 - Cured sample. Source: Author.



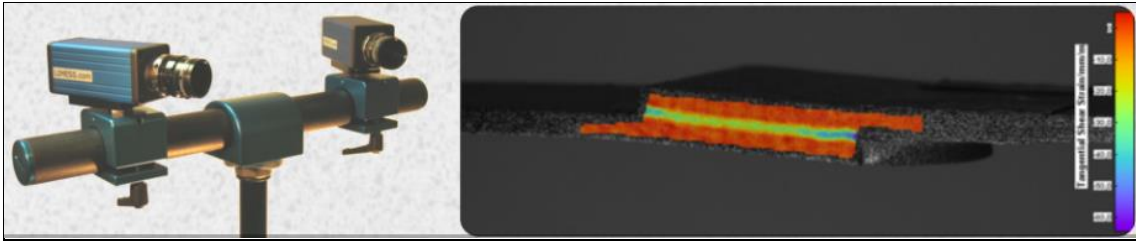
The excess of adhesive, shown in the sides of the overlap area of Figure 32, was removed from the sides with the usage of a grinder in order to avoid kame the load path uniform. The samples were then ready for the tensile tests, however, as mentioned in the beginning of this chapter, DIC analyses were also performed. So, a specific preparation was performed in order to accomplish this technique and will be explained in the next topics.

3.2.2 DIC technique

As mentioned in the overview of the research technique, the DIC is a measurement technique capable of correlating the results from the tensile shear tests to the strain of an analyzed area. It is a high capacity state of art technique for displacement and strain measurement of materials mechanical characterization, (YANG *et al.*, 2010).

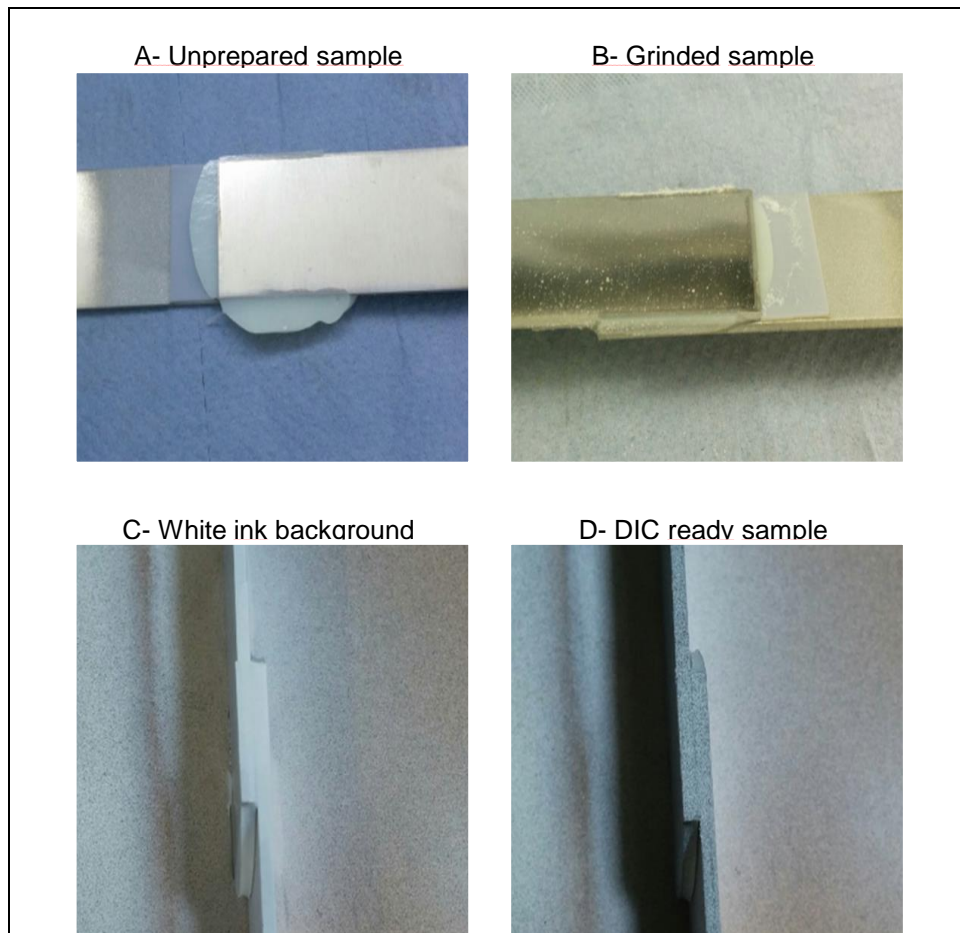
The DIC system used in this work was the Q-400-RT, from LIMESS GmbH, Krefeld, Germany. This system composed by two cameras of 2 megapixels and the software ISTR4 4D from the same company. It was set with 4Hz (4 pictures per second) to acquire the images of the analyzed area, which will be described in the following topics. An overview of the system is shown in Figure 33.

Figure 33 - The DIC example. Source: www.limes.com.



In order to analyze the mechanical behavior of the SLJ the overlap area (region or area of interest) the samples must be prepared for the DIC analysis. It's a simple process shown in Figure 34.

Figure 34 - Preparing samples for DIC. Source: Author.



Preparing samples for the DIC, process shown in Figure 34, consisted basically in 4 steps: A) get the just bonded sample; B) the excess of cured adhesive was carefully removed from the region of interest with a hand grinder; C) the region of interest was painted with a white ink, forming the background and; D) black ink was slightly

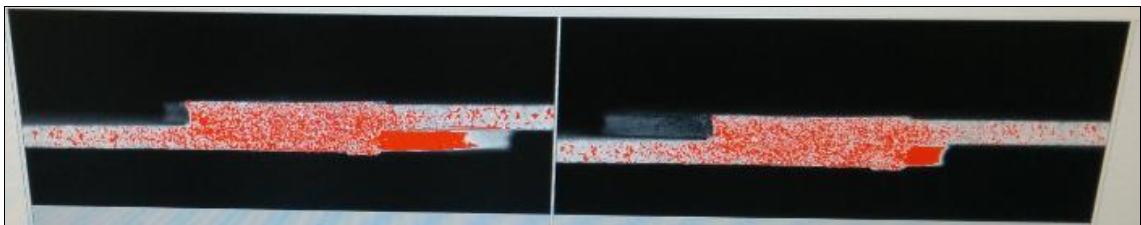
sprayed over the area of interest. For the steps C and D an air pump with an airbrush from Evolution GmbH was used with a pressure of 0.8 bar, shown in Figure 35.

Figure 35 - Air brushing the DIC sample. Source: Author.



The result was a contrast between the two colors over the area of interest, which also blocks the reflection of the metal adherend, what would result in bad images. Prior to the test, the DIC cameras identify each point of the analyzed region. Figure 36 presents one prepared sample being visualized by the DIC system at the ISTR4 4D software screen.

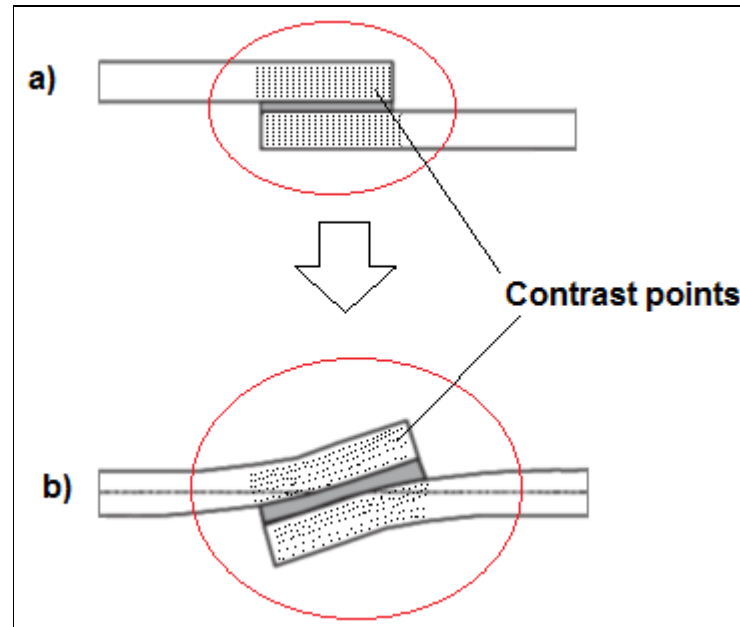
Figure 36 - Sample ready for the DIC. Source: Author.



Each red dot in Figure 36 represents a recognized black ink spot which is tracked by the DIC system during the tensile/shear test. The Figure 37 presents a scheme of a SLJ prepared for the DIC analysis and the area of interest, where a) represents the

sample before the tensile shear test (reference image) and b) represents the sample during or after the test (succeeding pictures after the beginning of the test).

Figure 37 – The DIC analysis model. Source: Modified from Guo, Dillard and Plautc, (2006).

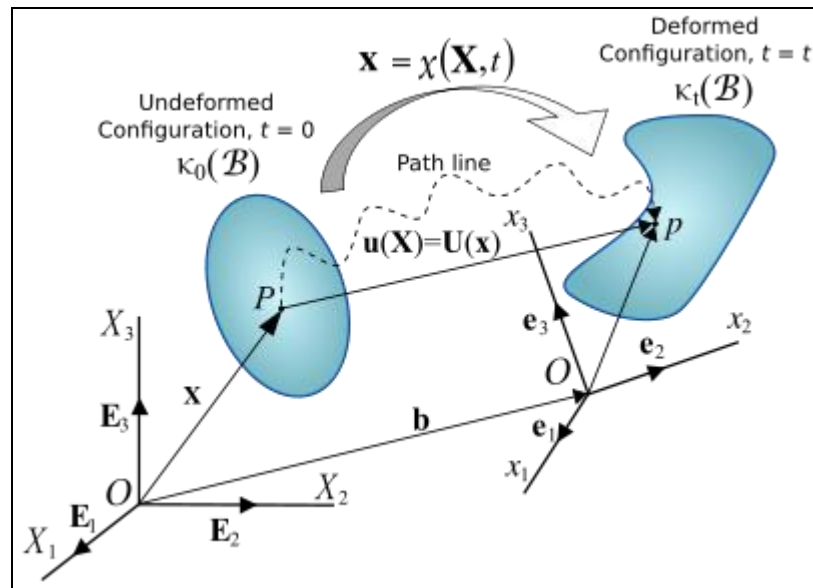


The DIC system quantifies the amount of displacement of each point during the test (picture after picture) and correlates it with the current applied load, informed by the tensile load test machine. By doing that, this system analyzes the amount strain and stress distribution of the region of interest of each sample, which allows a better understanding of the resulting SLJ FL and its mechanical behavior. The stress distribution was analyzed according to LaGrange principal strains method, which calculates the amount of strain of each point and plots a colored mask over the region of interest with its corresponding motion vectors.

3.2.3 LaGrange Principal strains

The LaGrange principal strains method is based in the comparison of each picture of DIC analysis with the reference picture (sample without load, as illustrated in Figure 37a). It calculates the LaGrange vector for the displacement of each identified point from the analyzed area. An illustration of the LaGrange principal strain method is shown in Figure 38:

Figure 38 - The LaGrange strain model. Source: DILL, (2006).

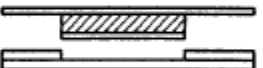
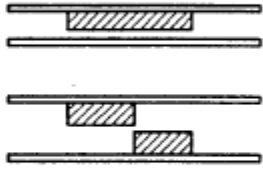


In Figure 38, “P” represents the original position of one of the analyzed points and “p” is the equivalent point after the application of a certain load (basically one of the points shown in Figure 37a and its equivalent point in Figure 37b). Despite the striped line indicates the path line, the method quantifies the amount of displacement in the two dimension plane (i.e. axis X2 and X3 in Figure 38) and calculates the intensity and direction of the resultant vector, known as LaGrange vector. After calculating, it is plotted on the analyzed area the LaGrange vector for each contrast point and a colored scale measurement is created indicating the amount of strain in each region. A concentration of vectors in a similar direction may indicate elongation and deformation of an analyzed surface.

3.2.4 Failure mode analysis

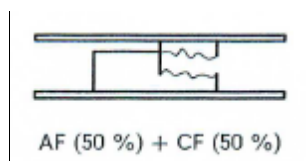
The ISO 10365 standard specifies designations for the main types of failure pattern of bonded assemblies and illustrates their respective appearances. This standard covers all kinds of bonded assemblies no matter the adherend or adhesive used in the joint. This designation is very important to understand better the result of any mechanical test, classifying the obtained failures and correlating it with the quantitative results. The failure patterns are classified according to Table 5.

Table 5 – Bonded joints failure mode classification. Source: ISO 10365.

Failure type		Designation
Adherend	 Failure of one or both adherends (Substrate failure)	SF
	 Failure of an adherend (Cohesive substrate failure)	CSF
	 Failure through delamination (Delamination failure)	DF
Adhesive	Types of cohesion failure  Cohesion failure  } Special cohesion failure 	CF SCF
	 Adhesion failure	AF
	 Adhesion and cohesion failure with peeling	ACFP

More than one type of failure part can result from a mechanical test. Figure 39 presents an example of an estimative of the failure pattern relation.

Figure 39 - Mixed failure mode pattern on SLJ. Source: ISO 10365.



4 RESULTS AND DISCUSSIONS

4.1 SLJ tensile tests results

In this chapter the results from the experimental program presented on the last chapter are presented and discussed. **Erro! Autoreferência de indicador não válida.** presents the failure loads of all the 27 SLJ configurations.

Table 6 – The experiments results. Source: Author.

Treatment	Material	Adhesive Thickness	Overlap (mm)	Average (N)	Std Dev. (N)
0001	AA5083 H111	0.1	7	5319.96	88.78
0002			12.5	6491.3	94.41
0003			25	8736.9	244.92
0004		0.5	7	4649.22	307.29
0005			12.5	6926.02	384.03
0006			25	9074.8	194.84
0007		1	7	3740.2	102.22
0008			12.5	5951.04	203.08
0009			25	8637.08	55.09
0010	Dissimilar	0.1	7	5633.24	351.59
0011			12.5	8056.62	234.68
0012			25	9167.66	295.42
0013		0.5	7	5127.68	107.48
0014			12.5	7784.24	400.14
0015			25	9609.14	164.84
0016		1	7	4586.06	113.75
0017			12.5	7126.88	350.83
0018			25	9499.62	91.55
0019	HSS DP600	0.1	7	6177.18	173.87
0020			12.5	9939.34	396.8
0021			25	16089.24	779.14
0022		0.5	7	5480.14	251.46
0023			12.5	8962.48	291.04
0024			25	17017.84	550.34
0025		1	7	4856.92	92.39
0026			12.5	8289.16	285.35
0027			25	14740.84	483.98

Analysis from the overlap length, adhesive thickness and material yield strength perspectives are done in the next topics. The influence of each variable over the SLJ FL was analyzed based on the ANOVA results from the DOE performed in this work.

4.1.1 ANOVA

The relevance of each variable was analyzed via a hypothesis test from the ANOVA, by observing the calculated results for P-Value and checking the validity of the null hypothesis H_0 , presented in the methodology section. As discussed previously, in order to reject a null hypothesis, its respective calculated P-value must be within the critical region which, in this case, for the set confidence interval ($\alpha=5\%$), is below 0.025.

Table 7 - ANOVA results. Source: Author.

ANOVA					
SOURCE	DF	SQ (AJ.)	QM (AL.)	F-VALUE	P-VALUE
OL	2	910229811	455114906	3074,65	0.0
AT	2	22190053	11095027	74,96	0.0
YS	2	314576794	157288397	1062,6	0.0
OL*AT	4	6279549	1569887	10,61	0.0
OL*YS	4	212202772	53050693	358,4	0.0
AT*YS	4	3830926	957732	6,47	0.0
ERROR	116	17170515	148022		
TOTAL	134	1486480420			

Table 7 presents the ANOVA results from the designed experiments of this work. It can be verified that the calculated P-values of the variables (OL, AT and YS) and its interactions were approximately 0 (zero). It is possible to infer that H_0 (The response - output - to the factors levels are equal: $FL_0=FL_1=FL_2$) was rejected. In other words, all the factors and its 2nd order interactions presented relevant significance over the SLJ FL.

In addition to the hypothesis test, the ANOVA results include calculated F-values in order to analyze the level of significance of the factors. For an $\alpha=5\%$, the reference F-values informed by the F Distribution table, shown in Attachment A, are 3.07 for the OL, AT, and YS (degrees of freedom of the factors is 2 and of the error is 116) and 2.45 for the 2nd order interactions between these factors (degrees of freedom of the

factors is 4 and of the error is 116). The ANOVA presented considerably higher calculated F-values than the references, as it is shown in Table 7:

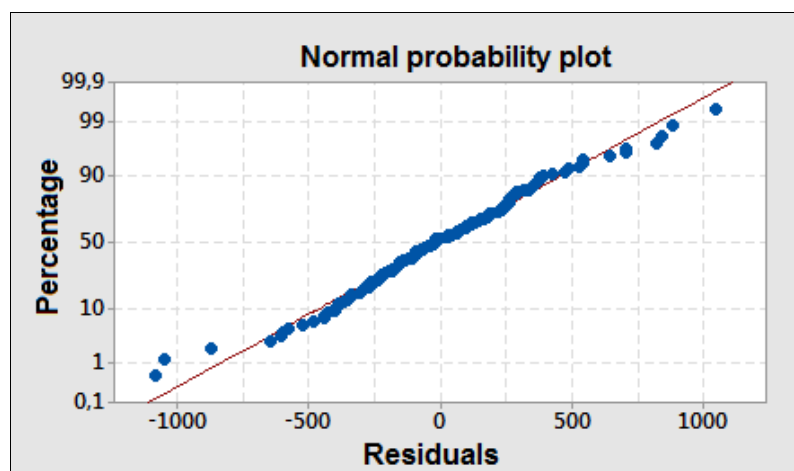
- OL - about 1000% higher, presenting 73% of significance;
- AT - about 25% higher, presenting 2% of significance;
- YS - about 345% higher, presenting 25% of significance.

The second order interactions presented about 3% of significance for the OL versus AT, 95% for OL and YS, and 2% for AT and YS. Such results converge with the hypothesis test and point out that the variability from the factors means (numerator) is considerably higher than the variability from the error means (denominator), indicating large influence from the factors over the output FL and low noise.

4.1.1.1 Model adequacy checking - residuals analysis

In addition to the hypothesis test and F-distribution, it is important to verify the model adequacy of the experiment, in order to verify if the factorial model was appropriated to the designed experiment, which can be investigated by examining the residuals of the treatments.

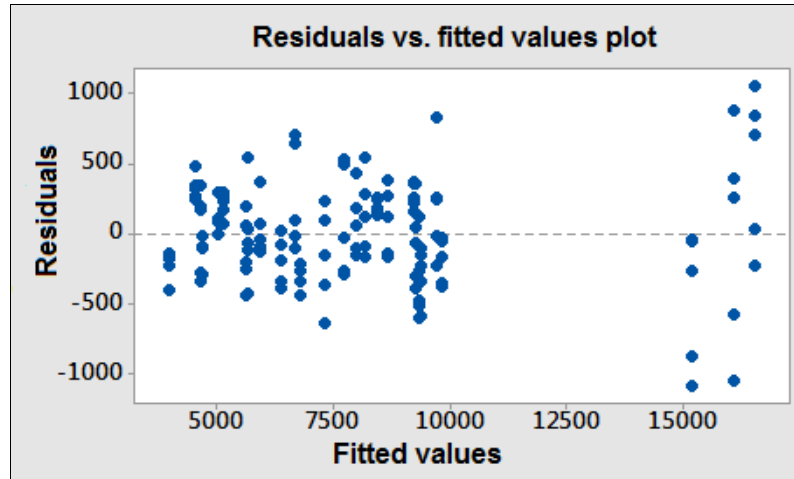
Figure 40 - Normal probability. Source: Author.



The normal probability plot, shown in Figure 40, is shaped as a straight line, underlying a normal distribution, indicating a robust ANOVA and an error distribution approximately normal. Also, the normal probability plot straight line presents more emphasis in the central values than in the extremes. It was not detected the

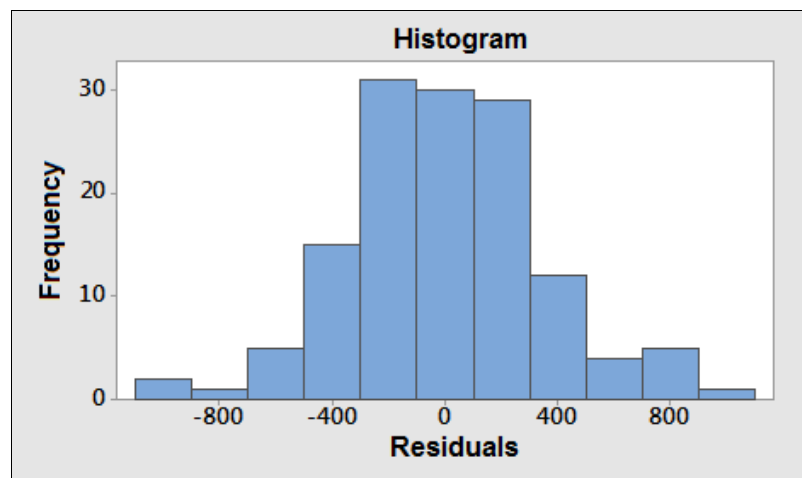
presence or outliers, which might indicate distort of the ANOVA, that could be caused by bad calculation, mistakes in data collection or copying errors.

Figure 41 - Residuals vs. fitted values. Source: Author.



According to Montgomery (2012), if the model is correct and the assumptions are satisfied, the residuals should be structureless, revealing no obvious pattern, trend or tendency. As it can be seen in Figure 41 the residuals vs. fitted values plot do not show tendencies or patterns. There is, however, a gap in between the fitted values around 10000 and 15000 N, which is related to the non-linear increase of the OL levels, the factor with higher significance, as analyzed in the previous section.

Figure 42 - Histogram. Source: Author.



The histogram graph presented the residuals congruent to a normal distribution. It can be analyzed in Figure 42 that the tendency of the residuals is central and the

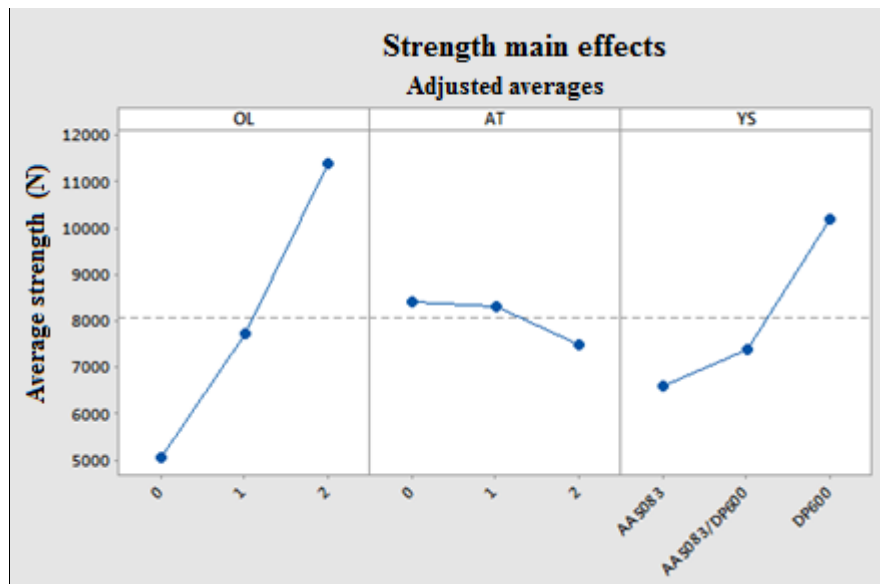
spread shapes a normal distribution curve, which indicates a centered experiments mean and controlled variance.

The R-values calculated by ANOVA where 99.3% (squared R), 99.14% (adjusted R) and 98.91%, justifying 98.91% of the obtained results, indicating a high quality level.

4.1.1.2 Effects from the OL, AT and YS over the SLJ FL

The Figure 43 compiles the full factorial analysis of tensile tests results regarding the effect of the three variables of this work, OL, AT and YS, over the SLJ FL. Each variable is analyzed according to its effect over the SLJ FL and behavior. Other author's results are used as reference.

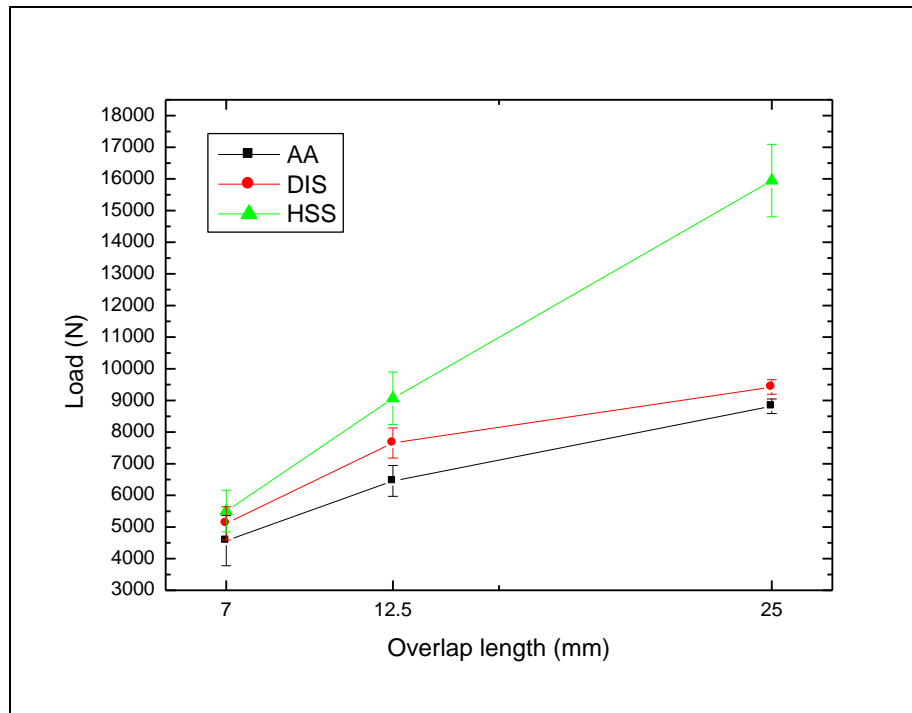
Figure 43 - Variables main effects over the SLJ FL. Source: Author.



4.1.1.3 The overlap length effect

Increasing the OL, as expected, increased the SLJ FL as the bonded area became larger. The SLJ set with 7mm of overlap presented the lowest results, followed by 12.5mm and then 25mm for all the material combinations, as it can be seen in Figure 44. It can be noticed that the effect of increasing the OL reduces as it gets longer. The similar AA and dissimilar SLJ presented a more pronounced when increasing from 7 to 12.5mm than from 12.5 to 25mm. The similar HSS SLJ presented a FL increase closer to linear than the other two, however with a small advantage also from 7 to 12.5mm.

Figure 44 - Overlap length vs. failure load. Source: Author



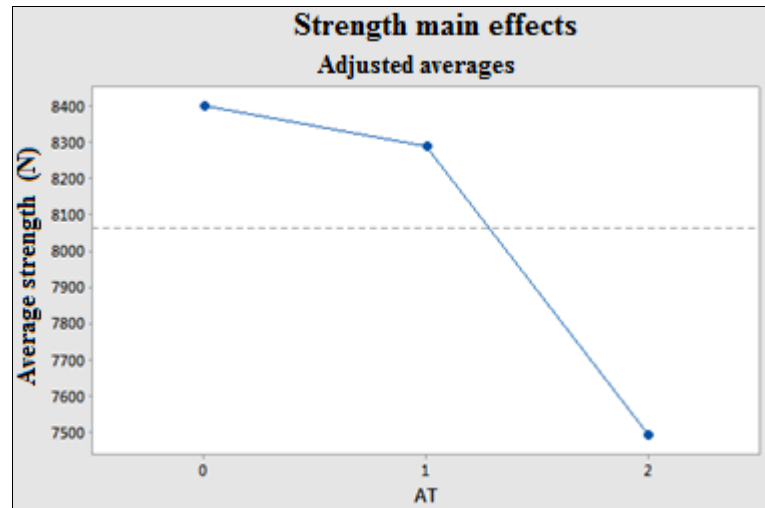
The effect of increasing SLJ FL as an effect of OL was also found in previous works, shown in Attachments B and C. Karachalios et al. (2013) work tested HSS adherends of 1800 MPa and verified that a linear increase in SLJ FL was found as the OL got longer. However, it expected a limit to it due to the adhesive strength. Da Silva et al. (2009), however, worked with high and low YS adherends and explained that with an elastic failure the adhesive can develop its full shear strength and make use of the full OL. In addition, encompassing plastic strain, the OL effect is lost. One reason for this second effect might be explained by analyzing Eq.3 and Eq.4, which shows that the longer the overlap the larger is the misalignment of the SLJ and the higher is the bending moment and the peeling stress. According to Silva and Nunes (2014), bending moments is strictly associated to incidence of peeling stresses, which, as discussed before, are the main reason for SLJ failures. Further discussions about these effects are done in the next sections based on the presence plastic strain, the stress state and incidence of stress concentrators.

4.1.1.4 The adhesive thickness effect

The AT had an inverse effect over the SLJ FL, as increasing the first reduced the second, as it can be seen in Figure 45. It is possible to notice, however, that the SLJ

FL drops more when increasing the AT from 0.5 to 1mm (levels 1 and 2, respectively) than from 0.1 to 0.5mm (levels 0 and 1, respectively).

Figure 45 - Adhesive thickness vs. failure load. Source: Author.



This effect was also found Grant *et al.* (2009) and Da Silva *et al.* (2009) works, shown in Attachments D and E, which states that SLJ are very sensitive to thicker AT due to three main reasons: a) increasing the AT increases also the interface stresses; b) thicker bond lines contain more defects such as voids and micro cracks and; c) increasing the AT increases also the bending moment, reducing the SLJ FL. The reason for this difference might be related to the presence or plastic strain and will be discussed further in this section.

4.1.1.5 The adherends yield strength effect

The results regarding adherend's YS effect over SLJ FL were also linear. The higher the YS, the higher the SLJ FL. Karachalios *et al.* (2013) stated that plastic strain at the adherends tends to change the stress state of the joint into a worse condition for the adhesive to withstand the applied load. So the results followed the expectation, as the AA adherends encompassed plastic strain (mainly for 12.5 and 25mm OL), as the similar adherends SLJ of AA presented the lowest results, the dissimilar adherends SLJ presented intermediate, however, closer than similar SLJ with AA adherends than the similar SLJ with HSS and the similar SLJ with HSS adherends presented considerably higher results than the other two adherend materials

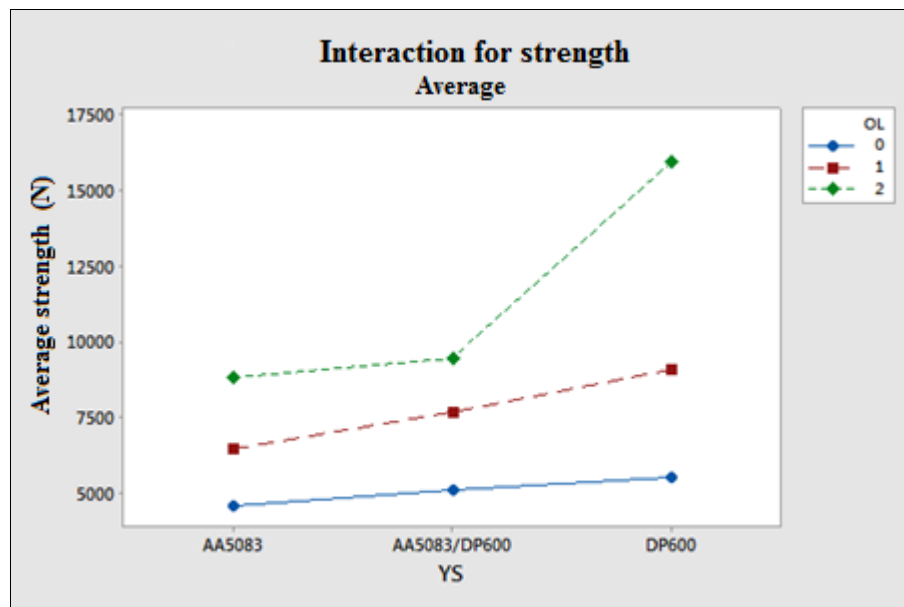
combinations. Figure 44 can be used to analyze the adherends different materials combinations and its respective failure load.

Similar results are found in Da Silva *et al.* (2009) work, seen in Attachment F. In such work, it was compared similar SLJ using as adherends material the low strength steel DIN St33, with 184 MPa of YS and the HSS DIN C65, with 1260 MPa of YS. Despite the larger difference among the mechanical properties of the adherends materials, the effect described before was the same.

4.1.1.6 Interactions

The interactions between the variables and how it influences the output SLJ FL was also analyzed. First, in Figure 46, the interaction between the OL and adherends YS was plot.

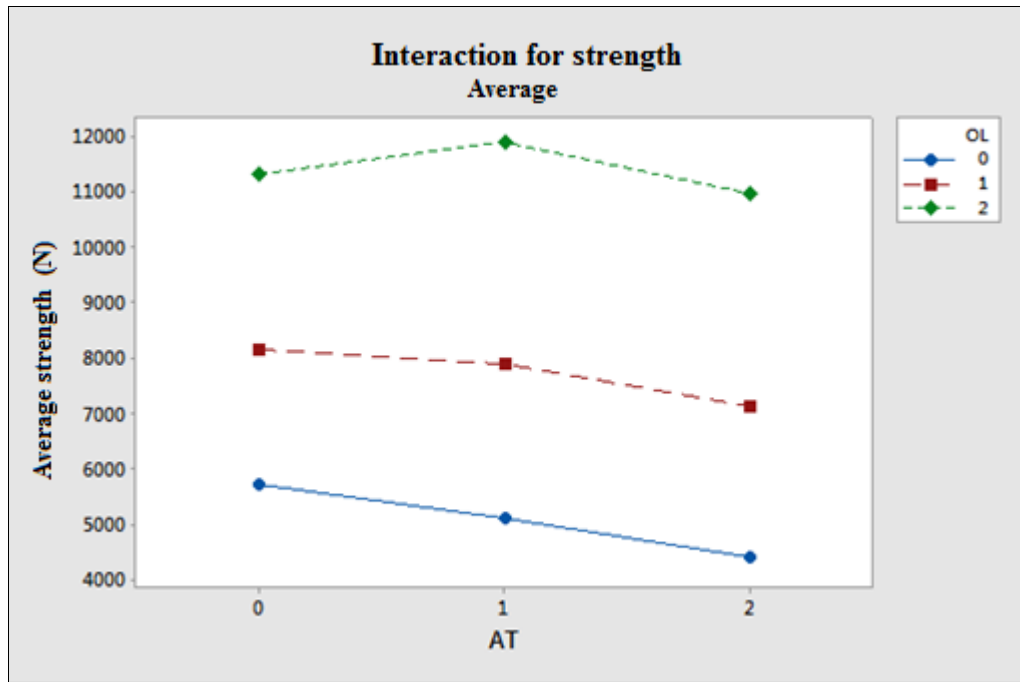
Figure 46 - Interaction between OL and YS vs. SLJ FL. Source: Author.



As discussed before, both variables affect positively the SLJ FL. However, it is possible to analyze that the increase of the SLJ FL, as a result of a larger OL, is more relevant for the similar HSS and dissimilar SLJ. The joints with 7mm of overlap presented a shorter difference among the failure load values of the different materials combination with the similar HSS configurations being the most resistant joints, the dissimilar joints the intermediate and similar AA joints the less resistant. For 12.5mm of OL, the difference between the configurations widens more but keeps the same

order between the different adherends configurations. When it comes to the longest OL of 25mm the order is still the same, however, the similar HSS presented a distinct improvement of SLJ FL, when compared to the other two material combinations. The dissimilar configurations presented failure load values closer to the similar AA SLJ.

Figure 47 - Interaction between OL and AT vs. SLJ FL. Source: Author.

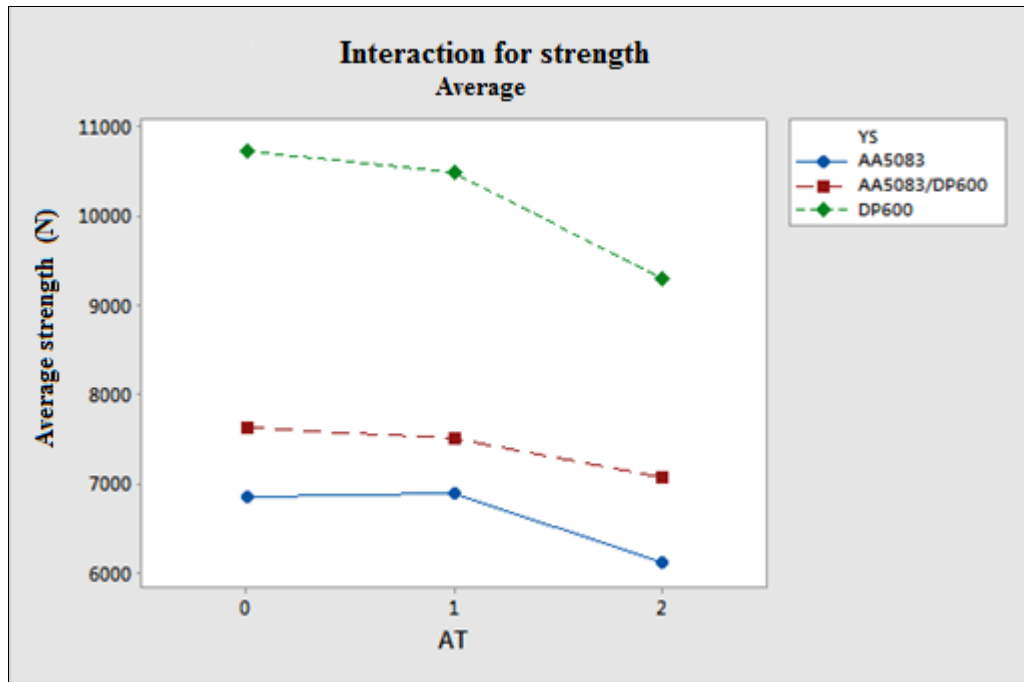


The next interaction analysis is about OL and AT. While the first positively affects the SLJ FL, the second affects negatively. Analyzing the Figure 47, it is possible to verify that the SLJ set with 7mm of OL have its FL decreased in a linear way, as the adhesive thickness increased. The 12.5mm of OL SLJ, despite also have its FL decreased, the effect was similar to the overall AT analysis described previously in this section, in which the SLJ FL drops more when going from 0.5 to 1mm than from 0.1 to 0.5mm. This may collaborate with the shape of the graph found in Figure 44. The SLJ set with 25mm, different from the other two discussed configurations, presented better joint FL with an AT of 0.5 than 0.1mm, being 1mm the one with the lowest FL. Contributing even more than the 12.5mm of OL SLJ for the behavior of the AT thickness effect curve, shown in Figure 45. This is different from what it is discussed for AT effect over SLJ effect, however, most studies are performed with high strength adherends (GRANT *et al.* (2009); Da SILVA *et al.* (2009); YANG *et al.*

(2014)) and it is known that this OL encompass more bending moment, as well as plastic strain. Both are discussed further in this chapter.

The last interaction analyzed was between AT and YS, is presented in Figure 48. The first affects negatively and the second positively the SLJ FL.

Figure 48 - Interaction between YS and AT vs. SLJ FL. Source: Author.

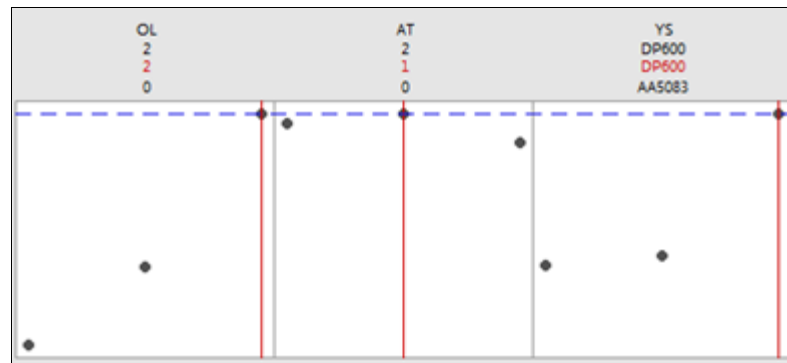


The similar AA SLJ presented and interaction with AT similar to the SLJ with 25mm of OL. Its FL results were higher when using an AT of 0.5mm than 0.1mm. The other two configurations (similar HSS and dissimilar SLJ) presented similar behavior: the joint FL decreased more changing the AT from 0.5 to 1mm than from 0.1 to 0.5mm. The similar AA SLJ are the configurations the ones with less YS, which makes it more suitable for plastic deformation (analyzed hereafter) to happen and may lead the interaction to this behavior.

4.1.1.7 Optimization

After analyzing the variables effects and its interactions, the last DOE analysis was the optimization of the SLJ FL by combining presented variables. The variables levels calculated and suggested by Minitab in order to maximize the output are presented in Figure 49.

Figure 49 - Output optimization. Source: Author.



The treatment that provided the highest FL was the number 0024, shown in Table 6, which was set with an OL of 25mm, HSS adherends and AT of 0.5mm. Based on what was discussed previously in this section about the variables effects, it is possible to analyze that the overlap length of 25mm encompass larger overlap area and, in consequence, increases the SLJ FL. Associated with HSS adherends it tends to minimize the effects of the higher levels of bending moment, as well as allow less plastic strains, due to the higher YS. Finally, as it was presented in Figure 47, the OL of 25mm presented better results when combined with the AT of 0.5mm. In addition, as in can be noticed in Figure 48, the SLJ with similar HSS adherends presented results close to each other when using 0.5 and 0.1mm of AT, despite the first was superior for this interaction.

4.1.2 Stress x strain curves analysis of plastic deformation

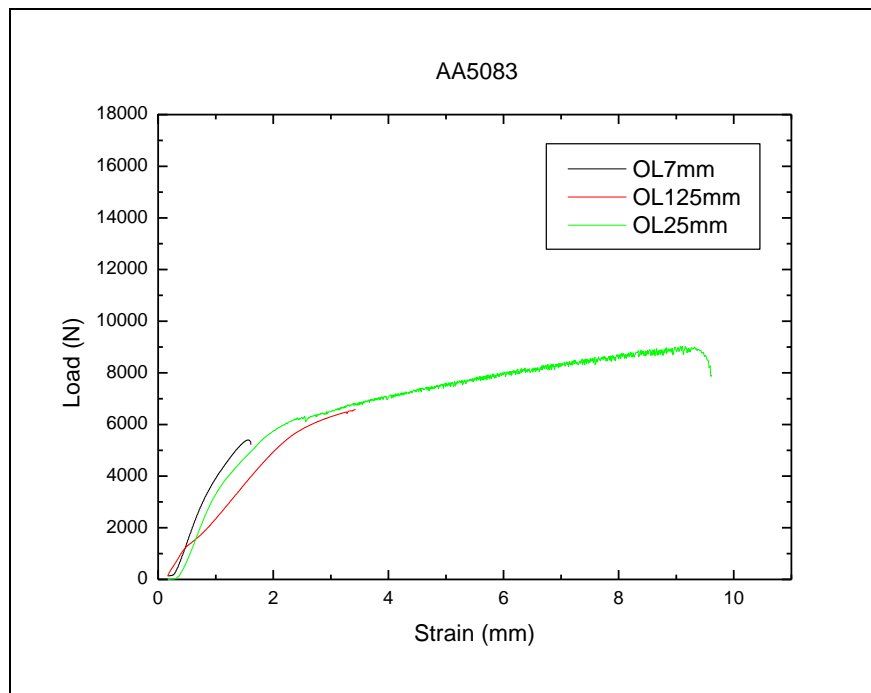
After analyzing the SLJ via DOE full factorial program, ANOVA, factors main effects and interactions, it was realized that some samples presented a behavior that differs from some adhesive bonding mechanical theories (HART-SMITH, 1994; GOLAND AND REISNER, 1944; VOLKERSEN, 1938). For example, the gain of SLJ FL as result of increasing the OL reduced as the first got longer. However, the decreasing of SLJ FL as a result of increasing the AT didn't happen for all the cases. Karachalios *et al.* (2013) stated that such theories are not strictly applicable when plastic deformation takes place in the SLJ. The stress strain curves from the tensile tests were then analyzed in order to investigate the incidence of plastic strain in the bonded joints. In addition, the dissimilar SLJ presented a behavior that deserves to

be investigated also, as its results of FL, for some cases, was closer to the HSS joints and, in other cases, closer to the AA joints.

4.1.2.1 Stress strain analysis of AA SLJ

Figure 50 presents the stress/strain results of the AA SLJ. As it is shown, the 7mm of OL SLJ seems to failure before the adherends face significant plastic deformation, with brittle failure characteristics, within the elastic region. The 12.5mm of overlap AA SLJ, however, seem to encompass some plastic deformation, characterizing an elastic-plastic failure, within the plastic region. And finally, the SLJ with overlap of 25mm failed within the plastic region, encompassing a large amount of plastic deformation.

Figure 50 - Stress strain curve from AA SLJ. Source: Author.



The AA SLJ with OL of 12.5mm, different from 7mm configurations, face some plastic strain, as it can be seen in Figure 50. The SLJ with 25mm of OL encompassed the highest plastic deformations of the AA SLJ, also shown in the stress/strain curves in Figure 50. These results might be related to two main aspects: the higher failure loads reached by these SLJ (due to the larger overlap length and larger bonded area, in consequence) associated to the low yield strength of the adherends cause these

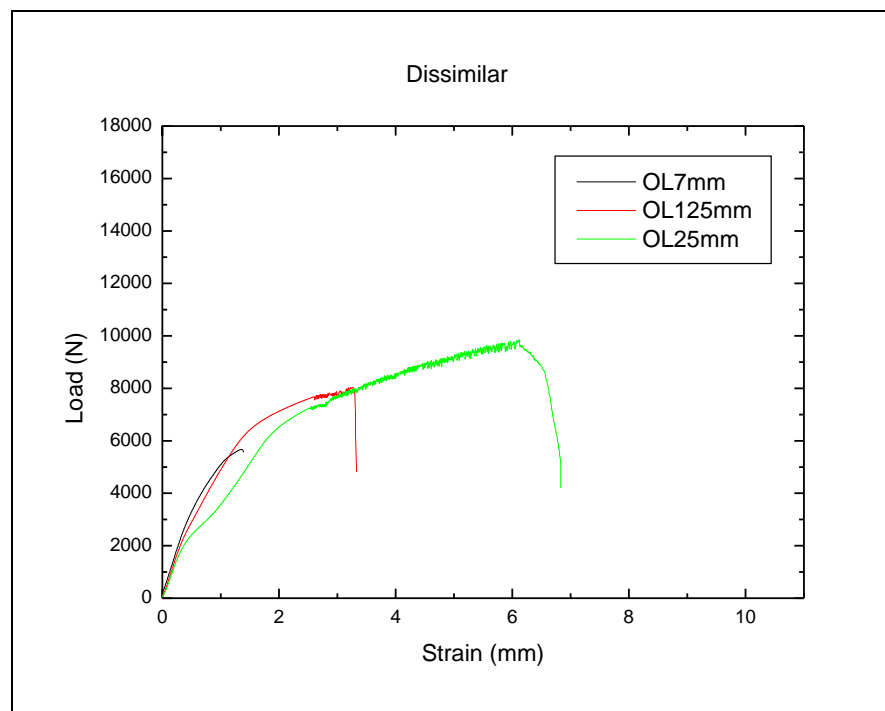
most significant deflections, what is expected for these cases, according to Grant et al. (2009); and the longer the overlap length the higher is the bending moment as well as the peeling stresses, in consequence, according to Silva and Nunes (2014) and Eq.3. Given this condition, the results from Da Silva et al. (2009), shown in Attachment C, can be related to the SLJ behavior presented here and in the sections 2.5.1 and **Erro! Fonte de referência não encontrada..** In their work, SLJ with adherends with 184 and 1260 MPa were tested and the results presented also a linear behavior (between OL and FL) when the failure happened within the elastic region. When it started to encompass plastic strain, the behavior was no longer linear and reduced the SLJ FL gain as function of OL.

Later in this chapter, in the DIC analyses, the plastic strains are related to the stress state of the bonded area, which is connected to bending moment and incidence of peeling stresses the edges of the bonded area.

4.1.2.2 Stress strain analysis of Dissimilar SLJ

The stress/strain curve, shown in Figure 51, presents the tensile tests results of the dissimilar SLJ.

Figure 51 - Stress strain curve from the dissimilar SLJ. Source: Author.



The 7mm of OL SLJ seems to break before the adherends face significant plastic deformation, failing within the elastic region, as the AA SLJ. Few relevance of inserting an HSS adherend is observed for this OL. The 12.5mm of OL dissimilar SLJ, however, presented significant plastic strain, as it can be seen in the stress/strain curve of Figure 51. It shows that the 12.5mm of OL dissimilar SLJ failed with plastic failure characteristics, which might show that the inserted HSS adherend seems to increase the joints resistance, encompassing, however, more plastic deformation as the failure load increased. This configuration presented values closer to the similar HSS than the AA SLJ. The dissimilar SLJ set with 25mm of OL presented also significant plastic deformation, as the 12.5 of OL SLJ. However, these configurations presented results closer to the AA SLJ, as shown previously in Figure 50. The 25mm of overlap SLJ encompassed the highest plastic deformations of the dissimilar SLJ (less than AA SLJ, however), as it can be seen in the stress/strain curve in Figure 50. The same assumptions of the AA5083 SLJ regarding bending moment, peeling stresses and plastic strain are observed here. The OL effect over the SLJ FL reduced as the first was increased. Later in this chapter, in the DIC analysis, the plastic strains in each adherend of the dissimilar SLJ will be analyzed and related to the stress state of the bonded area, which is connected to bending moment and incidence of peeling stresses the edges of the bonded area.

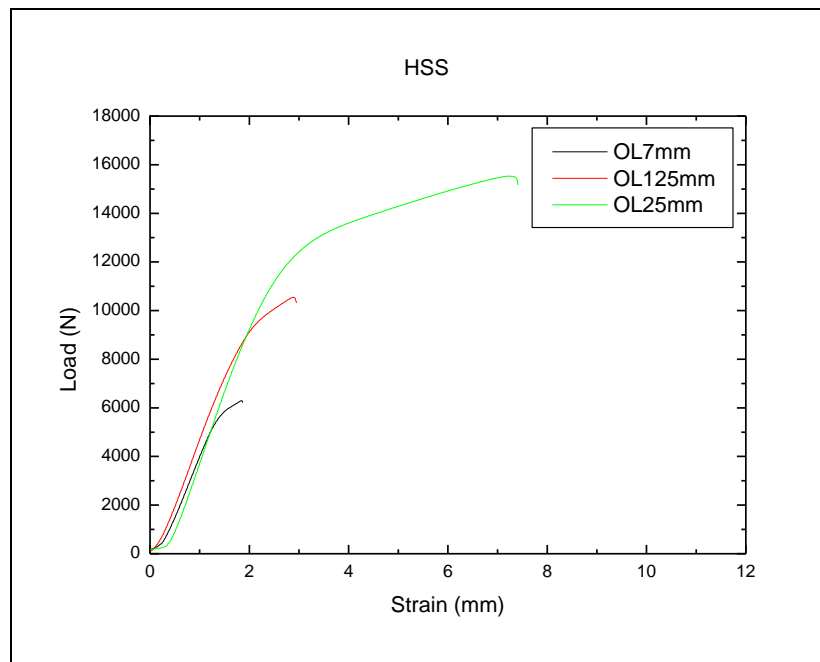
4.1.2.3 Stress strain analysis of HSS SLJ

It can be verified that for the HSS SLJ the 7mm of OL configuration presented a similar behavior if compared with of the other two equivalent material combinations. The joints failed within the elastic region, as it can be verified in the stress/strain curves in Figure 52. The HSS SLJ with 12.5mm of OL, however, behave different that the AA and dissimilar SLJ. Such joints also failed within the elastic region, encompassing irrelevant plastic strain until failure. In this case, the HSS adherends set as similar configuration seems to hold the bond together without relevant plastic strain, which let the adhesive layer develops more its shear strength (the main mechanical property of structural adhesives, as explained previously). This behavior was only noticed for OL of 7mm in the other materials configurations.

The stress/strain curve of Figure 52 shows that the 25mm of OL HSS SLJ presented similar results if compared to AA and dissimilar SLJ. It failed within the plastic region,

however with less plastic strain than the other two equivalent configurations. This was the first time that HSS SLJ presented plastic strain what might be related to the longer OL and higher failure load, as consequence of the larger area. As discussed before, the longer the OL the overlap length the higher is the bending moment as well as the peeling stresses, in consequence, Silva and Nunes (2014) and Eq.3. Also, increasing the OL increases SLJ FL, it makes the SLJ to encompass more plastic deformation, reducing the enhancement effect. However, as it can be analyzed in Figure 44, the HSS SLJ did not experience this. Different than AA and dissimilar SLJ, the OL effect over SLJ FL did not reduced notably as it got longer, fact that might be related to the use of HSS adherends, reducing the plastic strain of the joint, favoring the adhesive layer to develop better its shear strength. Deeper analyses about plastic strain at the adherends, stress state of the joints and presence of peeling stresses are done hereafter in the DIC section.

Figure 52 - Stress strain curve from HSS SLJ. Source: Author.



4.1.3 DIC analyses

In the previous section, it was presented the tensile-shear tests results, discussed the effects of the geometric variables overlap length and adhesive thickness as well as the adherends yield strength over the SLJ FL. Then, the behavior of the joints was

analyzed in order to verify elastic, elastic-plastic and plastic failure and its influence over the test results. In this section it was performed closer look on the SLJ during the tensile-tests with the aid of the DIC equipment in order to analyze the stress state of the joints. It was investigated the presence of plastic strains at the adherends, the distribution of the load along the adhesive layer and the presence of stress concentrators. The first, as explained previously, is related to the incidence of bending moment and peeling stresses. The second represents the stress state or load distribution of the bonded joint, which can be appropriated or not for the structural adhesive. The third represents a bad condition of stress state for the SLJ. The Table 8 presents an overview of the results detected by the DIC analysis, which will be discussed along this section.

Table 8 - DIC results summary. Source: Author.

OL	7			12.5			25		
SLJ Type	AA	Dissimilar	HSS	AA	Dissimilar	HSS	AA	Dissimilar	HSS
Plastic strain	Yes	Yes (AA)	No	Yes	Yes (AA)	No	Yes	Yes (AA)	Yes
Load distributed	Yes	Yes	Yes	No	Yes	Yes	No	No	Yes
Stress concentrator	Yes	No	No	Yes	Yes	No	Yes	Yes	Yes

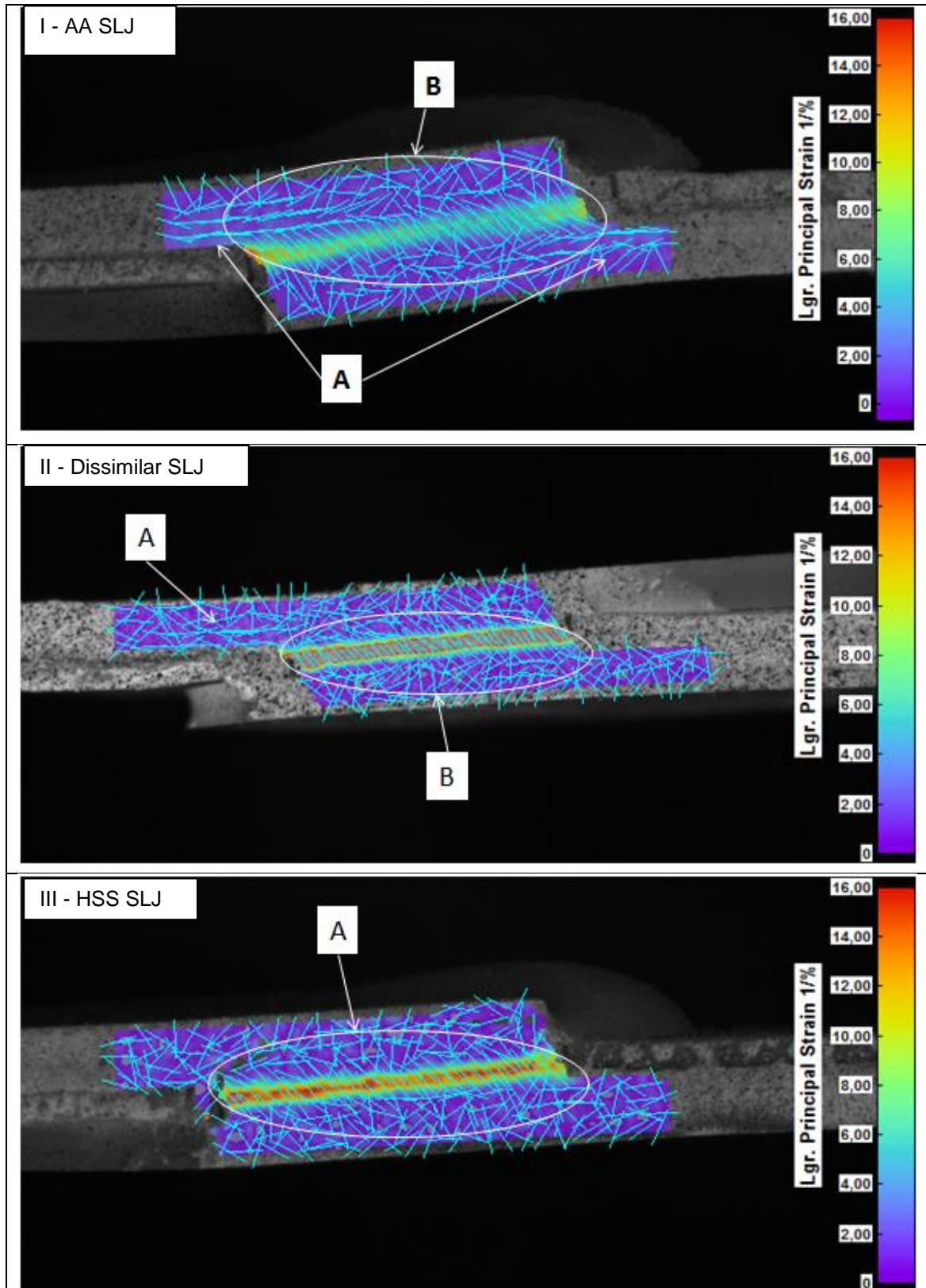
4.1.3.1 DIC analyses of the 7mm of overlap length

Figure 53 shows the DIC analysis of the SLJ with 7mm of OL with the three material combinations: similar AA5083, dissimilar and similar HSS DP600 adherends. It consists in stress state analyses of the SLJ at the failure moment.

The DIC analysis of the AA SLJ indicates, letter A in Figure 53-I, that it presented few relevant plastic strain at the adherends. The LaGrange vectors are concentrated in the same direction, parallel to the adherend, indicating elongation. The dissimilar SLJ presented also little relevant plastic strain, but only at the AA adherend, as indicated by letter A in Figure 53-II. The LaGrange vectors indicate the direction of the load barely parallel to the AA adherend side, indicating few plastic strain, also by elongation. Different from these two configurations, the DIC analysis of the HSS SLJ, shown in Figure 53-III, didn't present plastic strains at the adherends. The plotted LaGrange vectors are randomly orientated over the adherends surface, indicating no plastic strain in it. All the SLJ with 7mm of OL presented an adhesive layer fully under load, as indicated by letters B the AA and dissimilar SLJ and A for HSS in Figure 53.

The adhesive layers present a dense amount of perpendicular, indicating shear stress on it.

Figure 53 - DIC analysis of the SLJ with 7mm of OL. Source: Author.



The 7mm OL seems to deliver an interesting condition for the SLJ. As calculated by Eq.4, it encompasses the least misalignment if compared to the other two OL. That condition has reduced incidence of peeling stresses and bending moment, which is mostly induced by deflection and plastic strain at the adherends, according to Silva and Nunes (2014), Da Silva et al. (2009), Zhao et al. (2010) and Tsai and Morton (1994). Peeling stresses are the main responsible for bonded joints failures, according to Grant et al. (2009) and Da Silva, et al. (2009). Some plastic strains were found in the AA and dissimilar SLJ and might be related to the low yield strength of the adherends. However, the adhesive layer of all the 7mm of OL configurations remained under load and in shear. That means that the applied load is being resisted mostly by the adhesive layer, which has shear strength as its best mechanical property. This configures a very good stress state condition for bonded joints. It seems that the found plastic strain didn't affect too much the SLJ FL, which might be favored by the short overlap and the minimization of bending moment and peeling stresses. However, this may explain the failure loads presented for this configuration: AA SLJ with the lower average, dissimilar with intermediate average and HSS with the higher failure loads.

4.1.3.2 DIC analyses of the 12.5mm of overlap length

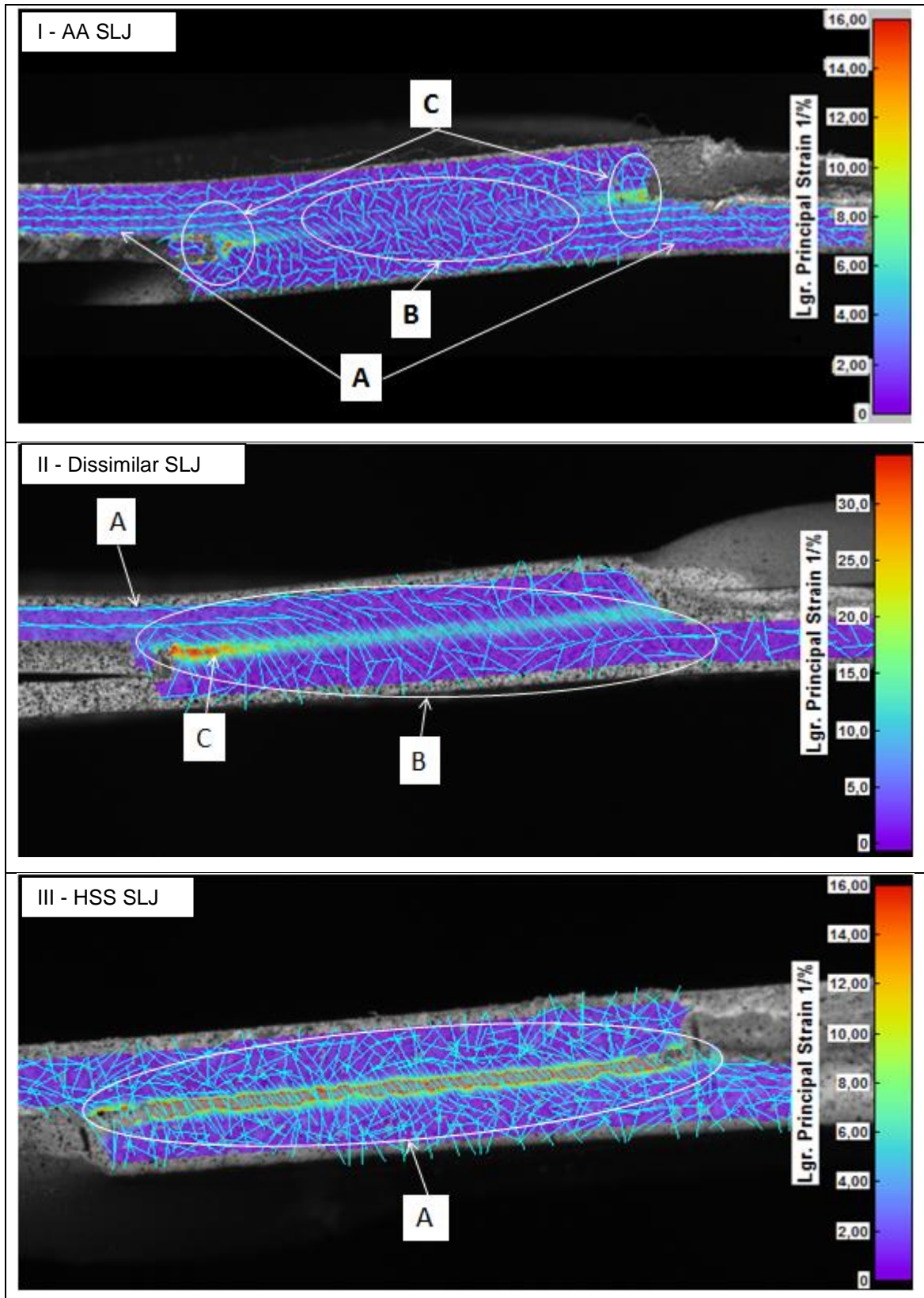
Figure 54 shows the DIC analysis of the SLJ with 12.5mm of OL for the three material combinations: AA5083, dissimilar and HSS DP600.

Different from the 7mm OL, the DIC analysis found relevant plastic strain in both adherends of the 12.5mm AA SLJ. That can be noted by analyzing the large amount of LaGrange vectors concentrated at the adherends in region of the edge of the overlap area (indicated by A in Figure 54-I). In addition, it can be seen that most of the applied load was not distributed along the adhesive layer (letter B in Figure 54-I). Just the edges of the adhesive layer are resisting most of the applied load, configuring a poor condition for the adhesive to develop its shear strength and indicating significant incidence of peeling stresses (letter C in Figure 54-I).

In the DIC analysis of the dissimilar SLJ with 12.5mm of OL, shown in Figure 54-II, the LaGrange vectors presented relevant plastic strain at the AA adherend – letter A – and no relevant strain at the HSS adherend. However, most of the applied load was distributed through the adhesive layer, indicated by letter B. This configuration

presented a stress concentrator region, shown by C, that seems to initiate a crack and propagate it until the joints failure.

Figure 54 - DIC analysis of the SLJ with 12.5mm of OL. Source: Author.



The HSS SLJ with 12.5mm of OL, show in Figure 54-III, presented no plastic strain at the adherends, as the LaGrange vectors seem to be random. As the previous HSS case, the applied load was distributed through the whole adhesive layer, as indicated by letter A in Figure 54-III. No stress concentrators were visualized, indicating a really good stress state for the SLJ.

As discussed in the previous sections, the effect of increasing the SLJ FL by setting a larger OL is very different for the different adherends materials configuration. The AA SLJ, when changing from 7 to 12.5mm of OL, no longer presented a stress distribution condition close to pure shear, presented larger stress concentrators at both edges of the bonded area, plastic strain in both adherends and most of the adhesive layer free of stress. The dissimilar SLJ presented even larger stress concentrators at the AA adherend side (changing from 7 to 12.5mm) and also plastic strain at it. However, this configuration kept the adhesive layer under load until the failure. Both joints configuration (AA and dissimilar SLJ) encompassed significant plastic strain, which led to bending moment and peeling stresses incidence. The 12.5mm of OL HSS SLJ configurations, however, remained in the elastic region until the SLJ failure and the whole adhesive layer resisted to the applied load, creating a very good stress condition of pure shear, similar to the HSS SLJ with 7mm of OL.

These analyses can justify the failure loads presented in Figure 44. Increasing the OL increases also the bonded area and may enhance the SLJ FL. However, for the AA SLJ it resulted in a worse stress distribution, plastic strains surged at the adherends, stress concentrators became more intensive and most of the adhesive layer didn't resist the applied load. Increasing the OL produced less gain of joints FL for the AA SLJ than the other materials configuration. The dissimilar SLJ was less affected, although also presented a worse stress condition, with more plastic deformations at the AA adherend and a more intensive stress concentrators region, compared with the previous shorter OL. However, as it could keep the full adhesive layer under load, which may justify the fact that the failure load for the dissimilar SLJ with 12.5mm OL had was closer than the HSS than the AA SLJ. The HSS SLJ was the only that kept a very similar stress distribution to the 7mm case (similar to pure shear), taking more advantage of the OL effect than the other materials configurations.

4.1.3.3 DIC analyses of the 25mm of overlap length

Figure 55 present the DIC analysis of the SLJ with 25mm of OL. That was the longest overlap length configuration used in this work and, consequently, obtained the highest failure load averages.

The AA SLJ with 25mm of OL, shown in Figure 55-I, followed the tendency observed in the respective joint configuration with 12.5mm. The LaGrange vectors, indicated by letter A, presented large amounts of plastic strain in both adherends. The letter B shows that most of the load was not distributed through the adhesive layer. As a result, stress concentrators were visualized in the both edges of the bonded area, indicated by letter C.

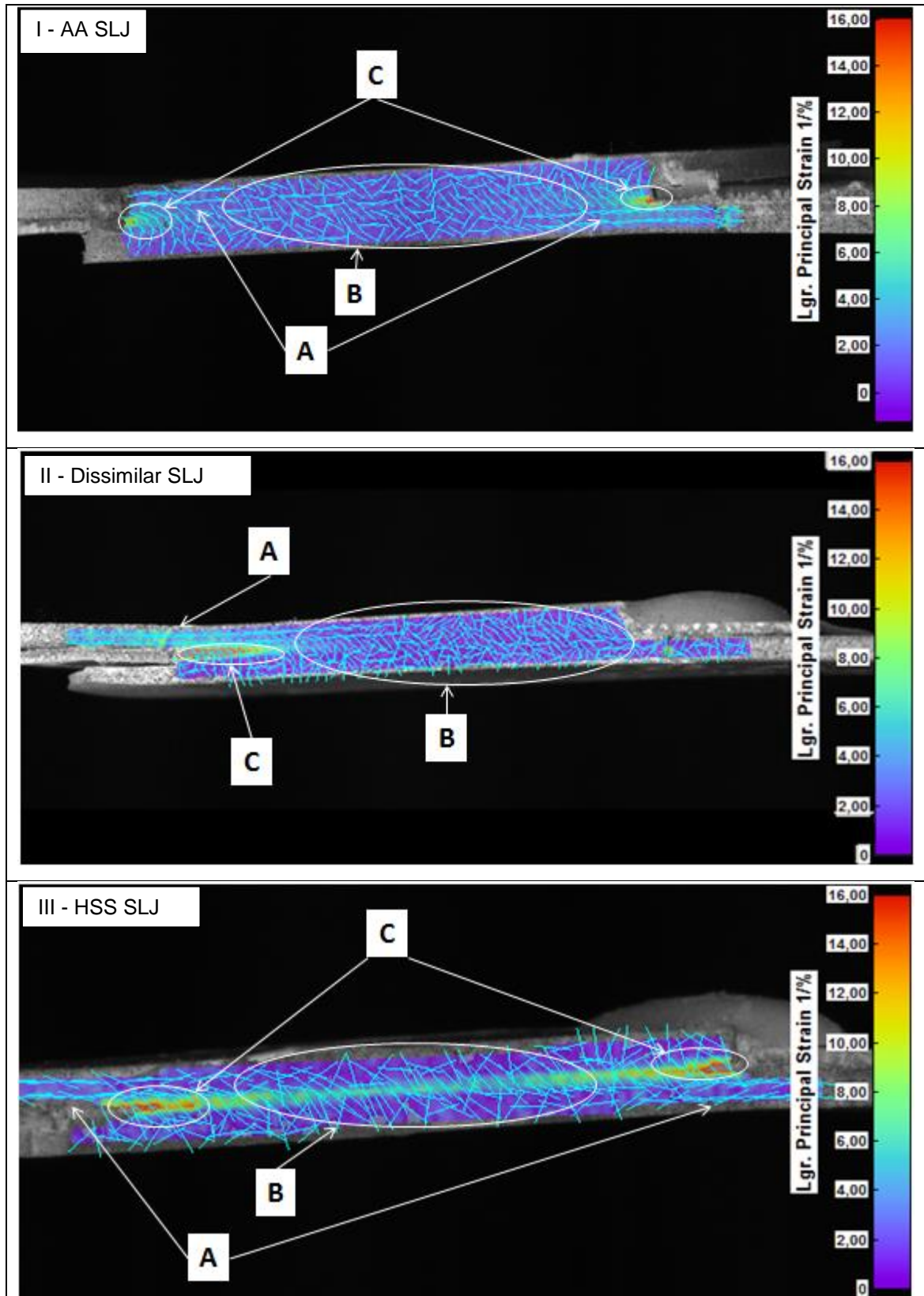
The dissimilar SLJ with 25mm DIC analysis results, shown in Figure 55-II, differ considerably from its similar SLJ results with 12.5mm of overlap. The letter A indicates large plastic strains were found at the AA adherends, as the previous dissimilar configuration. However, as shown by letter B, most of the applied load was not distributed along the adhesive layer. This can be noticed by analyzing the remarkable stress concentrator region at the edges of the bonded area by the AA adherend side, indicated by letter C. As consequence, the applied load is being resisted only by the edge of the bonded area. The failure of this joint, in consequence, resulted from a crack propagation originated in this area.

The DIC analysis of the HSS SLJ with 25mm of OL is shown in Figure 55-III. It presented differences and similarities comparing with the two previous equivalents HSS SLJ with 7 and 12.5mm. The adherends, for the first time when using HSS SLJ, presented plastic strain (letter A in Figure 55-III), as indicated by the aggregation LaGrange vectors parallel to the adherend. However, despite the detected plastic strain, the whole adhesive layer remained under load until the joints failure (indicated by B), which is the most appropriate condition for the adhesive to develop its shear strength. Stress concentrators were identified in the edges of the bonded area (pointed by letter C).

It could be seen that the joints with 25mm of OL presented similarities to 12.5mm, for the AA SLJ, but differences for the dissimilar and HSS SLJ. The AA SLJ stress state was even worse, as more plastic strain and stress concentrators were found. The dissimilar SLJ presented more plastic strain at the AA adherend and its stress state

was considerably worse than the previous configuration, as of the applied load was not being resisted by most of the adhesive layer.

Figure 55 - DIC analysis of the SLJ with 25mm of OL. Source: Author.



The HSS DP600 SLJ for the first time in these analyses, presented plastic strain at its adherends. Stress concentrators were identified in the bonded joint, however its adhesive layer remained under load until failure. The stress distribution, different from the previous HSS SLJ DIC analysis, was not close to pure shear.

It could be noticed, once again, the relation between OL, plastic strain, bending moment and peeling stresses. As discussed, increasing the OL in order worsen the stress state condition, which, as analyzed, augmented or generated bending moment and peeling stresses. Not only better SLJ FL is obtained. All the 25mm joints presented stress concentrators. Also, the adherends of these configurations presented relevant plastic strain, which created bending moment and peeling stresses mainly at the edges of the overlap area, primarily the AA and dissimilar SLJ. The HSS SLJ, however, despite the presence of stress concentrators, could keep a reduced amount of strain at the adherend and the full adhesive layer under load, reaching higher values of failure load, as shown in Figure 44. This might indicate the importance of higher yield strength when setting the SLJ with longer OL, in order to better use its effect.

4.1.3.4 DIC analysis of the adhesive thickness analysis

The adhesive thickness, as commented before, presented less influence over the SLJ FL. Several authors (GRANT *et al.*, 2009; DA SILVA *et al.*, 2009; SILVA and NUNES, 2014) state that increasing the adhesive thickness should decrease the SLJ FL. However, as presented in the tensile test results in

In this chapter the results from the experimental program presented on the last chapter are presented and discussed. **Erro! Autoreferência de indicador não válida.** presents the failure loads of all the 27 SLJ configurations.

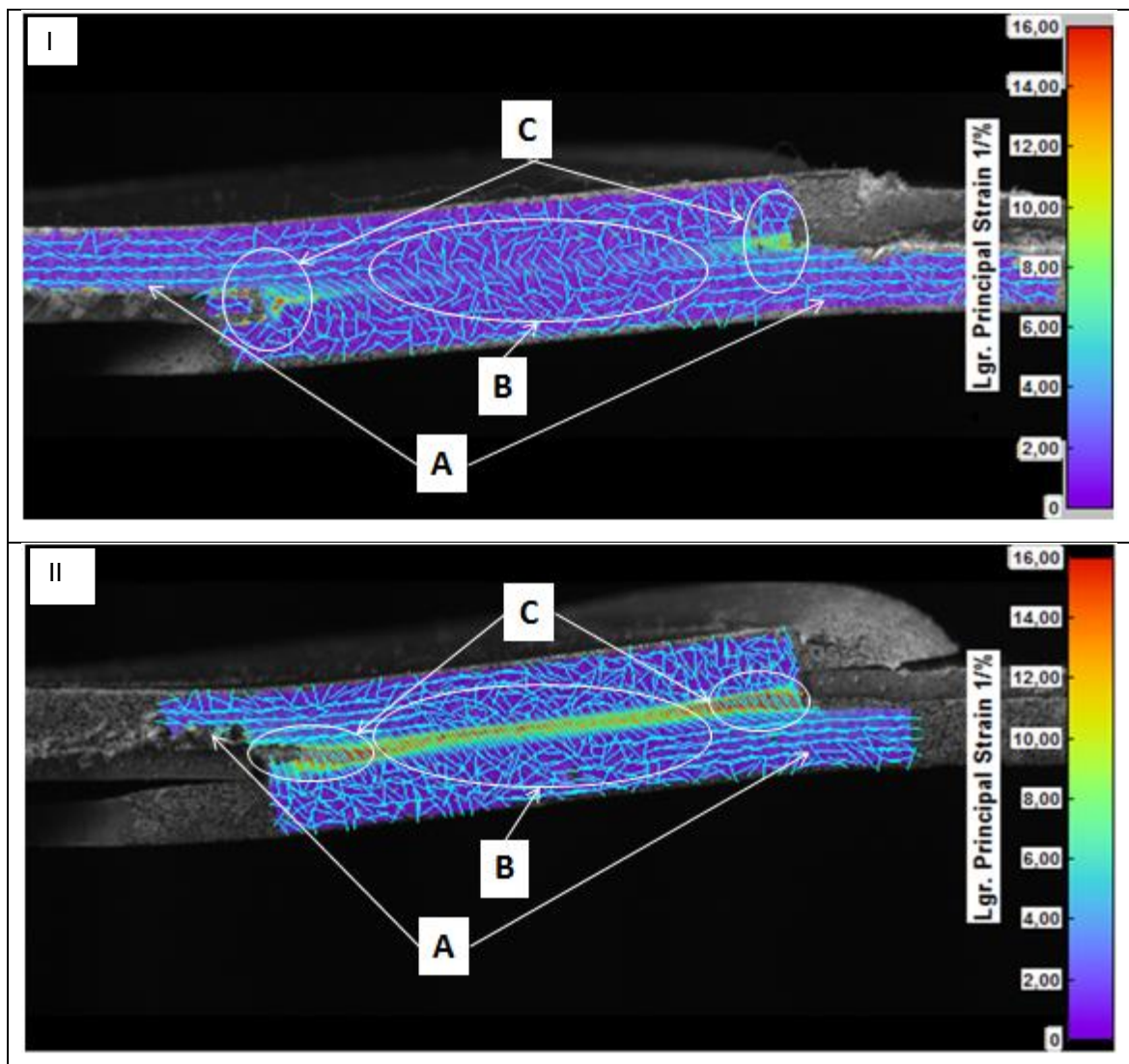
Table 6, some configurations presented higher average FL when set with 0.5mm than with 0.1mm, i.e.:

- AA SLJ OL 12.5mm: This configuration presented a failure load of 6491.30N using an AT of 0.1mm versus a failure load of 6926.02N with an AT of 0.5mm;
- AA SLJ OL 25mm: This configuration presented failure loads of 8736.9N and 9074.8N when using AT of 0.1 and 0.5, respectively;

- Dissimilar SLJ 25mm: The failure load of the SLJ with and AT of 0.1mm was 9167.66N and with 0.5mm was 9609.14N;
- HSS SLJ 25mm: The average failure load of the joints with 0.1mm of AT was 16089.24N and with 0.5mm was 17017.84N.

No SLJ with 7mm of OL presented this fact of higher failure load when using an AT of 0.1 than 0.5mm. The AA SLJ of aluminum presented for both 12.5 and 25mm of OL configurations, while the dissimilar and HSS SLJ just presented for the joints with 25mm of OL. It might be possible to analyze that all the cases that presented higher values of failure load for 0.1mm than for 0.5 were the ones which encompassed the highest amount of plastic deformation for the respective material combination (similar AA, dissimilar and similar HSS).

Figure 56 - DIC analysis of AT effect. Source: Author.



However, the DIC analysis just detected differences among different adhesive layer thicknesses only for the AA SLJ with 12.5mm, presented in Figure 56. It is possible to verify that both joints presented plastic deformation at the adherends and stress concentrators in the edges of the bonded area (letters A and C in Figure 56 I and II). However just the SLJ with 0.5mm of AT had the adhesive layer under load until the failure (letter B in Figure 56-II), which might justify the higher FL. The second condition is better for the SLJ FL, as commented in the previous section, as it has a larger adhesive area resisting to the applied load and a more uniform stress distribution.

Except the AA SLJ with 12.5mm, in the other cases that presented a higher failure load for 0.5mm of AT than for 0.1mm, no remarkable difference was detected by the DIC method. For all the analyzed cases, however, it was noticed that this fact is associated with occurrence is involved with relevant plastic strain. All the short SLJ with OL of 7mm presented few or irrelevant plastic strain. In consequence it had its FL reduced as the adhesive layer got thicker, following what the main structural adhesives theories state for SLJ free of strain, as described by (GRANT *et al.*, 2009; Da SILVA *et al.*, 2009). For the SLJ with 12.5mm OL cases, however, only the dissimilar and HSS SLJ, presented irrelevant plastic strain and the same behavior regarding increasing AT and decreasing FL, while the AA SLJ presented the commented effect of inversion between 0.1 and 0.5mm AT failure loads. According to Karachalios *et al.* (2013), when SLJ face plastic strain, the deformation of the adhesive layer (ductile adhesives mainly) may enhance the stress state condition and reducing energy of the cracks propagation. In the other hand, thinner layers may propagate faster the cracks as it has limited strain capacity, reducing the joint FL. In this case, the 0.5mm layer is five times thicker than 0.1mm but seems to still not thick enough to encompass the defects commented before, such as voids and micro cracks, as stated by Da Silva *et al.* (2009). The AT of 1mm seems to be excessive for every case in this study, since, in general, it reduced the SLJ. Further analyses are needed in order to better understand the AT effect when relevant plastic strain is involved and affects significantly the stress state of a SLJ.

4.1.4 Failure mode analysis

The failure pattern of a SLJ helps to understand the mechanical tests of it, according to the ISO 10365. The standard, as presented in 3.2.4 section, divides the failure patterns in two main groups referring to adherends and adhesives failure. The first occurs when the joint fails due to an adherends break or delamination. The second occurs when the failure happens in the adhesive or in the interface between the adhesive and the adherend, bringing up more sub-classifications, as presented in Table 5. According to Pocius (2012), an adhesive bonded joint should be designed in order to have adhesive failure and not adherends. In this work, three main types of failure were found: a) special cohesive failure (SCF); b) adhesion failure (AF) and; c) adhesion and cohesion failure with peeling (ACFP). Xu et al. (2013) state that the cohesive failure – a type of adhesive failure when the bonded joint fail occurs within the adhesive layer – is the most desirable as it assures the use of the maximum strain energy by the weaker part of the joint, the adhesive. The AF is related to unconformities in the surface preparation, brittle adhesives or wedge effect, as the one presented in Figure 7. The ACFP is an AF associated with the incidence of peeling stresses. In practice, both AF and ACFP might demand attention, due to the fact that they are related to aspects that weaken the SLJ FL – such as peeling stresses and stress concentrators, as commented in the previous sections.

Figure 57 – Failure modes of the SLJ: geometric aspects

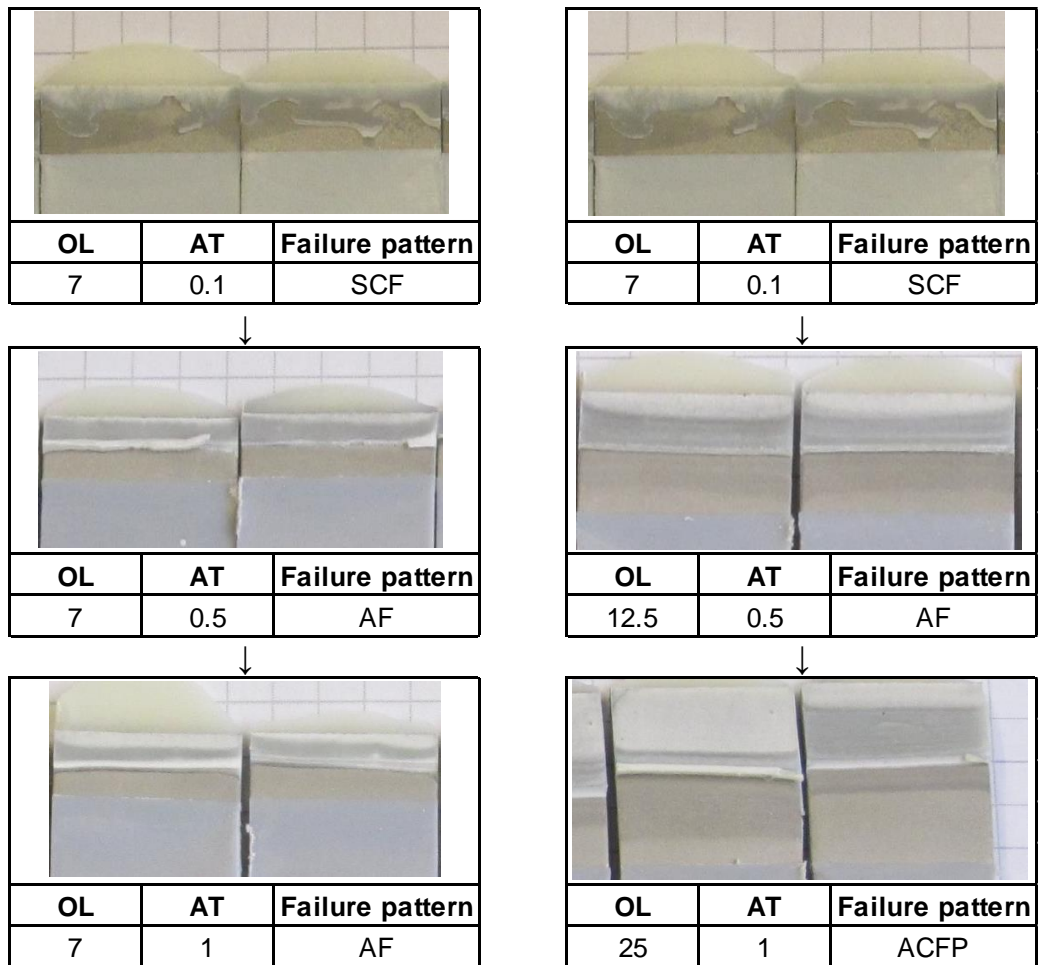


Figure 57 presents a resume of the resultant failure modes observed when changing the OL and AT levels. It can be seen that increasing the AT changed the failure mode from SCF to AF. In this case, only the AT with 0.1mm of AT remained as SCF while 0.5 and 1mm presented AF failures. Increasing the OL produced similar effect. While the OL with 7mm resulted in a CF, the 12.5mm resulted in a AF and 25mm ACFP. The AA adherends of the configurations with 12.5 and 25mm of OL presented elongation of the length.

Figure 58 – Failure modes of the SLJ: YS aspects

		
OL	Aderends	Failure pattern
25	AA	AF
↓		
		
OL	Aderends	Failure pattern
25	DIS	AF
↓		
		
OL	Aderends	Failure pattern
25	HSS	CF

The adherends YS produced an expected result. As shown in Figure 58, the longest OL of 25mm, which encompass more misalignment and bending moment, only resulted in a CF for the similar HSS treatments. The similar AA had an equally split AF. The dissimilar SLJ despite also resulted in an AF, held more adhesive in the HSS adherend, which might indicate that the failure was an effect of a crack propagation that resulted from the AA adherend plastic strain.

Akpinar et al. (2013) presented also SCF and CF in their work as result of tensile shear tests in SLJ, shown in Attachment G. In this case, an AT of 0.1mm was used and adherends of the AA 2024-T3, which has around 350 MPa of YS. According to Xu et al. (2013), CF represents the ideal condition for SLJ failure. However, as discussed previously, most works that study SLJ and its variables are done with high strength adherends and thin adhesive layers (usually no more than 0.3mm), Da Silva et al. (2009). The AF and ACFP analyzed in this work might be related to the presence of plastic strain at the adherends and peeling stresses. As discussed

previously, these are related mainly to long OL and low YS. In addition, Grant et al. (2009) state that increasing the AT results in larger bending moment, which also adds peeling stresses to the SLJ.

Another important observation is that the dissimilar SLJ seems to take advantage of the HSS adherends YS as it holds more the adhesive layer until failure, being less affected by bending moment and peeling stresses at this side.

5 CONCLUSIONS

Similar AA, HSS and dissimilar SLJ were tested and analyzed in this work in order to verify the influence of the OL, AT and YS over the FL and stress state of SLJ. Tensile tests and DIC analyses were performed and the main conclusions are:

-The incidence of plastic strains at the adherends when load is being applied changes the stress state of the SLJ, influencing the joints FL. It must be considered when changing the OL, AT or YS;

-The OL presented the larger influence over SLJ FL. Increasing the first increased the second. However, more bending moment, peeling stresses and, in some cases, plastic strain are associated with OL increasing, which worsens the stress state of the SLJ and handicaps the FL;

-The adherends YS presented noticeable influence over the SLJ FL. When longer OL are set, using a high YS adherend is recommended as it minimizes the amounts of plastic strains, resulting in a better stress state;

-The AT had less influence over the SLJ FL than the other two analyzed variables, though thicker adhesive layers should be avoided. The AT of 1mm used in this work, reduced the joints FL remarkably;

-As the OL, YS and AT impact the structures mechanical properties and also its cost and weight. Then, a business case of a new or changed bonded structure must accomplish an analysis over these variables;

-The DIC analysis is important for a richer mechanical characterization. It supplies information such as load distribution, stress state of the joint, presence of ending moment and peeling stresses to increment tensile-shear tests results.

6 FUTURE WORKS

By the end of this work, some future developments are identified and recommended below:

-Comparative study between adhesive bonding and rivets for aircrafts industry, encompassing mechanical and corrosion properties, as well as overall costs;

-Comparative study among adhesive bonding and RSW for automotive industry, encompassing weight reduction, fuel efficiency, crashworthiness, mechanical and corrosion properties, as well as overall costs;

-Viability study of adhesive bonding as a hybrid joining method to be used along with RSW (weldbonding), rivets and other techniques;

-Theoretical and experimental study comparing the main adhesive bonding and SLJ theories for dissimilar materials applications;

-Further works are necessary in order to better understand the influence of plastic strains over the stress state of SLJ and also of the OL, AT and YS over the joints failure pattern.

REFERENCES

Adhesive and glue, Adhesion theories, available at: <www.adhesiveandglue.com>, accessed in 05 of December of 2016.

Adhesives and Sealants Council, Safer cars with adhesives, 2015, available at: <www.adhesives.org/adhesives-sealants/market-overview-applications>, accessed in 30 of May of 2016.

AKPINAR, S. et al. The effect of the spew fillet on an adhesively bonded single-lap joint subjected to bending moment. *Composites Part B: Engineering*, v. 55, p. 55-64, 2013.

ASTM D907-15, Standard Terminology of Adhesives, ASTM International, West Conshohocken, PA, 2015.

ASTM D1002-10, Standard Test Method for Apparent Shear Strength of Single-Lap-Joint Adhesively Bonded Metal Specimens by Tension Loading (Metal-to-Metal), ASTM International, West Conshohocken, PA, 2010

BAMBERG, P.A.M.G.P. et al. Tensile Stress Analyses through Digital Image Correlation of Single Lap Joints of High Strength Steel and Aluminum Alloy Using Adhesive Bonding. In: *Materials Science Forum*. Trans Tech Publications, 2017, p. 363-368.

BARTCZAK, B.; MUCHA, J.; TRZEPIECIŃSKI, T. Stress distribution in adhesively-bonded joints and the loading capacity of hybrid joints of car body steels for the automotive industry. *International Journal of Adhesion and Adhesives*, v. 45, p. 42-52, 2013.

BENEVENTO, M. *Adhesive Opportunities and Outlook in Light Vehicles*, 2015. Available at: <www.adhesives.org>, accessed in 20 of October of 2016.

BRISKHAM, P. et al. Comparison of self-pierce riveting, resistance spot welding and spot friction joining for aluminium automotive sheet. SAE Technical Paper: 2006-01-0774, 2006.

CARLE, D.; BLOUNT, G. The suitability of aluminium as an alternative material for car bodies. *Materials & design*, v. 20, n. 5, p. 267-272, 1999.

COELHO, R.S. Friction-stir Dissimilar Welding of Aluminium Alloy to High Strength Steels: Mechanical Properties and Their Relation to Microstructure. *Materials Science and Engineering: A*, 556, p. 175-183, 2012.

Da SILVA, L.F.M. et al. Effect of material, geometry, surface treatment and environment on the shear strength of single lap joints. *International Journal of Adhesion and Adhesives*, v. 29, n. 6, p. 621-632, 2009.

Da SILVA, L.F.M.; ÖCHSNER, A.; ADAMS, R.D. *Handbook of adhesion technology*. Springer Science & Business Media, Heidelberg, 2011.

Da SILVA, L.F.M. et al. *Testing adhesive joints: best practices*. John Wiley & Sons, Weinheim, 2012.

Da SILVA, L.F.M.; ÖCHSNER, A.; ADAMS, R.D. *Handbook of adhesion technology*. Springer Science & Business Media, Heidelberg, 2011.

DILLARD, D. *Advances in structural adhesive bonding*. Elsevier, Cambridge, 2010.

DILL, E.H., *Continuum Mechanics: Elasticity, Plasticity, Viscoelasticity*. CRC Press. Germany, 2006.

DIN EN 1465:2009-07, *Adhesives – Determination of tensile lap-shear strength of bonded assemblies*, Deutsches Institut für Normung, Berlin, 2009.

DUNN, D.J. *Adhesives and sealants: technology, applications and markets*. iSmithers Rapra Publishing, Shropshire, 2003.

European Aluminum, Automotive and transport: Aluminum in use. Available at <www.european-aluminium.eu/>, accessed in 05 of December of 2016.

GOLAND, M; REISSNER, E. The stresses in cemented joints. Journal of applied mechanics, v.11, n.1, p. A17-A27, 1944.

GRANT, L.D.R.; ADAMS, R.D.; Da SILVA, L.F.M. Experimental and numerical analysis of single-lap joints for the automotive industry. International journal of adhesion and adhesives, v. 29, n. 4, p. 405-413, 2009.

HART-SMITH, L.J. The key to designing durable adhesively bonded joints. Composites, v. 25, n. 9, p. 895-898, 1994.

HER, S. Stress analysis of adhesively-bonded lap joints. Composite structures, v. 47, n. 1, p. 673-678, 1999.

ISO EN. 10365:1992, Adhesives - Designation of main failure patterns, Geneva, 1992.

HUSSEY, R.J.; WILSON, J. Structural Adhesives: Directory and Databook. Springer Science & Business Media, 1996.

JAMESTOWN, Cost advantages of the adhesive bonding technique, available at: <<http://www.jamestowndistributors.com/>>, accessed in: 10 of November of 2016.

KARACHALIOS, E.F.; ADAMS, R.D.; Da SILVA, L.F.M. Single lap joints loaded in tension with high strength steel adherends. International Journal of Adhesion and Adhesives, v. 43, p. 81-95, 2013.

KARACHALIOS, E.F.; ADAMS, R.D.; Da SILVA, L.F.M. Single lap joints loaded in tension with ductile steel adherends. International Journal of Adhesion and Adhesives, v. 43, p. 96-108, 2013.

KINLOCH, A. J. Adhesion and adhesives: science and technology. Chapman and Hall, London, 1987.

LEADLEY, S.R.; WATTS, J.F. The use of monochromated XPS to evaluate acid-base interactions at the PMMA/oxidised metal interface. The Journal of Adhesion, v. 60, n. 1-4, p. 175-196, 1997

MONTGOMERY, D.C. Design and analysis of experiments. John Wiley & Sons, 2008.

PLASTECH, Optimal bonding for industrial constructions, 2011, available at: <www.plastech.biz>, accessed in 05 of December of 2016.

POCIUS, A.V. Adhesion and adhesives technology: an introduction. Carl Hanser Verlag GmbH Co KG, Munich, 2012.

PORTAL ACTION, Cálculo e interpretação do P-Valor, Available at: <www.portalaction.com.br>, accessed in 10 of October of 2016.

Science of adhesion, Adhesives and Sealants Council, 2015, available: <www.adhesives.org/adhesives-sealants/science-of-adhesion>, accessed in 30 of May of 2016.

SILVA, T.C.; NUNES, L.C.S. A new experimental approach for the estimation of bending moments in adhesively bonded single lap joints. International Journal of Adhesion and Adhesives, v.54, p. 13-20, 2014.

SINGH, A.K. Mechanics of solids. PHI Learning Pvt. Ltd., New Delhi, 2007.

The aluminum joining manual, European aluminum association, 2015, available at: <www.drivealuminum.org/research-resources/2015-joining-manual>. Accessed in 30 of May of 2016.

TSAI, M.Y.; MORTON, J. An evaluation of analytical and numerical solutions to the single-lap joint. *International Journal of Solids and Structures* 31.18, p. 2537-2563, 1994.

TSAI, M.Y.; MORTON, J. Three-dimensional deformations in a single-lap joint. *The Journal of Strain Analysis for Engineering Design*, v. 29, n. 2, p. 137-145, 1994.

VOLKERSEN, O. Die Nietkraftverteilung in zugbeanspruchten Nietverbindungen mit konstanten Laschenquerschnitten. *Luftfahrtforschung*, 15:41–7, 1938.

XU, W. et al. Tensile and fatigue properties of weld-bonded and adhesive-bonded magnesium alloy joints. *Materials Science and Engineering: A*, v. 563, p. 125-132, 2013.

YANG, L. et al. Measure Strain Distribution Using Digital Image Correlation (DIC) for Tensile Tests: Final report. *Auto/Steel Partnership*, 2010.

ZHAO, X.; ADAMS, R.D.; Da SILVA, L.F.M. A new method for the determination of bending moments in single lap joints. *International Journal of Adhesion and Adhesives*, v.30, n. 2, p. 63-71, 2010.

APPENDICES

APPENDIX A – Order of experiments runs (Part I)

OrdemPad	OrdemEns	OL	AT	YS	FL
67	1	1	1	0	6759
28	2	0	0	0	5384,2
127	3	2	0	0	8478,5
34	4	0	2	0	3784,6
13	5	1	1	0	7308
47	6	2	0	1	9283
120	7	1	0	2	9985,3
79	8	2	2	0	8701,1
52	9	2	2	0	8577,3
97	10	1	2	0	5823,2
89	11	0	2	1	4396,3
99	12	1	2	2	8430,7
21	13	2	0	2	16366,8
54	14	2	2	2	15165,4
57	15	0	0	2	6178
92	16	1	0	1	7873,8
15	17	1	1	2	8793,7
9	18	0	2	2	4844,9
36	19	0	2	2	5004
42	20	1	1	2	9431,8
23	21	2	1	1	9750,2
93	22	1	0	2	9489,1
61	23	0	2	0	3733,9
69	24	1	1	2	9048,5
124	25	1	2	0	6288,7
129	26	2	0	2	16499,4
43	27	1	2	0	5984,7
66	28	1	0	2	10549
50	29	2	1	1	9636
20	30	2	0	1	8938,8
82	31	0	0	0	5185,8
131	32	2	1	1	9423,7
49	33	2	1	0	9204,6

APPENDIX B – Order of experiments runs (Part II)

OrdemPad	OrdemEns	OL	AT	YS	FL
3	34	0	0	2	6038,2
81	35	2	2	2	14331,4
14	36	1	1	1	7674,4
41	37	1	1	1	7402,6
25	38	2	2	0	8593,3
46	39	2	0	0	8914,2
45	40	1	2	2	8266,8
65	41	1	0	1	8037
122	42	1	1	1	8227,6
17	43	1	2	1	7138,9
112	44	0	1	0	4804,7
71	45	1	2	1	6930,7
51	46	2	1	2	16567,7
59	47	0	1	1	5118,4
106	48	2	2	0	8627,1
38	49	1	0	1	7813,5
58	50	0	1	0	4828
53	51	2	2	1	9589,4
60	52	0	1	2	5665,4
26	53	2	2	1	9592,6
114	54	0	1	2	5170,5
88	55	0	2	0	3786,2
105	56	2	1	2	17382,5
11	57	1	0	1	8160,8
90	58	0	2	2	4769,3
18	59	1	2	2	7991,2
55	60	0	0	0	5403,5
86	61	0	1	1	5111,9
4	62	0	1	0	4971,9
109	63	0	0	0	5347,3
118	64	1	0	0	6571,8
76	65	2	1	0	9253,7
134	66	2	2	1	9380,3

APPENDIX C – Order of experiments runs (Part III)

OrdemPad	OrdemEns	OL	AT	YS	FL
40	67	1	1	0	6556,4
6	68	0	1	2	5404,3
77	69	2	1	1	9781,5
73	70	2	0	0	9028,5
31	71	0	1	0	4291,8
117	72	0	2	2	4875,4
39	73	1	0	2	9709,3
63	74	0	2	2	4791
68	75	1	1	1	8185,8
72	76	1	2	2	8695,1
123	77	1	1	2	8706,1
103	78	2	1	0	9019,6
98	79	1	2	1	6650,9
107	80	2	2	1	9451
95	81	1	1	1	7430,8
128	82	2	0	1	8847,1
94	83	1	1	0	6637,6
24	84	2	1	2	16308,9
96	85	1	1	2	8832,3
111	86	0	0	2	5977,9
29	87	0	0	1	5214
108	88	2	2	2	15147,7
104	89	2	1	1	9454,3
62	90	0	2	1	4589,3
91	91	1	0	0	6521,2
80	92	2	2	1	9484,8
85	93	0	1	0	4349,7
8	94	0	2	1	4674,5
48	95	2	0	2	15061,8
75	96	2	0	2	16990,4
100	97	2	0	1	8500,2
30	98	0	0	2	6296,1
12	99	1	0	2	9964

APPENDIX D – Order of experiments runs (Part VI)

OrdemPad	OrdemEns	OL	AT	YS	FL
135	100	2	2	2	14120,9
113	101	0	1	1	5304,1
22	102	2	1	0	9132,2
1	103	0	0	0	5279
119	104	1	0	1	8398
35	105	0	2	1	4595,7
130	106	2	1	0	8763,9
83	107	0	0	1	6182,9
56	108	0	0	1	5526
64	109	1	0	0	6350,6
126	110	1	2	2	8062
5	111	0	1	1	5092,6
74	112	2	0	1	9176,8
125	113	1	2	1	7389
110	114	0	0	1	5572,6
78	115	2	1	2	17245,1
2	116	0	0	1	5670,7
133	117	2	2	0	8686,6
84	118	0	0	2	6395,7
44	119	1	2	1	7524,9
33	120	0	1	2	5800,4
19	121	2	0	0	8763,1
116	122	0	2	1	4674,5
37	123	1	0	0	6443,1
27	124	2	2	2	14938,8
70	125	1	2	0	5785,5
16	126	1	2	0	5873,1
102	127	2	0	2	15527,8
10	128	1	0	0	6569,8
121	129	1	1	0	7369,1
115	130	0	2	0	3567,5
87	131	0	1	2	5360,1
101	132	2	0	1	9592,6
7	133	0	2	0	3828,8
32	134	0	1	1	5011,4
132	135	2	1	2	17585

APPENDIX E – Preliminary results

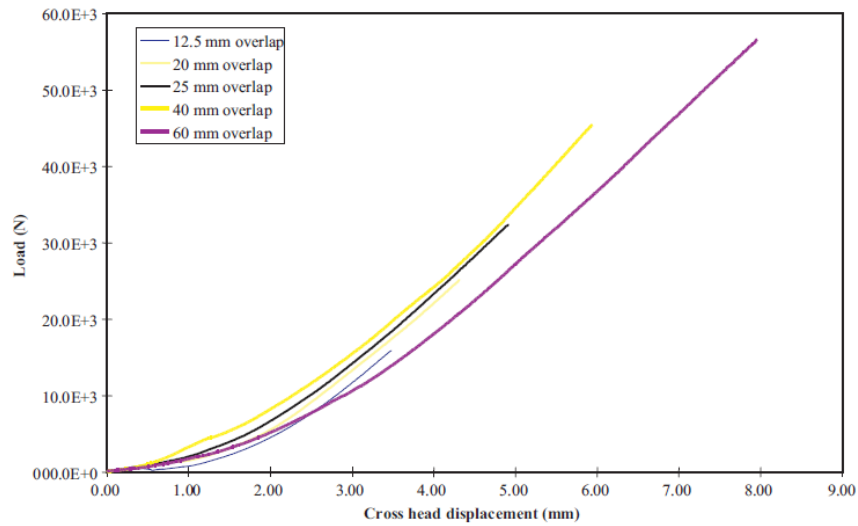
OL (mm)	AT (mm)	Sample	Failure load (N)	Average (N)	Standard deviation (N)
7	0.1	1	4633,46	4454,12	169,85
		2	4424,32		
		3	4617,1		
		4	4356,78		
		5	4238,93		
12.5	0.1	1	6425,4	6062,44	474,97
		2	5424		
		3	6495,04		
		4	6269,83		
		5	5697,9		
25	0.1	1	8881,8	8502,02	443,2
		2	8072		
		3	8728,3		
		4	7972,5		
		5	8855,5		

ATTACHMENTS

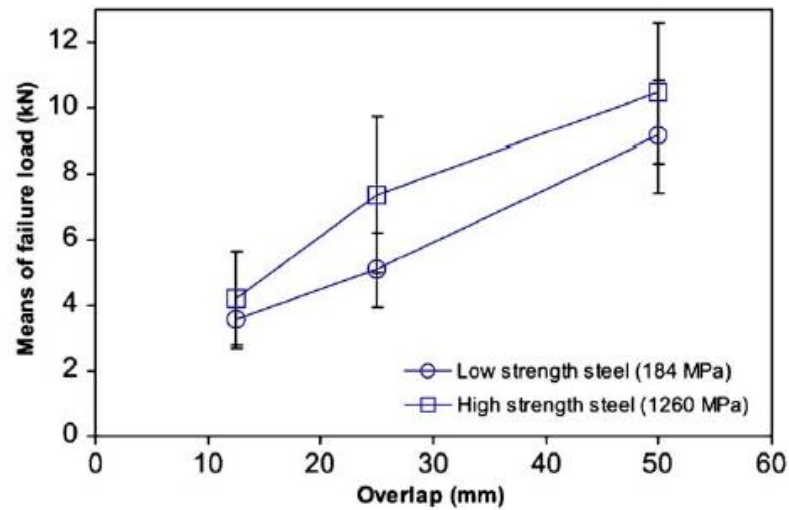
ATTACHMENT A – Reference F values – adapted from MONTGOMERY (2008)

		DF for the numerator	
		2	4
DF for the denominator	120	3.07	3.45

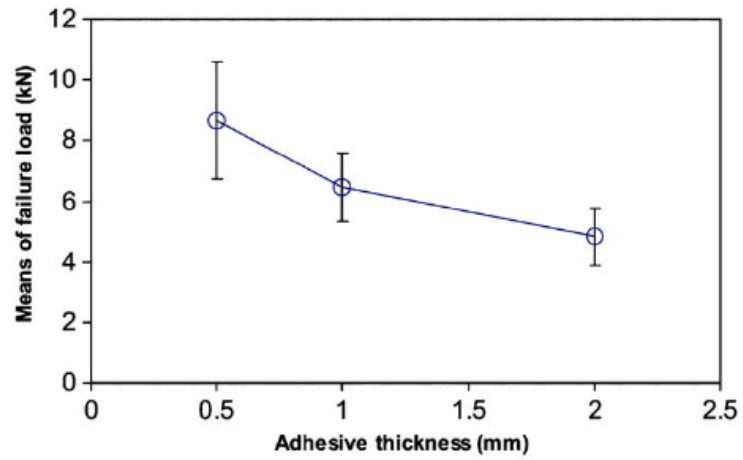
ATTACHMENT B – OL effect over SLJ FL – KARACHALIOS *et al.* (2013)



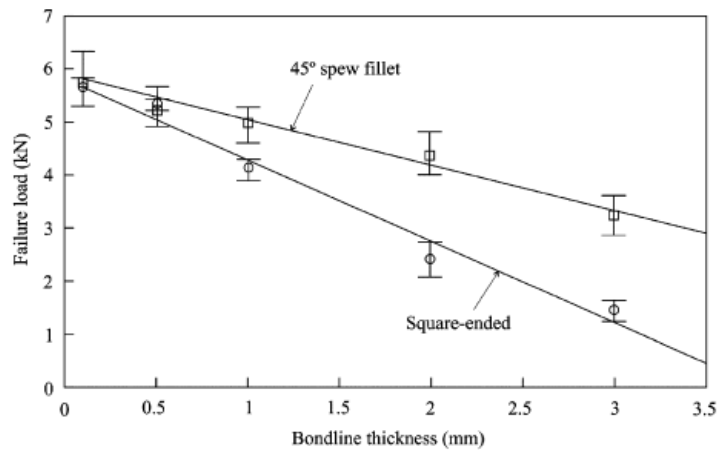
ATTACHMENT C - OL effect over SLJ FL – Da SILVA *et al.* (2009)



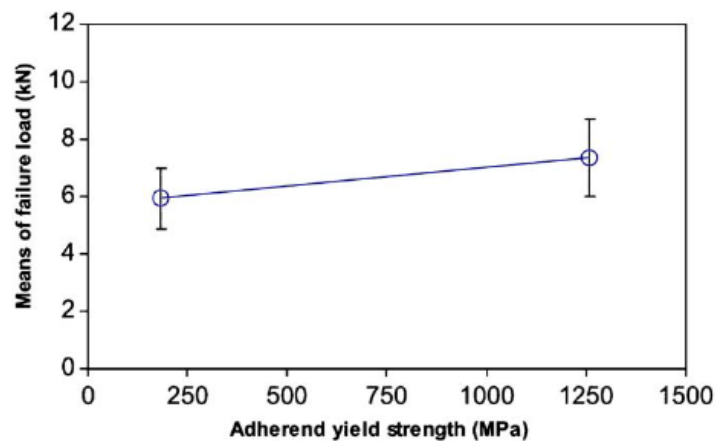
ATTACHMENT D - AT effect over SLJ FL – Da SILVA et al. (2009)



ATTACHMENT E - AT effect over SLJ FL – GRANT et al. (2009)



ATTACHMENT F – YS and OL effect over SLJ FL – Da SILVA et al. (2009)



ATTACHMENT G – SLJ failure modes – AKPINAR et al. (2013)

											
Sample	Failure patterns	F (N)	Sample	Failure patterns	F (N)	Sample	Failure patterns	F (N)	Sample	Failure patterns	F (N)
Type-I a	S.C.F.	2945	Type-I b	S.C.F.	1911	Type-I c	S.C.F.	1538	Type-I d	C.F.	1138